Improving, characterizing and predicting the lifetime of organic photovoltaics

Topical Review

Gevorgyan, Suren A.; Heckler, Ilona Maria; Bundgaard, Eva; Corazza, Michael; Hösel, Markus; Søndergaard, Roar R.; Benatto, Gisele Alves dos Reis; Jørgensen, Mikkel; Krebs, Frederik C

Published in:
Journal of Physics D: Applied Physics

Link to article, DOI:
10.1088/1361-6463/50/10/103001

Publication date:
2017

Document Version
Peer reviewed version

Improving, characterizing and predicting the lifetime of organic photovoltaics

Suren A. Gevorgyan*, Ilona Maria Heckler, Eva Bundgaard, Michael Corazza, Markus Hösel, Roar R. Søndergaard, Gisele Alves dos Reis Benatto, Mikkel Jørgensen and Frederik C. Krebs

Department of Energy Conversion and Storage
Technical University of Denmark
Frederiksborgvej 399, 4000-Roskilde, Denmark
E-mail: surg@dtu.dk

Abstract

This review summarizes the recent progress in the stability and lifetime of organic photovoltaics (OPVs). In particular, recently proposed solutions to failure mechanisms in different layers of the device stack are discussed comprising both structural and chemical modifications. Upscaling is additionally discussed from the perspective of stability presenting the challenges associated with device packaging and edge protection. An important part of device stability studies is the characterization and the review provides a short overview of the most advanced techniques for stability characterization reported recently. Lifetime testing and determination is another challenge in the field of organic solar cells and the final chapters discuss the testing protocols as well as the generic marker for device lifetime and the methodology for comparing all the lifetime landmarks in one common diagram. These tools were used to determine the baselines for OPV lifetime tested under different ageing conditions. Finally, the current status of lifetime for organic solar cells is presented and predictions are made for the progress in near future.

Contents

1 Introduction 3

2 Device architecture 4

3 Photoactive layer 6

3.1 Recent chemical advances 6

3.1.1 Chemical diversification of the side chain of the light absorbing polymer 6

3.1.2 Chemical diversification of the light absorbing polymer backbone 9

3.1.3 Chemical diversification of the acceptor molecules in the photoactive layer 11

3.2 Structural properties and external impact 16

3.2.1 Intrinsic stability: additives and ternary blends 16

3.2.2 Resistance against extrinsic impact 18

3.2.3 Mechanical stability 19

4 Intermediate layers 21

4.1 Hole transport layer 22

4.2 Electron transport layer 27

5 Electrodes 30

5.1 Non-transparent electrode 30

5.2 Transparent electrodes 31

6 Upscaling and packaging 33

7 Stability and lifetime characterization 38

7.1 Advanced characterization of stability 38

7.2 Lifetime measurements and reporting 40

7.2.1 Before and after ISOS standards 40

7.2.2 Lifetime marker 43

7.2.3 Lifetime comparison: O-diagram and baselines 48

8 Current status and predictions of OPV lifetime 49

9 Conclusions 54

References 55

1 Introduction

The emerging thin film solar cell technologies, such as organic solar cells, perovskites and others alike, have a strong potential for producing very cheap energy, which is one of the key motivations for the research in these fields and it is believed that successful commercialization of the products based on such technologies may revolutionize the energy sector. One of the key criteria for commercialization of these technologies however is the achievement of the necessary level of durability and lifetime for a given application. The lifetime of the aforementioned technologies today is still not sufficient for most of the energy production applications and therefore a significant effort is necessary to improve device stability in order to bring them into the market. Among these technologies some of the most prominent ones are organic photovoltaics (OPVs) and hybrid technologies, such as perovskite and dye synthesized solar cells. While this review will primarily focus on stability of OPVs and in particular polymer solar cells (PSC), many of the discussed challenges and their solutions are also applicable to the other technologies due to vivid similarities in device architectures [1].

Organic solar cells tend to lose their initial performance with time, which is due to failing of either one or several components (materials) in the device. It all comes down to two types of modifications that cause the failure of a material: chemical and physical modifications, as will be shown further in the text. Chemical modifications are associated with alterations in the chemical structure of the molecules in the material due to reaction with another material or substance, such as breaking of the polymer bonds due to oxidation processes [2]. Physical changes are associated with structural modifications in the material structure, where the material may for example transform from crystalline into less favorable amorphous structure with poorer electron transport properties or in the case of commonly used donor/acceptor mixture in the device, the reorganization of the mixture may lead to less favorable phase separation due to clustering of the individual components [3]. Such modifications may be caused by internal and/or external factors, as is depicted in Figure 1. Internal factors are associated with reaction between two materials or substances inside the device, such as the reaction between the electrode and the active mixture in the device, or the influence of additives on the active mixture morphology etc. [4]. External factors may accelerate internal processes i.e. an elevated temperature facilitate the morphological reorganization of the active mixture [5]. Elevated temperature may also grant access to new harmful processes, such as diffusion of moisture inside the device or increased corrosion rates for the metal electrodes [6]. The main external factors that are well known to deteriorate device performance are oxygen, moisture, light, temperature, mechanical and electrical stresses and the reader is referred to a number of reviews that have discussed each

mechanism in detail for each factor influencing device stability [7–13]. This review will instead focus on proposed solutions for the different failure mechanisms that have been reported recently.

The review provides a complete overview of solutions for the entire chain of stability issues ranging from material chemistry and device architecture to upscaling and characterization and complements these with an overview of the current status of OPV lifetime and predictions for the future. The review is split into several parts. In the second chapter a general overview of the architectural challenges of the OPV devices is presented. In the third to fifth chapters the different layers of traditional architecture of OPV device are discussed in terms of stability by covering chemical, physical and architectural issues. This is then followed by discussions of upscaling and packaging in sixth chapter. The final chapters cover the advanced characterization of stability and measuring of the lifetime, present the status of the OPV lifetime today and make predictions for the near future.

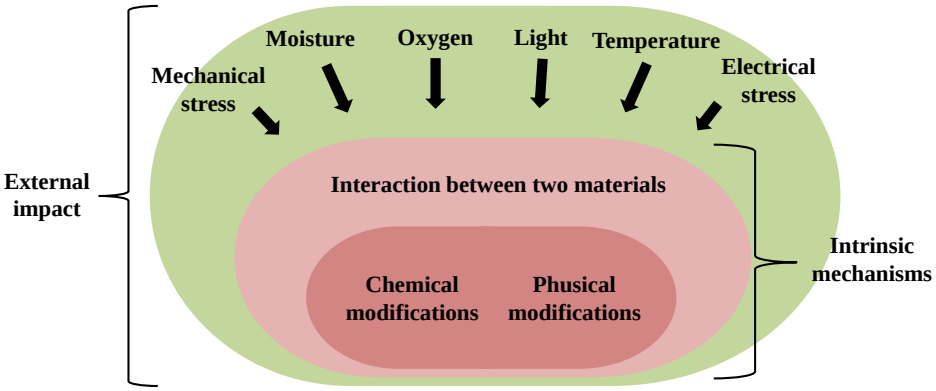

Figure 1 Diagram of the internal ageing mechanisms inside the devices and the external impact from environment is presented. The internal mechanisms are associated with chemical and structural modifications of the materials caused by interaction between two materials inside the device. External impact is associated with oxygen, moisture, light and electrical and mechanical stresses.

2 Device architecture

One of the common ways for improving the stability is optimization of device architecture. The latter constitutes improved combinations, thicknesses and order of layers in the device, protected device terminals, improved packaging with appropriate edge sealing and other similar solutions. As of today the market of OPVs has not been completely defined yet and thus, there are still no existing standards for the final product architecture of these devices, which leaves a broad space for making variations in architectural modification of OPVs. However, the challenge with certain architectural modifications is that, although, these lead to lifetime improvement, such modifications may be in

opposition to the envisioned architecture of an OPV end product and therefore, their usefulness may be a subject of dispute. Several examples are discussed in this section.

The use of thick layer or even a multilayer of top evaporated electrodes has been frequently reported to significantly improve the stability of OPVs (see for example [14,15]). While the method has shown orders of magnitude improvements in stability of unencapsulated devices [16], this has primarily been demonstrated by comparing lab scale devices with a glass substrate on one side protecting the device and the top electrode on the other. Since the thick glass substrates comprise an impervious barrier with zero transmission rate for air and moisture diffusion, the top part of the device including the top electrode obviously becomes the only path for the diffusion of the environmental agents and will therefore be the defining factor for the device stability. Therefore, changing the thickness of the top electrode can have a major impact on the stability of such a non-symmetric device. Similarly, changing the material of the electrode can also drastically affect the device stability, such as for example when switching from the aluminum (Al) used in normal structure devices to silver (Ag) used in inverted structures [17,18]. In a traditionally envisioned structure of a large scale processed flexible OPV device the stack of the layers is sandwiched between two barriers with one side serving as the substrate, which allows avoiding additional layer of costly substrate [19,20]. Alternatively, a cheap polyethylene terephthalate (PET) with no barrier properties is often used as an extra substrate for the convenience of processing. In such configurations, the front transparent electrode will be equally vulnerable to environmental impact and therefore, the above suggested architectural modifications of the back electrode or the layer sequence may become useless in this case. Moreover, the non-transparent electrode on the back of the device is easier to substitute with a cheap flexible solid metal foil, while finding cost efficient flexible transparent electrode with strong resistivity towards environmental impact for the front side of the device may be much more challenging.

Another questionable architectural modification is associated with sample dimensions. Often, laboratory scale samples of 1 cm^2 and smaller, packaged in much larger barrier materials are used for stability measurements. While these are useful for comparing the stability of the particular samples with other samples of similar nature, due to the edge diffusion effects the obtained stability data cannot be utilized for assessing the potential of the technology in terms of lifetime, since the actual end products (in forms of modules and panels) will not have the same dimensional ratio between the device and packaging and may therefore be prone to stronger edge effects.

One of the most important assets of OPVs is potentially low cost of the technology, and while often new materials or material modifications are reported, which significantly improve the stability

of OPV devices, in most cases it remains unclear whether such materials are cheap or can be made cheaply available eventually, as majority of the reports do not discuss this subject.

It is therefore recommended to always bear in mind the eventual product design and competitiveness while carrying any architectural modifications for improving the device performance.

3 Photoactive layer

The chapter discusses the recent achievements related to improvement of stability of the active layer by chemical or physical modifications. While the first section covers the chemical solutions for improving the material properties, the second section addresses the effects related to structural alterations and the external impact.

3.1 Recent chemical advances

In recent years a great amount of articles and reviews have addressed the stability of polymer solar cells (PSCs) with a specific focus on the chemical manipulation of the materials used in PSCs to improve the thermal and morphological stability for a longer lifetime of the PSCs [9,10,21–24]. Different pathways of degradation make it necessary to be creative in terms of material manipulation which can lead to their stabilization. In this section recent chemical improvements are shown for improving the stability of photoactive layer (PAL) against both intrinsic and extrinsic ageing mechanisms. The section is divided into three parts, one discussing new approaches to improve the stability of the PSCs by chemical diversification of the side chains, the other considering the backbone alterations of the light absorbing polymers and the third part discussing the acceptor materials.

3.1.1 Chemical diversification of the side chain of the light absorbing polymer

As the side chains in organic materials represent a weak point in the light absorbing layer, several new approaches have been presented in recent times that address this issue. Peng *et al.* [25] investigated the influence of the branching (linear or branched) and dimensionality (alkoxy or thienyl) of the side chains of a polymer based on benzodithiophene (BDT) and monofluorinated quinoxaline (Qx) on its thermal stability. The 2D conjugated structures were shown to increase the thermal stability of the polymer. An increased degree of branching induces higher lamellar-like ordering of the polymer, leading to a more stable PAL. However the research was performed on the pure polymer, but not on a polymer:PCBM blend and neither on a PSC [25]. Similarly, Tournebize *et al.*

reported a study on poly[(benzo[1,2-b:4,5-b]dithiophene)-alt-(thieno[3,4-c]pyrrole-4,6-dione)] (PBDTTPD) and while comparing the photostability of this polymer with traditional polymers discovered that PBDTTPD significantly outperformed the others [26]. The reason was ascribed to the fact that the alkoxy side-chains on BDT subunits mitigate the photodegradation of the whole polymer. Tierney *et al.* [27] investigated the impact of different types of side chains on the (photochemical) stability of BDT - diketopyrrolopyrrole (DPP) based PSCs (Figure 2). The stability of the bulk heterojunction (BHJ) is controlled by two different processes: the PCBM crystallization and dimerization, which means that the stability depends on the rate of crystallization. The authors claimed that this could be influenced by the type of side chains; whereas the stability decreases from linear alkyl side chain > no side chains > alkoxy side chains > branched side chains. The branched side chains cause steric hindrance in solid films, locking the polymer chain in place and reducing the paths in the 3D space for the fullerene diffusion. An increase of the steric hindrance as well as the rotational freedom can be seen for the alkoxy and thienylethylhexyl side chains. However, polymer with linear side chains are the most stable ones due to an even distribution of the chains along the backbone and dense packed polymer aggregates, where no PCBM molecule can migrate through (Figure 2), leading to a low diffusion rate for the series due to thermal instability of the polymer:PCBM BHJ [27]. Not only the type of side chain but also the different length of the conjugated side chains is directly influencing the thermal and morphological stability of the devices. The study by Yang *et al*. [28] deals with the use of different amounts of thiophenes in the side chain of BDT. The alkyl-thienothiophene substituted polymer with the longest side chain revealed the optimal morphology and best thermal stability in comparison to alkoxy and alkyl-thiophene substituted polymers.

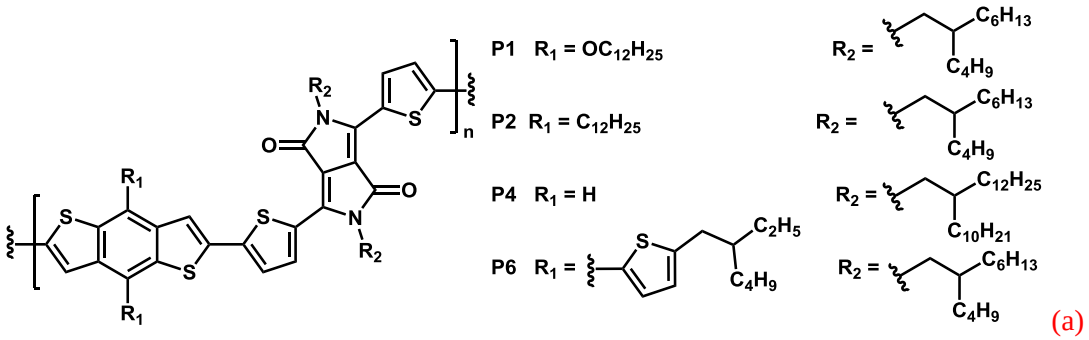

(a)

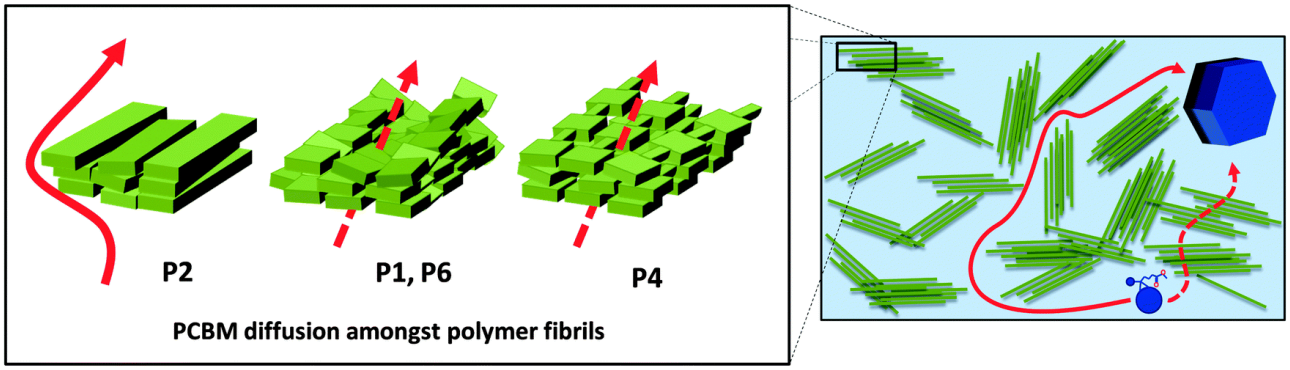

(b)

Figure 2 Illustration of different polymer (a) aggregate formations based on side chain distribution and rotation (b, left). In a BHJ material these aggregates regulate the transport of PCBM which can either pass around the aggregates or through them (b, right). Reprinted with permission from [27].

Maes *et al.* [29] reduced the side chain density in a polymer based on cyclopentadithiophene (CPDT) and Qx leading to a PSC with increased efficiency and device stability under continuous thermal stress. This tuning of the side chain pattern led to an optimized morphology of the PAL [29].

The immutability of the morphology of the BHJ to have an optimal function of the solar cell is one of the main focuses of the chemical diversification of light absorbing polymers. Instability of the BHJ morphology is often a result of prolonged thermal annealing leading to a phase separation/demixing of the polymer and PCBM (crystallization of the PCBM). One approach would be to do a side chain functionalization/modification to yield a polymer with higher glass transition temperature (Tg). This has already been done in 2011 by Vanderzande *et al.* [30] on a polyphenylvinylene (PPV) derivative using a phenylethoxy side chain. Recently this concept was adopted (also from the same group) [31] and applied to various more promising (advanced conjugated) polymers for PSCs. The usage of alcohol or ester (and cinnamoyl) groups as part of the side chains of polythiophene (Figure 3a) [21,31–33] or a polymer based on CPDT and benzothiadiazole (BT) (Figure 3b) [34] resulted in a higher Tg and thus an enhanced thermal stability (Figure 3a). In the case of polythiophene (PT) the specific functional moieties were introduced in a small ratio (10%) into a random poly(3-alkylthiophene) improving the thermal stability significantly through a decay in demixing of the PAL. [21,31–33] The phase separation and morphology development are shown in the images of transmission electron microscopy (TEM) and selected-area electron diffraction (SAED) patterns (Figure 3c). [32] In case of the CPDT based polymer the specific functional groups are incorporated into the whole polymer. These results show an absence of phase separation and crystallization as well as an enhancement in the long-term stability of the solar cell parameters, as shown in Figure 3d for samples stored in nitrogen at 85 ^{o}C temperature. [34] However, the adoption of this concept on advanced conjugated polymers (like polymers based on BT or thiazolothiazole) using the phenethyl group to partially exchange the solubility side chain, did not

lead to a clear enhancement of the stability of the BHJ PSCs [35]. This means that this approach cannot be applied to all suitable advanced conjugated backbones for PSCs.

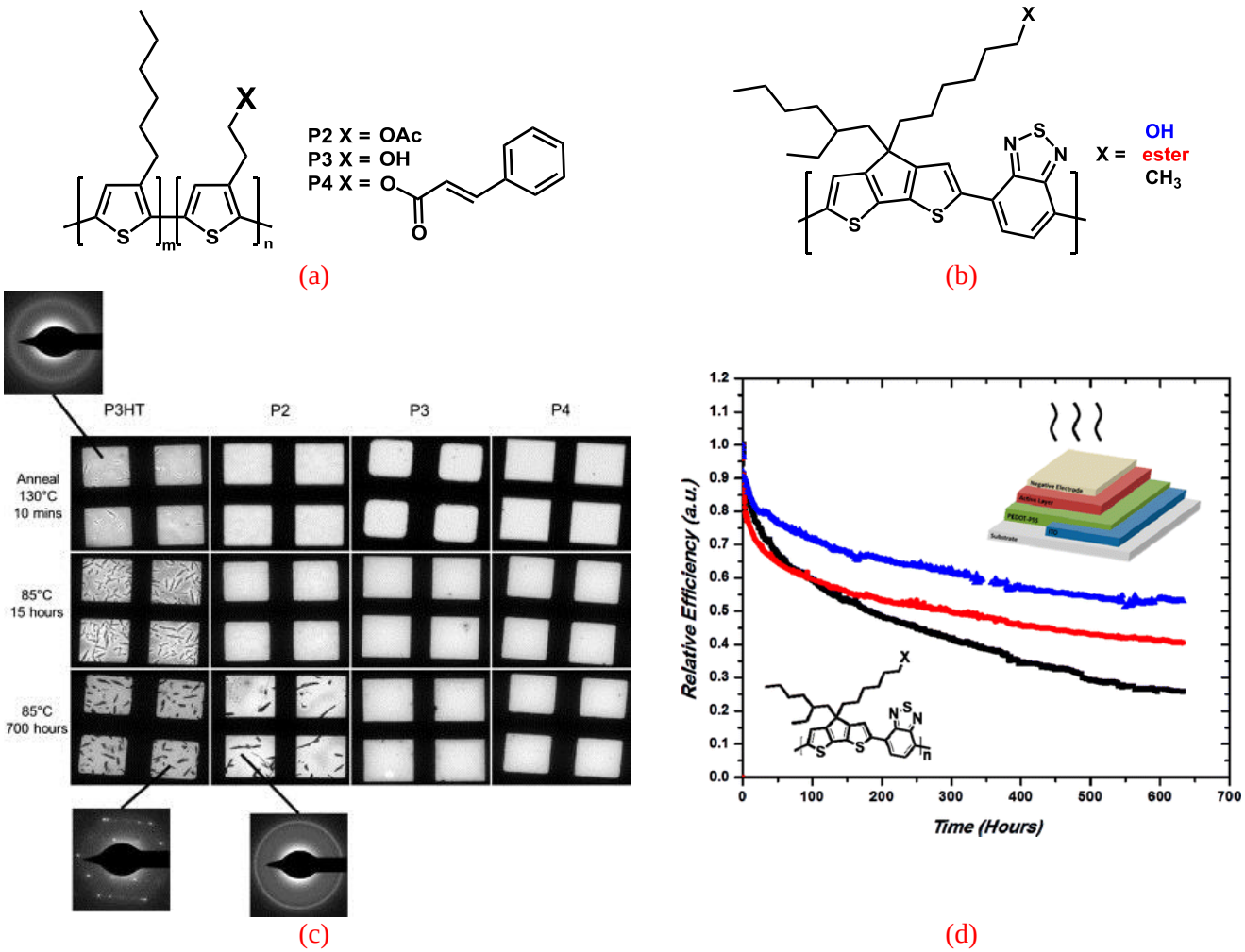

Figure 3 Molecular structure of modified a polythiophene (a) and a CPDTBT based polymer (b), TEM and SAED images of PT based:PCBM blends (1:1) degraded at 85°C (c) [32] and the thermal degradation of the efficiency of PSCs based on CPDTBT polymers with different side groups stored in nitrogen at 85 °C (d). Reprinted with permission from [34].

In another approach the alcohol moieties were used to crosslink with another molecule. Shiao *et al.* described a series of maleimide-thiophene copolymers containing partial 2-hydroxyethyl or 6-hydroxyhexyl units, which were cross-linked with 3,3'-dimethoxy-4,4'-biphenylene diisocyanate (DMBPI) leading to an increased thermal stability [36].

3.1.2 Chemical diversification of the light absorbing polymer backbone

The structure of the polymer backbone can also have an influence on the stability of the PSCs. However, this influence is not as drastic as it is for the side chains. It is already well known that the stability depends on the monomer units. For example a polymer containing fluorene is less stable than a polymer containing BDT as the donor unit [24,37]. Gedefaw *et al.* studied a series of p-type

copolymers, which combined a fluorinated quinoxaline (FQ) acceptor unit either with a differently substituted BDT or an unsubstituted thieno[3,2-b]thiophene (TT) and showed their effect on both film and device stability [38]. In particular, the authors demonstrated that while in the form of pristine films the polymer with TT showed the best photostability, in the form of devices the polymers with BDT led to the most stable devices retaining 85% of the performance after 72 hours of light exposure. In another study dithienobenzodithiophene (DTBDT) donor was fused with 2-ethyl – 1 -(thieno [3,4-b] thiophen-2-yl) hexan – 1 - one (TTEH) or 6 – octyl – 5 H –thieno [3′,4′:4,5] thieno [2,3-c] pyrrole - 5,7 (6H) - dione (DTPD) acceptor units and the stability was investigated. Due to its flat structure pDTBDT-TTEH formed crystalline structure, while pDTBDT-DTPD had highly twisted structure resulting in very amorphous structure and therefore, the former significantly outperformed the latter in terms of shelf life highlighting the importance of the morphology in the stability [39]. Hou *et al.* [40] showed that there is also influence of the chemical structure of the backbone units. A polymer which contains two fused thiophenes is theoretically more thermodynamically stable, than a polymer with two non-fused thiophenes (Scheme 1). The more rigid and stable backbone confirmation is more stable thermodynamically. The thermal properties (melting and crystallization temperatures) are also higher.

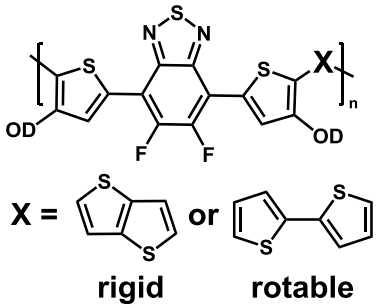

Scheme 1 Polymers with different backbone structures

Further, direct substituents on the monomer units can influence the stability of the polymers. In another study Carlé *et al.* [41] showed that with increasing number of fluorine substituents on a BT unit in two different polymer groups, the photochemical stability of the polymers were clearly enhanced. As a result the incorporation of fluorine substituents in the polymer backbone has a positive effect on the stability of the solar cell devices. Similar results were shown by Livi et al. (Figure 4) and Li et al. demonstrating clear enhancement of the efficiency and stability of such PSCs (Figure 4) [42,43].

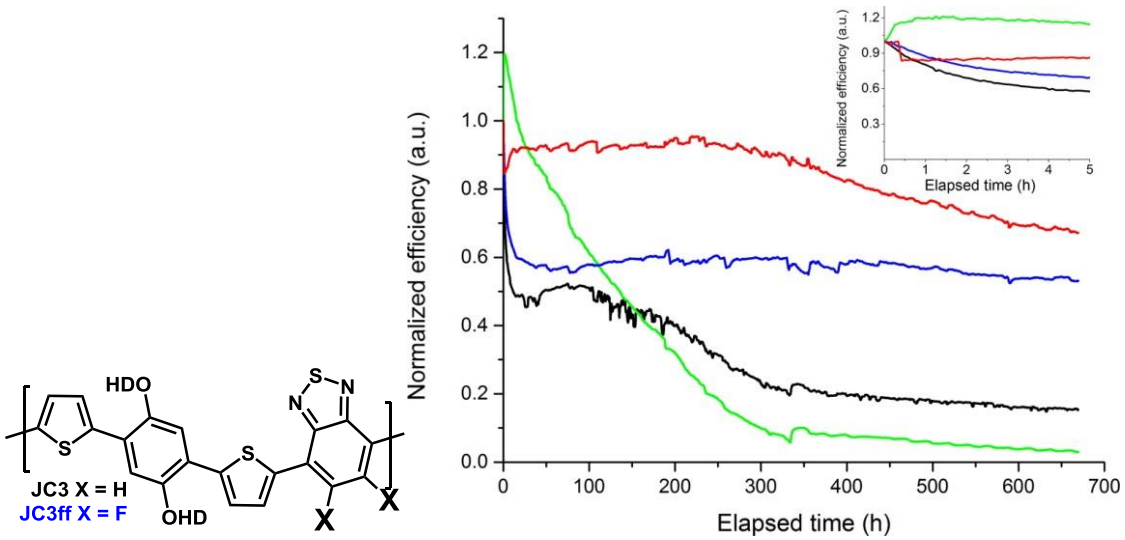

Figure 4 Lifetime studies of JC3 (black in (a) and (b)), JC3ff (blue in (a) and (b)) and poly(3-hexylthiophene) P3HT (green in (b)). (Red curve in (b) is out of scope of this review). The encapsulated samples were exposed to 1.2 Sun light illumination at 130 ºC temperature. Reprinted with permission from [43].

Other ways to stabilize the intrinsic stability of the donor, were the use of polythiophene block copolymers selectively functionalized with isoorotic acid moieties and a diaminopyridine tethered fullerene derivative (PCBP), which showed strong complexation through hydrogen bonding. Solar cell was fabricated by Li *et al.* employing the polythiophene block copolymers with issoorotic acid moieties and by varying the amount of PCBP and PCBM. The authors found that such complementary hydrogen bonding not only led to improved device stability, but also to tunable and long-range ordered morphologies by adjusting the amount and nature of fullerene derivatives [44].

3.1.3 Chemical diversification of the acceptor molecules in the photoactive layer

In the processing of the PAL in the solar cells specific solvent additives are often used to influence the morphology of the PAL and thus the efficiency of the PSCs. This principle is similar to adding or (partially) exchanging (10-15%) the PCBM with small molecules to influence (the morphology and thus) the stability of the PAL. In the approach of Chuang *et al.* [45], a cross-linkable open-cage fullerene (Scheme 2a) was partially incorporated into the PAL. The cross-linking can be induced via heat treatment of the styryl moiety resulting in a longer lifetime of the correspondent PSCs under thermal stress. Cross-linkable azido C60-fullerene derivatives were also used in poly(3-hexylthiophene) P3HT and PCBM mixture based solar cells to drastically suppress the formation of PCBM crystals in the BHJ and macro-phase separation, leading to a very stable morphology [46].

Andersson *et al.* [47] modified fullerenes with pyridine and amine groups, respectively (Scheme 2b). Partial incorporation of these fullerene derivatives into the PAL blend of a thiophene-Qx donor

polymer:PCBM shows significant increase of the thermal stability of the BHJ nanostructure, where the fullerene crystallization is hindered at the annealing temperature. In addition, these materials can also be used as self-assembling interlayers on the indium tin oxide surface.

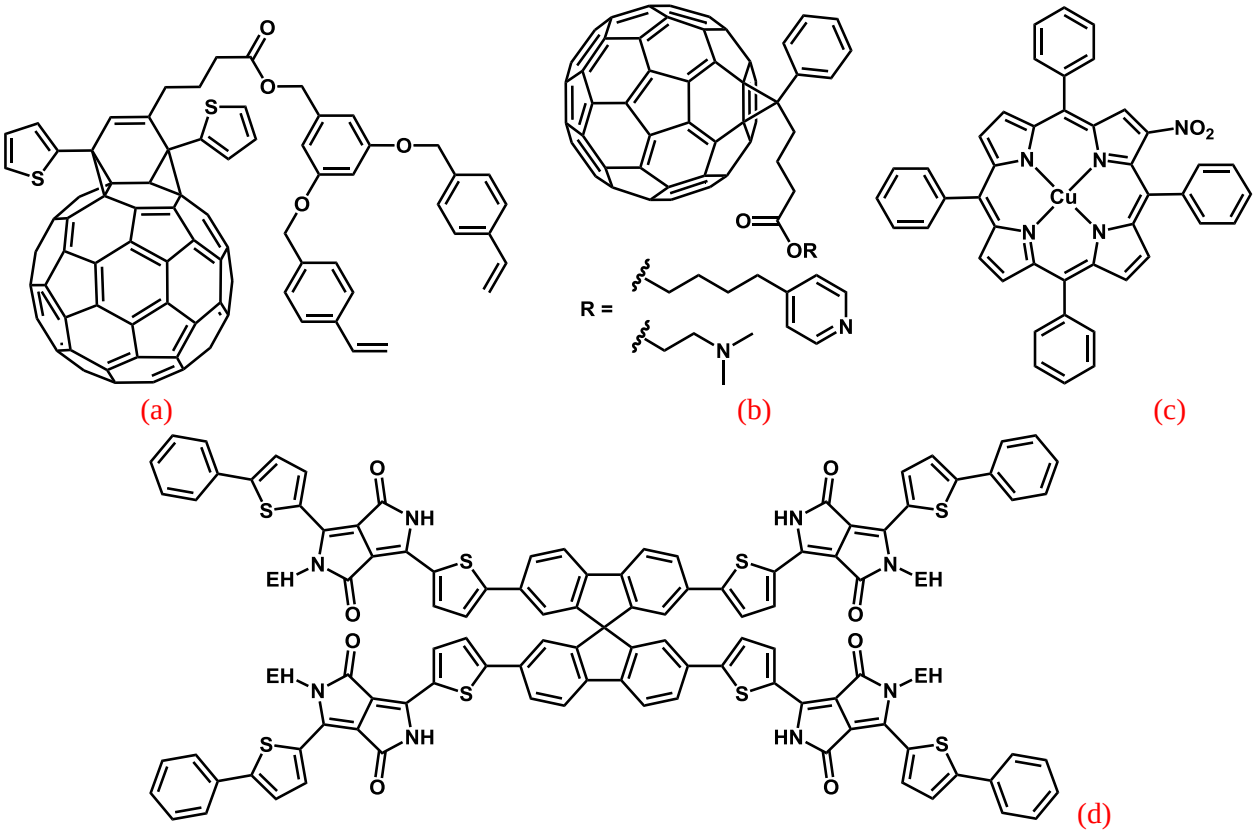

Scheme 2 Small molecule additives to the PAL (cross-linkable open cage fullerene [45] (a), and PCBM derivatives [47] (b) and porphyrin compound [48] (c) and PCBM replacement (spirobifluorene [49](d)) to improve the stability of the PSC.

Another strategy to prevent fullerene aggregation is to stabilize the PAL via incorporation of a porphyrin compound. This addition does not only stabilize the morphology of the polymer:PCBM film, but depresses the PCBM crystallization. After discovering that these compounds are sufficient for PSC stability [50], Yang *et al.* [48] performed a small screening of different porphyrin compounds including different metals (Cu, Zn, Ni, non-metallized) or different substituents (NO_2, C_4F_6Cl, non-substituent) to see the influence on self-aggregation and photo-thermal stability. The PSC (P3HT:PCBM), which was doped with 8 wt-% of the most promising porphyrin compound (Scheme 2c), showed the smallest decrease in efficiency preserving 83% of initial photoconversion efficiency (*PCE*) after 48h at 130°C in comparison to the pristine devices, which retained 28.4% after 3h at 130°C [48]. Liao *et al.* developed a [6,6]-phenyl-C 61 butyric acid pentafluorophenyl ester ($PC_{61}BP^F$) and used together with PCBM. Such a mixture is responsible for creating a supramolecular attraction between the pentafluorophenyl group of $PC_{61}BP^F$ and the C60 cores of $PC_{61}BP^F$/PCBM, which can prevent the $PC_{61}BP^F$/PCBM materials from severe aggregation [51]. By doping only 8.3 wt%

($PC_{61}BP^F$), in a P3HT:PCBM device, a *PCE* of 3.68% was reached after 25 h of heating at 150 °C, preserving 95% of its original value. In sharp contrast, the *PCE* of the device that used a traditional P3HT:PCBM blend decayed drastically. Such an approach was effective also with low band-gap polymer such as PDTBCDTBT, which is based on dithienobenzo-carbazole (DTBC).

To prevent fullerene crystallization in the PAL, the PCBM can be replaced by a fullerene free material. After a decade of slow progress, non-fullerene acceptors are now undergoing rapid development and are emerging as a focus area in the field of organic semiconductors [52]. The novel non-fullerene electron acceptor spirobifluorene with four diketopyrrolopyrrole endcapped with a benzene ($SF(DPPB)_4$) (Scheme 2d) was designed to suppress strong intermolecular aggregation. Excellent thermal stability was shown upon thermal treatment of the P3HT:$SF(DPPB)_4$ PSC at 150°C for 3h. Its efficiency remained unchanged, whereas the efficiency of the fullerene based PSC dropped significantly [49]. In another study, as an acceptor {[N,N0-bis(2-octyldodecyl)-naphthalene-1,4,5,8-bis(dicarboxi- mide)-2,6-diyl]-alt-5,50-(2,20-bithiophene)} (P(NDI2OD-T2)) was used and as a donor 7,70-(4,4-bis(2-ethylhexyl)-4H-silolo [3,2-b:4,5-b0]dithiophene-2,6-diyl)bis(6-fluoro-4-(50-hexyl-[2,20-bithiophen]-5-yl)benzo[c][1,2,5] thiadiazole), p-DTS ($FBTTh_2)_2$ was used, which led to a device exhibiting excellent thermal stability in air without encapsulation preserving 70 % of initial performance after heating at 180 °C for 20 h (see a comparison with other polymers in Figure 5) [5].

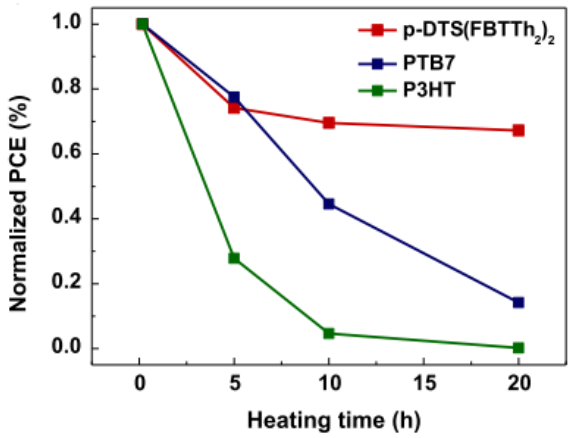

Figure 5 Degradation curves of unencapsulated devices with different polymers coupled with the acceptor P(NDI2OD-T2) tested in air. The heating temperature was 180 °C and was applied before the deposition of the front electrode. Reported with permission from Elsevier [5].

Chen *et al.* [53] used ter(ethylene oxide) (TEO) functionalization to manipulate the polymer donor (P-BDTT-TT-TEO) and fullerene acceptor (PCB-TEO) [53]. The TEO side chains induce more ordered molecular packing leading to a well-defined morphology and enhanced stability of the PAL. PCB-TEO is an effective compatibilizer located at the interface of the acceptor and donor to strengthen and manipulate the interaction between PCBM and PBDTT-TT-TEO (Figure 6 I). Direct

blending of the TEO manipulated acceptor and the donor results in poor performance. Therefore, appropriate amount (5%) of PCB-TEO was incorporated in the PAL blend. Thermal stability in inert atmosphere of the different PSCs (Figure 6 II) and films (Figure 6 III) showed increased stability with incorporation of TEO in acceptor or acceptor and donor. This approach is very promising in terms of thermally stable devices with well-defined and stable morphology [53].

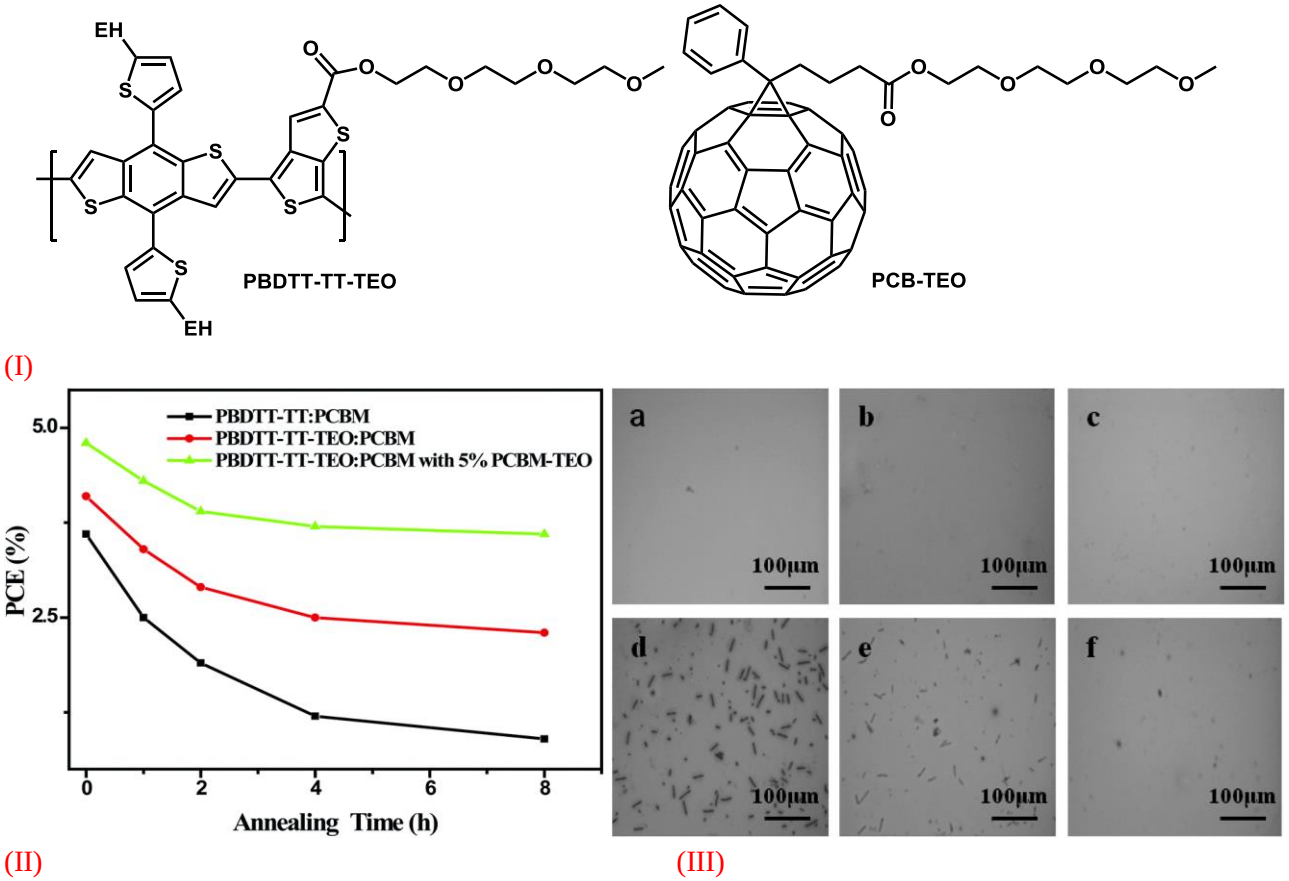

Figure 6 (I) Illustration of the TEO modified polymer and fullerene derivative (PBDTT-TT-TEO and *PCE*-TEO), (II) Lifetime of PSCs based on these materials in terms of their *PCE* under 150 °C and inert atmosphere and (III) optical micrographs of films based on PBDTT-TT:PCBM (a and d), PBDTT-TT-TEO:PCBM (b and e) and PBDTT-TT-TEO:PCBM:PCB-TEO (c and f) before (a-c) and after (d-f) annealing at 150°C for 8 h. The dark areas correspond to PCBM crystals. Reprinted with permission from [53]

Table 1 outlines the improvements discussed above. It is difficult to pin point the best solutions among the reported data, since the conducted tests and samples vary greatly and therefore, are incomparable. The comparability for the general lifetime of OPV devices was addressed in 2011 by developing ISOS testing guidelines, which will be discussed in Chapter 7. It would however be relevant in addition to ISOS guidelines to develop common testing procedure for determining film photostability. This would allow easily comparing and determining the reported chemical modifications of the films that lead to the best photostability.

Table 1 Overview of all chemical diversifications in this review.

Affected molecule[1]	Affected unit[2]	Comparison/ realization[3]	Chemical diversification	Effect on stability/morphology	Ref
Diversification in donor/polymer					
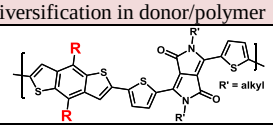	Side chain	dimension	R = no/**linear**/ branched/alkoxy/ alkyl-thiophene	even distribution (=linear alkyl chain) →reduces the PCBM diffusion rate →more stable polymer solar cell	[27]
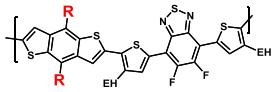	Side chain	dimension	R = alkoxy/ alkyl-thiophene/ **alkyl-thienothiophene**	increasing number of thiophene →improved morphological/ thermal stability	[28]
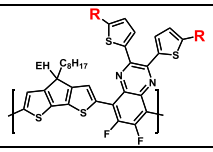	Side chain	reduction	copolymer with R = EH and R = **H**	partly removal of the side chains →enhances the thermal stability →more fine intermixed blends	[29]
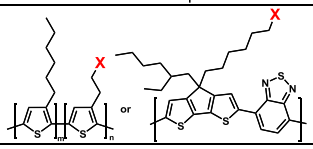	Side chain	Doping/ exchange	X = ester or **alcohol** group	(partly) incorporation → increase of the glass transition temperature →enhances thermal and morphological stability	[21,31 –34]
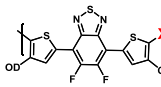	Back-bone	Fused/ non-fused	X = bisthiophene or **thienothiophene**	Fused thiophenes: more rigid backbone/ stable confirmation →higher melting and crystallization temperatures →stronger interchain interaction.	[40]
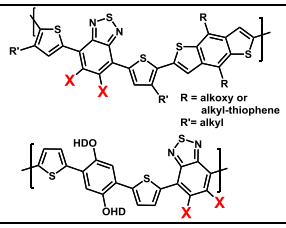	Back-bone	doping	X = hydrogene or **fluorine**	Fluorination of benzothiadiazole →better photochemical stability of the polymer →slower decay rate of the PSC device	[41,43]
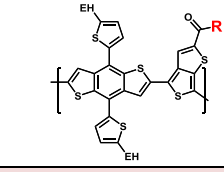	Side chain	exchange	R = **ter(ethylene oxide)**	Functionalized copolymer (and fullerene acceptor) →changes morphology →manipulates miscibility between polymer and fullerene →more thermally stable PSCs.	[53]
Diversification in acceptor/PCBM (see Scheme 2 and Figure 6)					
PCBM	Side chain	doping	cross-linkable group	Addition of crosslinkable fullerene →reduce the PCBM phase aggregation rate →highly stable PSCs.	[45]
PCBM	Side chain	doping	pyridine or amine groups	Addition of functionalized fullerene →hinders the PCBM crystallization →increased thermal stability	[47]
PCBM	Molecule	doping	porphyrin	Addition of porphyrin →supramolecular interactions →depresses PCBM crystallization (decreased T_m and increased T_c) →stabilized morphology.	[48,50]
PCBM	Molecule	exchange	spirobifluorene	Non-fullerene electron acceptor →suppressed intermolecular aggregation →improved thermal stability.	[49]
PCBM	Side chain	doping	Ter(ethylene oxide)	see the entry in row 7 above, in this table (side chain, exchange)[4]	[53]

[1]Chemical structures: EH = 2-ethylhexyl, OD = 2-octyldodecyl, PCBM = phenyl-fullerene (C61 or C71)-butyric acid methyl ester, P3HT = poly(3-hexylthiophene), PEDOT:PSS = poly(3,4-ethylenedioxythiophene)-poly(styrenesulfonate); [2]part of the molecule is which is affected by the chemical diversification, [3]comparison or realization which affected the molecule part, [4]effect is only described with the manipulation of both polymer and PCBM.

3.2 Structural properties and external impact

This section addresses the studies related to structural and morphological aspects of PAL stability and is split into three parts. The first part primarily deals with structural and morphological modifications within the active mixture and the effect of the third components. Such changes often originate from the properties of the materials and are not linked to external impact. The discussion in the second part is oriented more towards the impact of the external agents on the PAL and presents certain solutions for making the PAL more resistive towards such agents. The final part addresses the mechanical properties of the PAL.

3.2.1 Intrinsic stability: additives and ternary blends

In a bulk heterojunction of polymer solar cell an optimal interpenetrating network of donor and acceptor is a key for optimal performance. However, the morphology of such a network often is not stable and may deteriorate after certain period of operation or storage resulting in device performance decay. It is therefore vital to develop methods for stabilizing the morphology of the mixture in order to preserve the optimal performance for extended period of time. As was discussed in the previous chapter optimizing the side chains is one way to improve the morphological stability of the film. On the other hand, solvent vapor annealing was also found to have strong influence on both efficiency and stability, by altering the blend morphology [54]. However, while the additive can improve the *PCE*, it often impacts the stability negatively. As an example, when 1,8-diiodoctane (DIO) was used as a solvent additive in active mixture of Poly[[4,8-bis [(2-ethylhexyl) oxy]benzo[1,2-b:4,5-b'] dithiophene-2,6-diyl] [3-fluoro-2-[(2-ethylhexyl) carbonyl] thieno[3,4-b] thiophenediyl]] (PTB7) and PCBM [55] or Poly[2,6-(4,4-bis-(2-ethylhexyl)-4H-cyclopenta [2,1-b;3,4-b′]dithiophene)-alt-4,7(2,1,3-benzothiadiazole)] (PCPDTBT) and PCBM [56], it significantly improved the efficiency of the devices, but reduced the stability bringing the samples to the same level of *PCE* after prolonged exposure to air for 300 hours. Meanwhile in another study, Huang *et al.* reported that using the poor anti-solvent isopropanol (IPA) during the spin coating of Poly[4,8-bis(5-(2-ethylhexyl)thiophen-2-yl) benzo[1,2-b;4,5-b'] dithiophene-2,6-diyl-alt-(4-(2-ethylhexyl)-3-fluorothieno[3,4-b]thiophene-)-2-carboxylate-2-6-diyl)] PBDTTT-EFT (also known as PCE10) and $PCBM_{[70]}$ helped removing the residual DIO and led to an improved photochemical stability [57]. Kettle *et al.* instead looked at alternative additives while studying PCPDTBT polymer, which would be less harmful for stability and proposed less volatile napthalene-based additives, such as 1-bromo-naphthalene (BrN) or 1-chloro-naphthalene (ClN) for improving PAL performance [58]. The author demonstrated that, although these additives increased the surface roughness of the active films resulting in somewhat

reduced *PCE*, the stability was improved by a factor of three. The improvement was ascribed to reduced morphological changes and reduced oxidation of the thiphene ring. It was also possible to employ additives that promoted a cross-link. Khiev *et al.* effectively improved the thermal stability by using a poly(3-hexylthiophene) (P3HT) end-capped with anthracene (P3HT-A) in a blend with PCBM, treaded with UV light. It was proposed that the P3HT-A chain reacts with PCBM fullerene via a [2+2] cyclo-addition to stabilize the blend. When comparing the UV-cured device with the device without UV treatment, only the latter presented large fullerene crystallization after thermal ageing [59]. Therefore, efforts were made on stabilizing the donor and/or the acceptor, as they both had major role in the stabilization process.

Another example of intrinsic instabilities in the photoactive material has been reported lately by Bracher et al [60]. The authors studied the effect of the residual palladium catalyst left inside the material from the synthesis of poly[N-9″-hepta-decanyl-2,7-carbazole-alt-5,5-(4′,7′-di-2-thienyl-2′,1′,3′-benzothiadiazole)] (PCDTBT) on the efficiency and stability of the devices based on this material and revealed that palladium self-assembles into nanoparticles, which initiate growth of large aggregates inside the polymer. The authors used photocurrent mapping to demonstrate that such aggregates result in shunts in the device which reduces the photocurrent and contributes in rapid initial burn in of the device performance (see Figure 7) during light soaking in air.

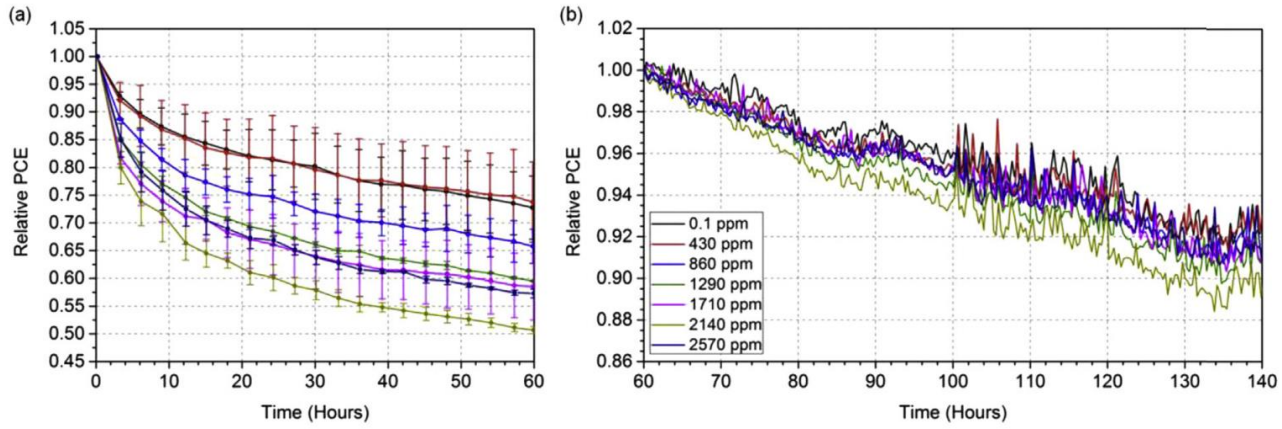

Figure 7 The ageing of encapsulated samples with various concentrations of palladium as a function of exposure to light in air. Reprinted with permission from [60].

A relatively new branch of organic solar cells (OSCs) consist of PAL with a third component besides the donor and acceptor (organic or inorganic, semiconductor or insulator). Cheng *et al.* presented a broad review of different third components that have been used in OPVs and argued that the use of such an extra component allowed broader and stronger absorption, more efficient charge transport pathways, better charge extraction at the electrodes and improved stability [61]. The reason

for a better stability was attributed to the fact that fullerene tends to aggregate into big clusters after some time or after thermal treatment, which deteriorates the morphology of the active layer and reduces the *PCE* drastically. The use of a third component can suppress aggregation of PCBM by means of solidifying the morphology of the active layer as a cross-linker, or freezing the scale of phase separation via some special intermolecular interactions. For example, PTB7:$PCBM_{[60]}$ degraded by more than 80% after 16 h of exposure to thermal heating at 150 °C, while the same device with the third component of 2 wt% bis-azide cross-linker 4,4′-bis(azidomethyl)-1,1′-biphenyl (BABP) degraded only by 20% after the same thermal exposure [61,62]. Another way to increase both performance and stability is to incorporate Ag and Al nanoparticles (NPs) into the active layer [63,64]. In poly(p-phenylene-ethynylene)-alt-poly(p-phenylene-vinylene):phenyl-C61- butyric acid methyl ester (AnE-PVstat:PCBM)-based bulk heterojunction solar cells, by incorporating Ag NPs of 6 nm in diameter in the PAL, the *PCE* was increased from 2.46 % to 3.10 %. Moreover the devices were testes under indoor solar simulator, showing a three-fold improvement of stability with the Ag NPs [64].

3.2.2 Resistance against extrinsic impact

It is well established that agents, such as oxygen and water combined with light significantly affect the stability of polymer solar cells and resistance towards these agents is described here as extrinsic stability. The morphology of the active layer is not only influencing the intrinsic, but also the extrinsic stability. One of the recent works demonstrated for instance how the more crystalline and denser materials showed improved stability towards light exposure compared to more amorphous materials [65]. In particular, when crystalline and amorphous materials were compared, only the amorphous materials showed a significant decrease of open circuit voltage (V_{OC}) after aging [66]. This was explained by the energy state disorder caused by light induced traps. In amorphous materials, the energy state disorder has a significant influence on V_{OC}, while in the crystalline materials since the charge carrier density is higher several times such a disorder does not play a major role [67]. Oxygen is known to cause drastic degradation, especially in combination with light [68]. The use of single-crystalline P3HT nanofibril with tightly packed π- π bonding was found to effectively reduce the permeation of oxygen, which led to an improved stability compared to standard P3HT. In particular, after 30 days of constant sunlight illumination, the standard P3HT lost 80 % of the initial performance, while the nanofibril one only 20 % [69].

Using hindered phenols as additives, substantial improvement of the stability was achieved for samples exposed to 1000 W/m^2 constant illumination under ambient condition. In particular, the use of octadecyl 3-(3,5- di-tert-butyl-4-hydroxyphenyl)propionate in P3HT:PCBM solar cells led to

increased power by a factor of 3, compared to the reference device without the stabilizing additive. Turkovic *et al.* suggested the hydrogen donation mechanism in combination with the radical scavenging properties of the propionate type hindered phenols was responsible for the significant reduction of radicals within the photoactive layer, which could in turn stabilize the performance by decreasing the exciton recombination [70].

A common issue for OPVs is the quick drop of the performance experienced during the initial stage of ageing, which is called "burn-in". Voroshazi *et al.* suggested that burn-in depend on the external impact and in particular is light dependent [71]. By altering the thickness or the acceptor in the bulk of active mixture they found that upon continuous illumination of P3HT:$PCBM_{[60]}$ cells, the burn-in, which was mostly caused by the drop of the short circuit current density (J_{SC}), was due to the ageing of the active bulk, while in PCDTBT:$PCBM_{[70]}$ the drop of the efficiency was mostly originating from the drop of the fill factor (*FF*) due to the blend/anode interface degradation. The authors suggested that a stable device without burn-in is possible by accurately engineering the employed materials. Meanwhile, Kong *et al.* by selectively extracting the trap-free high molecular weight components in PCDTBT showed that it is possible to reduce the burn-in loss and the resulted optimized device showed burn-in free behavior with 40% increased performance [72].

3.2.3 Mechanical stability

In recent years, the interest towards studying and solving issues related to the mechanical stability of organic solar cell is rapidly growing, since roll-to-roll (R2R) printed flexible devices are often subjected to high mechanical stress during processing and handling, which may impair device stability. Kim et at. studied the mechanical stability of the photoactive layer of OPVs and proposed a method for improving the mechanical and thermal stability of PAL by adding the novel compatibilizer poly(3-hexylthiophene)-graft-poly(2-vinylpyridine) (P3HT-g-P2VP) in the active blend of P3HT and fullerene derivative [73]. This led to a better interface between P3HT and the fullerene derivative, which improved both thermal stability and as a result, the cell having 5 % P3HT-g-P2VP, lost less than 10% of initial performance after 72 h thermal ageing at 150 °C compared to almost full degradation of the reference device without the compatibilizer. Moreover, while studying the mechanical properties the authors recorded around 20% increase in the fracture energy in the blend, indicating a much more mechanically stable device.

Corazza *et al.* studied the effect of external stresses, such as heat, UV light or humidity exposure on the mechanical properties of different layer in the device [74]. It was found that the combination of humidity and annealing (45 % R.H. and 85 °C) caused growing of macrostructures in the active

layer exposed directly to these conditions, resulted in development of weak layer within the bulk leading to mechanically unstable layer. Interestingly, when UV light exposure was added to the experiment, the mechanical deterioration of the PAL by the external stresses was reduced. This was ascribed to the fact that the UV light may have dried the samples and therefore protected it from the impact of humidity. The authors suggested that optimized treatment of the device with different external stressors may eventually lead to more stable device. In another study, Kim *et al.* substituted fullerene with poly[[N,N′-bis(2-hexyldecyl)-naphthalene-1,4,5,8-bis(dicarboximide)-2,6-diyl]-alt-5,5′-thiophene] P(NDI2HD-T), which not only improved the efficiency, but also significantly enhanced the strength and flexibility of the PAL, with an improvements of 60 and 470 times respectively in elongation at break and toughness [75]. Such improvement originated from the fact that the polymer based acceptor is intrinsically more ductile and is therefore better able to entangle with polymer chains of the donor. Savagatrup *et al.* studied the different mixtures of fullerenes $PCBM_{[70]}$ and $PCBM_{[60]}$ in varying rations in the active blend with P3HT polymer and analyzed the effect of the different ratios on the mechanical stability of the blend [76]. The studies revealed that the films of pure $PCBM_{[70]}$ had approximately five times higher mechanical compliance (robustness, flexibility, and stretchability) than films of pure $PCBM_{[60]}$. It was also found that BHJ films comprising technical grades (with purity of $\geq$ 90%) of $PCBM_{[60]}$ or $PCBM_{[70]}$ were approximately two to four times more compliant compared to 99% purity. This proved that that technical grade not only lowers the cost of the manufacturing, but may simultaneously increase the mechanical stability of the film and the device. The smallest range of stretchability was found for BHJs with 99% $PCBM_{[60]}$ (fracture at 3.5% strain), while the greatest was found for technical grade $PCBM_{[70]}$ (11.5% strain) (see Figure 8). The same authors proposed in another article a rational way of designing molecularly stretchable electronics, in order to ideally allow a chemist to synthesize a material that could exhibit both the mechanical and electronic properties required for a particular application [77]. The idea was to design materials that allowed for the best compromise of compliance and charge mobility. For example, poly(3-heptylthiophene) (P3HpT) which combines low-T_g amorphous domains, but well-ordered crystalline domains, reports to be the most efficient and most elastic material considered in the study.

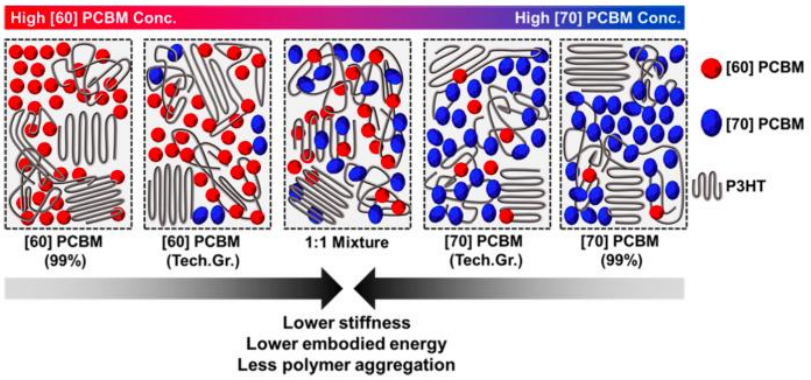

Figure 8 Schematic summary of the effect of mixed grades of methanofullerenes on the mechanical properties of P3HT:methanofullerene blends. Reported with permission from Chemistry of Materials [76].

Bruner *et al.* studied the effect of the molecular weight (M_w) of P3HT on the temperature dependent decohesion behavior of the BHJ of P3HT:PCBM in inert atmosphere [78]. The authors discovered that the de-cohesion readily occurs within the BHJ layer at loads well below the fracture resistance. It was also observed that in the P3HT with higher M_w, the decohesion threshold became higher, indicating that larger domains of entangled and bridged P3HT limited the crack propagation. Dupont *et al.* studied normal and inverted structure devices and found that the interface P3HT:PCBM/PEDOT:PSS (where PEDOT:PSS stands for poly(3,4-ethylenedioxythiophene)-poly(styrenesulfonate)) is the weakest in inverted structures with the configuration: Ag/PEDOT:PSS/P3HT:PCBM/ZnOx/ITO (where ITO is indium tin oxide), while in the case of a normal geometry device with configuration: Al/Ca/P3HT:PCBM/PEDOT:PSS/ITO, the fracture occurred within the bulk of P3HT:PCBM [79]. This was explained by the formation of a strong $P3HT^+$:PSS^- interface for the normal device due to P3HT-rich regions gradually diffusing towards the PEDOT:PSS interface. This effect is reduced in inverted structure due to the different device configuration. For the inverted geometry, several techniques were proposed for improving the mechanical properties: 1) surface activation of the underlying layer by means of O_2 plasma treatment with the addition of a few percent of CF_4 could provide extra reactivity to the surface. 2) solvation could soften the surface of the polymer layer and therefore increase the degree of intermixing between the two polymer layers. 3) Microgels, such as poly(allylamine hydrochloride) and dextran (PAH-D), could be used as an adhesive interlayer [79].

4 Intermediate layers

The layers that are typically placed between the active absorbing layer and the electrodes are often referred to as intermediate or buffer layers or depending on whether they are positioned adjacent

to cathode or anode they are called electron or hole transport layers respectively. The main functions of the intermediate layers in terms of electric properties are better aligning the work functions of the electrodes with the energy levels of active mixture and selectively conducting either the positive or negative carriers through the layer while blocking the opposite carriers. Such properties help to drastically reduce the recombination mechanisms in the carrier transport and improve device efficiency. In terms of processing, the intermediate layers can both smooth out the rough surface of the front electrode and protect the active layer from the direct deposition of the back electrode, since both often result in shunts. Intermediate layers play a crucial role also in terms of device lifetime and depending on the type of materials can significantly improve or deteriorate device stability. This section discusses the recent discoveries associated with the intermediate layers and their impact on the device stability.

4.1 Hole transport layer

Hole transport layer (HTL) is the buffer layer between the anode and active layer and has the role of transporting the positive carriers and blocking the negative carriers. The most commonly reported HTL is poly(3,4-ethylenedioxythiophene) polystyrene sulfonate (PEDOT:PSS). The effect of PEDOT:PSS on stability of devices has been debated for several years already and it remains unclear to which extent PEDOT:PSS limits the device stability. The hygroscopic nature of aqueous solution of PEDOT:PSS results in a rapid uptake of water, which leads to loss of conductivity of the HTL itself [80] and corrosion of other materials in the device [81]. In particular, if the PEDOT:PSS layer is used in combination with transparent electrode indium tin oxide (ITO), the acidic PSS starts etching the ITO [82–84]. UV light sensitivity of PEDOT:PSS has also been claimed to result in conductivity loss of the material [85]. Nevertheless, there have also been instances where PEDOT:PSS was shown not to have an effect on device stability [86] or even to slow down the ageing compared to other HTLs [87,88]. The recent study addressed this controversy by analyzing a large number of articles with lifetime data reported in literature and constructing comparative plots of the lifetimes for samples with and without PEDOT:PSS [16]. In this study the lifetime and initial *PCE* values were determined from the reported ageing curves and collected in one plot. In Figure 9 the upper plots represent the so called o-diagram, which depicts the initial performance (Y-axes) of the sample against the lifetime (X-axes) and the time is expressed in logarithmic scale with base 4, which allows associating the time blocks with the common time units. The detailed description of o-diagram can be found in section 7.2.3. The lower plots show the distributions of the corresponding numbers of data per time blocks. The study demonstrated that indeed most of the reported PEDOT:PSS based unencapsulated devices

(blue squares) show inferior stability compared to PEDOT:PSS free devices (green circles), when tested in dark or under light exposure. The only exception was PEDOT:PSS used in combination with Ag electrode in inverted structure tested in the dark (red triangles), where the shelf-life of these samples was similar to PEDOT-free samples. The results indicated that PEDOT:PSS based devices with normal structure are particularly susceptible to ageing in the dark, which is possibly due to the direct contact of PEDOT:PSS and ITO and the presence of Al electrode, which is sensitive to humidity. The fact that inverted devices with PEDOT:PSS show comparable stability only in dark conditions, but degrade rapidly under light, confirms that PEDOT:PSS is sensitive to light exposure. In the same study, the encapsulated samples (not shown in the plots) revealed similar lifetimes independent of the presence of PEDOT:PSS and ageing conditions, which suggests that the encapsulation sufficiently protected the samples from humidity, minimizing the effect of the device structural differences on stability.

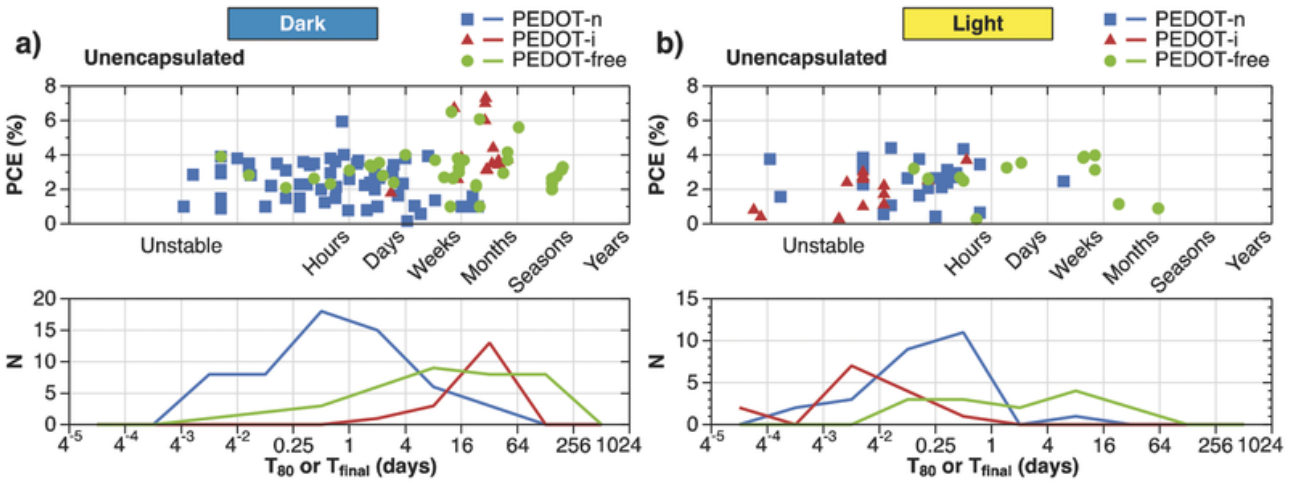

Figure 9 Distribution of lifetimes for unencapsulated samples grouped into three categories: samples with PEDOT:PSS between anode and the PAL in the normal architecture (blue squares), between the PAL and anode in the inverted architecture (red triangles) and PEDOT:PSS free samples (green circles). Plots are grouped according to dark (a) and illumination (b) tests. Each data point corresponds to one aged sample reported in the literature. The upper plots show the initial performance against lifetime (the scale is expressed in logarithmic scale with base 4 and is associated with common time units). The bottom plots show the distribution of the data in a histogram format, where the y-axis represents the number of the reported data points. Reprinted with permission from [16].

An additional proof of this is the recent study by Kumar *et al.*, where the authors compared stability of normal devices with PEDOT:PSS or MoOx under different environmental conditions and showed that while some differences were observed for unencapsulated samples under different conditions, these were diminished, when the samples were encapsulated [89]. Unfortunately, the tests were interrupted after 400 hours and therefore, for the encapsulated samples the rates of ageing in the

stabilized phases were not possible to determine, making it difficult to understand if a difference would eventually appear during longer period of tests. At this point it is important to stress therefore that conducting the ageing for sufficiently long period is vital for extracting reliable data. For example, as Voroshazi *et al.* suggested longer term tests may reveal secondary effects that shorter term studies do not uncover [88]. In their long term shelf-life studies the authors demonstrate, that the inverted structures, where PEDOT:PSS or MoOx was used in combination with Ag electrode, showed similar ageing in the first 1000 hours of storage, but significantly faster ageing was recorded for MoOx devices at a later stage (see Figure 10). The results corroborate well with the Figure 9 data and statement that in inverted structures PEDOT:PSS does not impose limitation on device shelf-life at least on a scale of a few years.

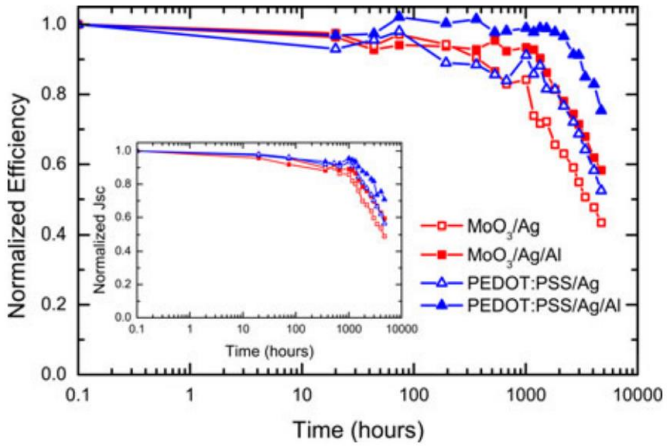

Figure 10 Normalized device efficiency as a function of air exposure time for inverted unencapsulated cells with various HTL/anode combinations. The values are averages over 12 cells. Inset: Normalized J_{SC} as a function of air exposure time for the same devices. Reprinted with permission from [88].

The study recently published by Glen *et al.*, showed instead the superior performance of MoOx devices compared to PEDOT:PSS in normal structure devices tested in dark, demonstrating that in normal structures PEDOT:PSS is rather problematic, which again well corroborates with Figure 9 and statement that PEDOT:PSS is problematic in normal structures [90].

In a different study Bovill *et al.* conducted comparative light exposure studies of normal structure devices utilizing three different HTLs, such as PEDOT:PSS, MoOx and V_2O_5 and PCDTBT as active material [87]. The study revealed a superior stability performance of PEDOT:PSS based devices compared to the other two and the reason was claimed to be the fact that PCDTBT is less sensitive towards humidity and therefore the hygroscopic nature of PEDOT:PSS did not do much harm to the device. However, the studied samples were encapsulated in glass and obviously the water content inside the device was already limited in the first place and it is highly likely that this was the reason

that the hydrophilicity of PEDOT:PSS was not problematic for this short term (600 hours) study. Greenbank *et al.* conducted thermal stress tests of inverted structure devices in the dark to explore the stability properties of PEDOT:PSS, MoOx and WOx as HTLs and in combination with Al or Ag.[91] The experiments were conducted in a glove box (N_2 atmosphere) in dark at 85^{o}C temperature, although were wrongly referred to as ISOS-D-2 tests according to common ISOS test guidelines (the latter mainly assumes tests in the air, as will be discussed in section 7.2.1 and tests in inert atmosphere do not qualify as ISOS tests). One of the important revelations was that when PEDOT:PSS was paired with Al, the device showed very fast ageing compared to the one paired with Ag, which suggests that the combination of PEDOT:PSS and Al is rather harmful for device stability. For samples with Ag electrode PEDOT:PSS showed slightly slower ageing rate compared to the two metal oxides.

Alteration of the composition of PEDOT:PSS for improving the device stability is another approach that has recently been addressed in literature a number of times. As an example Savva *et al.* studied different compositions of PEDOT:PSS, where after comparative studies it was shown that the PEDOT:PSS PH derivative treated with Zonyl:Dynol produced the most stable interfaces and thus, led to the most stable devices[92]. S. J. Lee *et al.* mixed PEDOT:PSS with MoOx, and succeeded demonstrating reduced water transmission rate and therefore improved stability of devices stored in dark, although the measurements were again not sufficiently long and lacked sufficient data to make certain conclusions[93]. A different way of PEDOT modification was proposed by J. J. Lee *et al.* that constituted condensation reaction of the PEDOT:PSS with poly(ethylene glycol) methyl ester (PEGME) (Figure 11) [94]. This resulted in significantly slowed uptake of water by PEDOT:PSS and reduced the In diffusion from ITO into PEDOT:PSS, which enhanced the stability of the resulting PSCs shown by an increase of the half-life by up to 3.5 times for the device consisting of a 1:1 weight ratio of PSS-PEGME in comparison to a pristine layer.

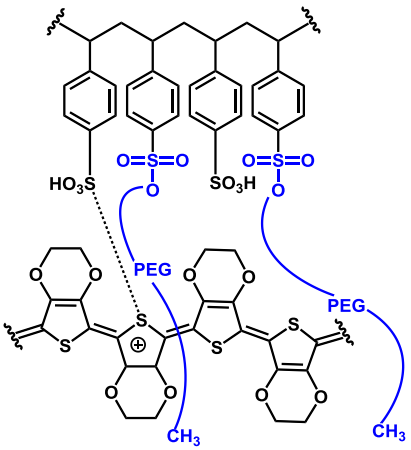

Figure 11 Schematic description of the PEDOT:PSS-g-PEGME graft copolymer. Reprinted with permission from [94].

Doping of PEDOT:PSS with amphiphilic perfluorosulfonic copolymer (Nafion) was proposed as an alternative method for improving the performance and stability. The highly hydrophilic $–SO_3H$ groups of the Nafion interacts with the PSS, while the highly hydrophobic fluorocarbon backbone prefers interaction with PEDOT. The consequence is the enhanced conductivity and increased surface roughness of the doped layer. The stable Nafion skeleton stabilizes the PEDOT:PSS film, due to its excellent thermal and mechanical stability. The compensation of the decohesion of the PEDOT:PSS layer leads to an improved efficiency and long-term stability of the PSCs as was shown for encapsulated samples during dark storage (Figure 12) [95].

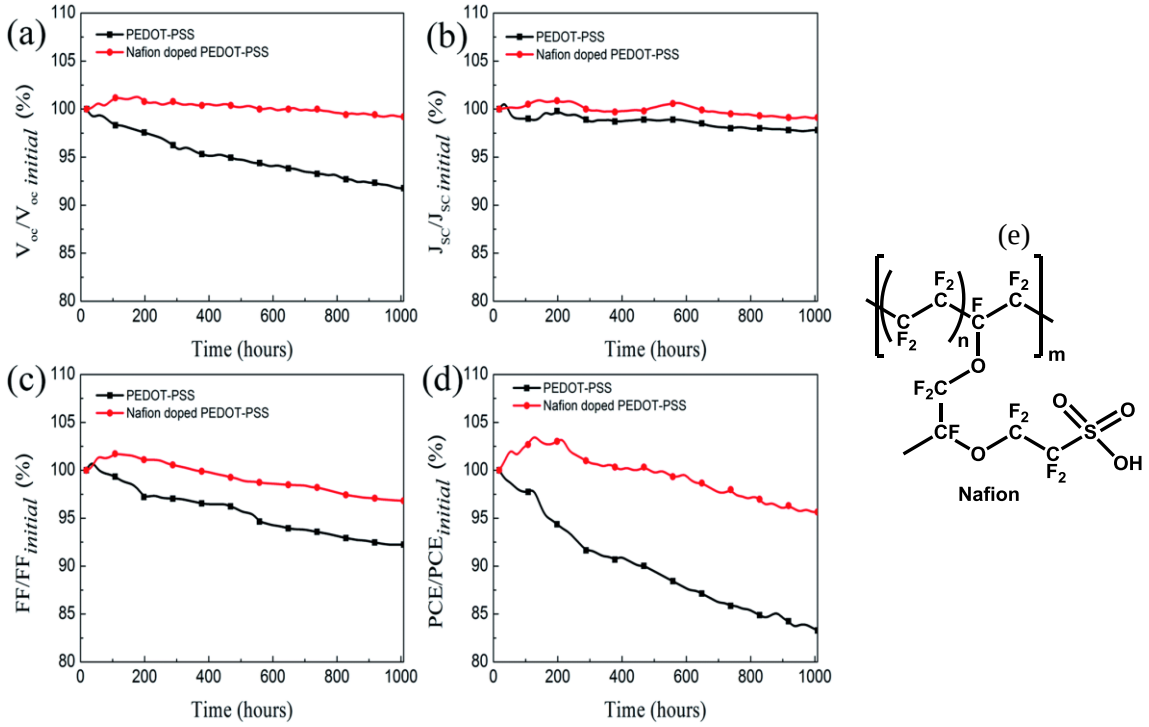

Figure 12 Lifetime V_{OC} (a), J_{SC} (b), *FF* (c) and *PCE* (d) of encapsulated devices based on PEDOT:PSS or Nafion (e) doped PEDOT:PSS (1:2). The devices where stored in dark under ambient conditions. Reprinted with permission from [95].

Some alternative HTL concepts have also been reported recently, such as for example Yuan *et al.* suggested using bismuth selenide (L-Bi2Se3) as HTL.[96] Although the superiority of the novel HTL over well-known MoOx in terms of *PCE* was only minor and in terms of stability there was no sufficient data to reliably determine the ageing rate difference, it may be worth investigating L-Bi2Se3 further to reveal the true potential of the material. Another method was proposed by Kim *et al.*, where microwave-reduced graphene oxide was utilized as HTL and when compared to PEDOT:PSS a major improvement in stability in dark was demonstrated [97]. Unfortunately, no information was provided for the performance of the devices under light in order to truly estimate the potential of this approach.

Shi *et al.* [98] modified P3HT with triethylene glycol (TEG) to receive the conjugated diblock copolymer poly(3-hexylthiophene)-b-poly(3-triethylene glycol thiophene) (P3HT-b-P3TEGT) (Figure 13a). The incorporation of this copolymer into the PAL forms a self-assembled anode buffer layer through spontaneous migration towards the PAL surface. Upon chelation of the lithium ions of the TEG side chains, the buffer layer can form an interfacial modification and ohmic contact between the Ag electrode and the PAL, through a reduction of the contact resistance and an increase of the electrical conduction. The lifetime of PSCs containing PEDOT:PSS as HTL (ITO/ZnOx/P3HT:PCBM/PEDOT:PSS/Ag) in comparison to PSCs containing P3HT-b-P3TEGT and P3HT-b-P3TEGT:Li^+, respectively, as an anode buffer layer (ITO/ZnOx/P3HT:PCBM:P3HT-b-P3TEGT(:Li^+)/Ag) was investigated by the group (Figure 13b), showing an enhancement of the unencapsulated device stability in air. The formation of a anode interfacial layer led to preferred BHJ morphology with improved transport of holes and electrons to anode and cathode, respectively [98].

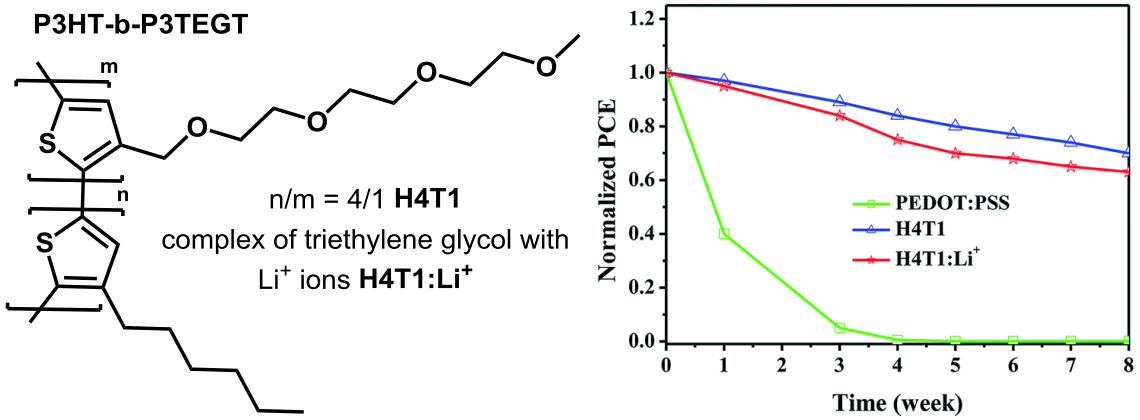

(a) (b)

Figure 13 Chemical structure of P3HT-b-P3TEGT (a) and its influence on the lifetime of a PSC (b). The unencapsulated PSC devices were stored in air under ambient conditions. Reprinted with permission from [98].

4.2 Electron transport layer

Electron transport layer (ETL) is the intermediate layer adjacent to the cathode and has the role of transporting electrons and blocking the holes. Similar to HTL, ETL can have a major impact on the stability of the device and many reports have addressed this earlier [11,13]. This section will primarily focus on recent developments related to ETL stability.

The most commonly used ETL for OPVs is ZnOx. The easy processing and good electron transport properties make ZnOx as one of the best candidates for inverted structure solar cells. MacLeod *et al.* investigated the effect of ZnOx processed from different precursors on the stability of devices [99]. In particular, ZnOx processed from diethylzinc (deZn) precursor appeared to be more

stable than the one processed from zinc acetate (ZnAc). Moreover, the modification of both types with dipolar phosphonic acid (PA), which is known to change the work function, resulted in the alteration of both *PCE* and stability behavior. Although PA treatment resulted in improvement of stability for ZnAc based devices and somewhat stronger burn in for deZn based devices, the overall ageing rate of the stabilized phase of the curves appeared to improve for both types of devices when the samples were exposed to light in air while maintaining low temperature via active cooling (see Figure 14). Nevertheless, the measurements were interrupted before clear patterns of stabilized ageing rates could be identified and therefore, firm conclusions cannot be made at this point.

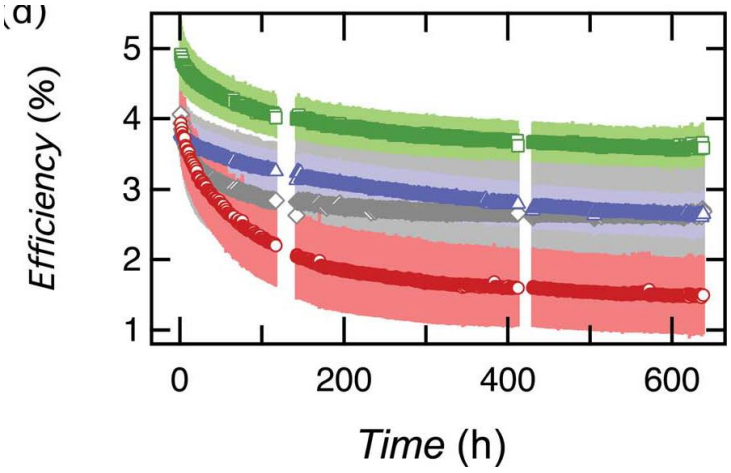

Figure 14 PCE ageing of unencapsulated devices with ZnAc (red circles), deZn (blue triangles), PA-modified ZnAc (green squares), and PA-modified deZn (gray diamonds) electrodes. The samples were exposed to sulphur plasma lamp with intensity close to 0.8 sun. Sample temperature was kept close to 25 °C via active cooling. Tests were conducted in air. Bars indicated ± one standard deviation of the mean. Reprinted with permission from [99].

Doping of ZnOx with aluminum has been reported to improve the conductivity of the film increasing device *PCE* [100]. Chen *et al.* investigated the stability of inverted structure devices utilizing aluminum doped ZnOx and demonstrated that the samples could retain up to 86% of initial performance after 900 hours of dark storage in air [101]. Unfortunately, there was no direct comparison with non-doped ZnOx presented in the study and therefore, it was unclear whether the doping improved the stability. Meanwhile Kam *et al.* thermally deposited a thin layer of Al on top of ZnOx layer and showed that this eliminated the rapid drop of open circuit voltage (burn in) observed in the standard devices during exposure to UV light. Based on the UV and UV-free exposure tests and ultraviolet photoelectron spectroscopy (UPS) analyses authors concluded that the reason of V_{OC} drop was the reduction of the barrier height of the films and as a consequence, the hole blocking properties, which was compensated by insertion of thin aluminum layer [102]. Bai *et al.* instead

suggested to apply ethanedithiol (EDT) treatment to passivate the surface of the solution processed ZnOx film, which led to increased *PCE* and somewhat increased stability [103].

Additionally, there have been a number of attempts to substitute ZnOx with novel materials. In particular, George *et al.* presented a number of polymer based intermediate layers, which were utilized in inverted devices as ETLs, and although no gain was achieved in terms of *PCE*, the devices with novel ETLs showed as good stability as titanium oxide (TiOx) based devices and offered novel easy processable materials for ETL [104]. As another alternative of ETL Weerasinghe *et al.* recently reported roll-to-roll coated and printed OPV modules with polyethylenimine–ethoxylate (PEIE) utilized as ETL [105]. Authors claimed that the novel ETL increased the module *PCE* by 20% compared to traditional ZnOx ETL, although no comparative data was presented. Authors additionally claimed that PEIE did not impair device stability and robustness, although again comparative data with other materials was not provided. The important advantage of PEIE was that it could be obtained by simple dilution and did not require steps, such as sol-gel synthesis. In another study Raïssi *et al.* employed copper phthalocyanine-3,4´,4´´,4´´´ tetra-sulfonated acid tetrasodium salt (TS-CuPc) as ETL in an inverted OPV device with active layer of P3HT:PCBM and combination of MoOx/Ag acting as anode [106]. Solution processed TS-CuPc led to stable (unencapsulated) devices showing no degradation after 140 days of storage in air in dark (Figure 15).

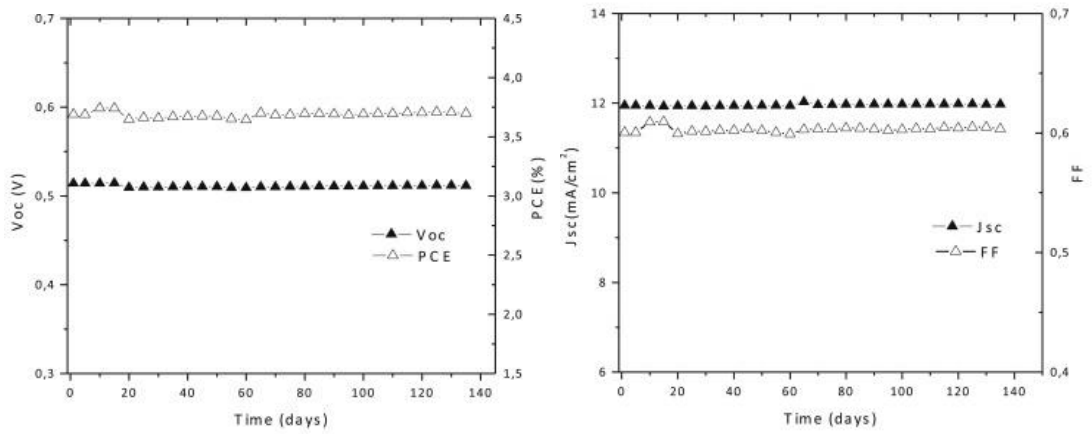

Figure 15 Studies of all parameters of ITO/TS-CuPc/P3HT-PCBM/MoO3/Ag devices over the time stored in air without encapsulation. Reprinted with permission from [106].

Wang *et al.* compared a range of different ETL materials in a traditional normal structure OPV configuration based on P3HT:PCBM active layer [107]. In particular, lithium fluoride (LiF), sodium chloride (NaCl), NaCl/Mg combination, tris-(8-hydroxy-quinoline) aluminum (Alq3), bathocuproine (BCP) and 1,3,5-tris (2-N-phenylbenzimidazolyl) benzene (TPBI) were tested in encapsulated devices stored in dark in inert atmosphere for 350 hours. Except for LiF, NaCl and NaCl/Mg the

samples of the remaining three ETLs rapidly degraded demonstrating that the ETL can indeed have a drastic effect on intrinsic stability of OPVs. Chen *et al.* [108] synthesized a fluorine-based organic small molecule electrolyte (SME) with different conjugated backbones (Scheme 3) and used it to substitute ZnOx. An enhanced efficiency (26% improvement) in comparison to ZnOx could be achieved. The authors additionally claimed that the stability of the device can be improved by SMEs as buffer layer, although, no comparative data was presented to prove that [108].

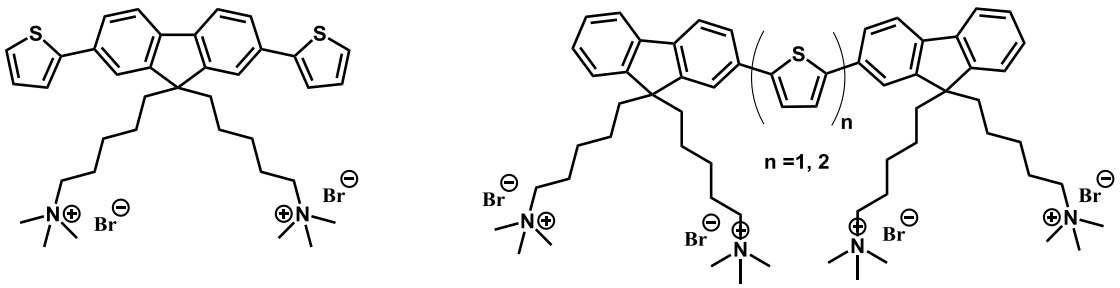

Scheme 3 Fluorine based small molecule electrolyte as cathode interfacial layer in PSCs.

5 Electrodes

5.1 Non-transparent electrode

The most commonly used non-transparent electrodes are aluminum (Al) for normal structure and silver (Ag) or gold (Au) for inverted structures. Al is very reactive towards water and in the previous section examples were already discussed showing that the combination of hydrophilic PEDOT:PSS and Al is detrimental for the devices tested in an environment with presence of humidity, while Ag based devices remained stable in the same environment [90,91]. Han *et al.* found that replacing the Al electrode (100 nm) in a normal geometry organic solar cells with an Al/Cu bilayer (25 nm Al and 80 nm Cu) drastically improves the devices lifetime when tested under highly damp conditions (90 % R.H. and 27 °C), making it comparable to the inverted OSCs. They attributed this to lower water vapor transmission rate (WVTR) of the Al/Cu bilayer compared to single Al layer [6]. Glen *et al.* studied the dependence of device stability on the grain size of Al top electrode and revealed that the electrodes with larger grain sizes showed slightly better stability compared to smaller grain sizes [109]. In the case of PEDOT:PSS free devices Yeom *et al.* compared the stability of devices with Al, Ag or Au as back electrode during storage in dark without any external protection [110]. The samples were based on PTB7:$PCBM_{[70]}$ blend with ZnOx and MoOx as intermediate layers. Al based devices showed much faster ageing confirming that even without PEDOT:PSS Al still acts as a bottleneck in an environment with the presence of humidity.

A different study by Voroshazi *et al.* showed that the combination of MoOx/Ag/Al multilayer electrode can also be a source of instabilities. In particular the advanced characterization showed that during light exposure due to heating Al tends to migrate through Ag and possible react with MoOx by creating an oxide layer at the interface. Due to such interfacial alterations the reflection of the light inside the devices is changed resulting in up to 20% drop in short circuit current [111]. An example of multilayer protective top electrode layer was presented also by Romero-Gomez *et al.*, who used MgF_2/MoOx as the top electrode [112]. The use of this layer resulted in manifold improvement of device stability, when tested in dark.

5.2 Transparent electrodes

The most commonly used transparent electrode in OPVs is ITO due to its good conductivity and high transparency. However, ITO is well known to be brittle and although flexible ITO substrates have been demonstrated, these typically tend to brake and rapidly lose conductivity upon multiple bending [113]. Additionally ITO is expensive to process and therefore, solar cells produced with ITO will inevitably have higher energy payback time (EPBT) [114,115]. ITO is also harmful to the device stability and this is particularly evident when it is used in combination with PEDOT:PSS [116], as was also discussed earlier in this review. One of the recent studies by Kettle *et al.* confirm the migration of indium (In) and tin (Sn) through the entire device, which is a result of the etching of ITO by PEDOT:PSS [56]. Therefore, the research in recent years has been largely focusing on replacing ITO with alternative electrodes.

Replacement of ITO with aluminum doped zinc oxide (AZO) was proposed by Chen *et al.*, an approach that was already discussed in the section describing the electron transport layers. In particular, the use of AZO combined with 1 nm Ca as transparent cathode in inverted structure devices was proven to provide comparable *PCE* with a reference ITO based device and slightly increased air stability in dark [117]. Wang *et al.* used the multi-structure ZnOx/AgOx/ZnOx (ZAOZ) as a transparent conductive electrode (TCE) [118]. Such an electrode deposited on PET provided an average transmittance of 91 %, and a sheet resistance of 20 Ω sq^{-1}. The device with configuration TCE/PTB7-F20:$PCBM_{[70]}$/PEDOT:PSS/Ag showed only 10 % drop in *PCE* after bending radius of 1 mm, whereas ITO device *PCE* dropped by approximately 60 %. Another sandwiched electrode consisting of nickel oxide (NiO)/Ag/NiO (known as NAN) having high transmittance of ~82% combined with a low sheet resistance of 7.6 $\Omega \cdot sq^{-1}$ was proposed by Xue *et al.* [119]. This electrode also improved the flexibility of the devices and was show to preserve carrier transport properties and

carrier density after storage at elevated temperature and humidity conditions for 1 day or prolonged 1 year shelf life, as can be seen in Figure 16.

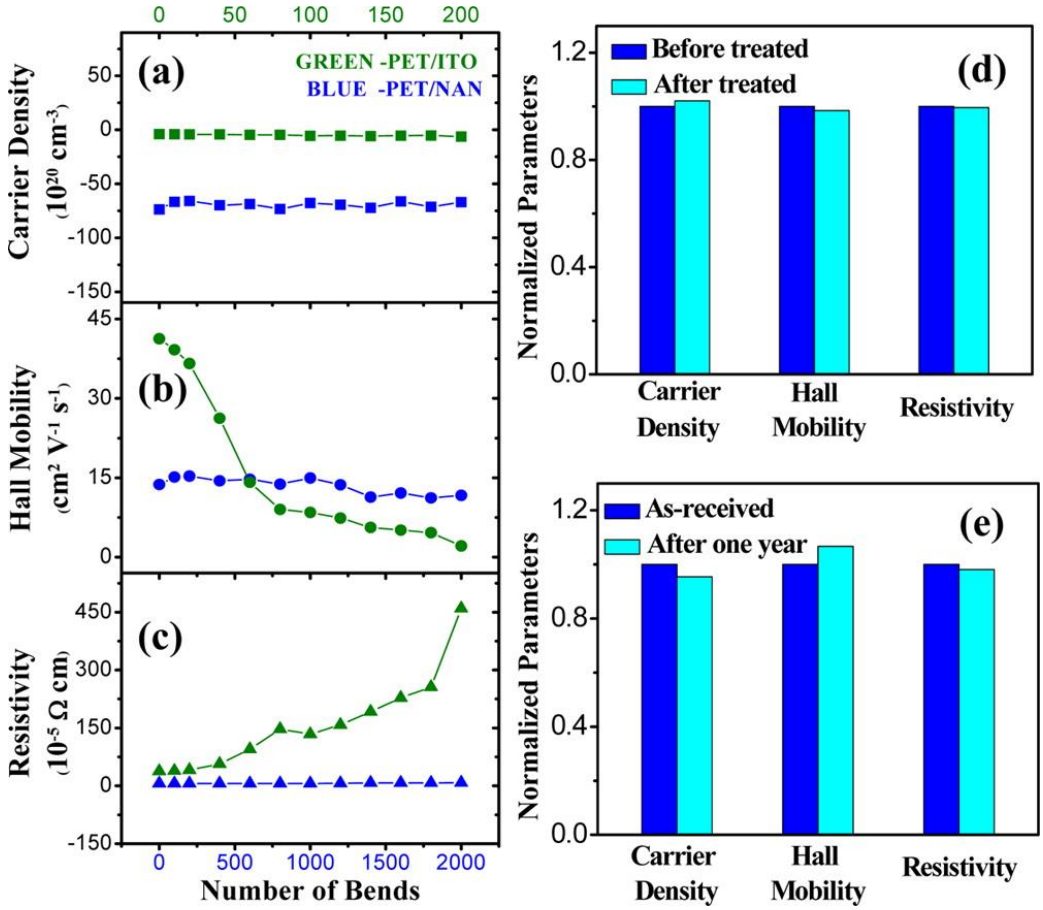

Figure 16 (a) Carrier density, (b) Hall mobility, and (c) resistivity of the PET/ITO and PET/NAN flexible electrodes after repeated bending. The green curves are for the PET/ITO (top x axis) electrode, and the blue curves are for the PET/NAN (bottom x axis) electrode. The bending angle was about 90°. (d) Carrier density, Hall mobility, and resistivity before and after the NAN electrode was stored at a constant temperature of 60 °C and relative humidity of 90% for 24 h. (e) Normalized changes in carrier density, Hall mobility, and resistivity of the NAN electrode before and after it was preserved in air for 1 year. Reprinted with permission from [119].

The replacement of ITO with highly conductive PEDOT:PSS or a combination of PEDOT:PSS and for example Ag grid has been widely utilized already for a number of years. Here we propose the recent advances related to these configurations. Fan *et al.* replaced ITO with PEDOT:PSS, which was treated with methanol and methanesulfonic acid (MSA) in order to improve its conductivity up to 3560 S cm^{-1} [120]. With such a layer normal structure organic solar cell Ca / Al / P3HT:PCBM / PEDOT:PSS (buffer) / PEDOT:PSS (electrode) / PET achieved *PCE* of 3.92 % (compared to 4.30 % for the standard ITO electrode). Using PEDOT:PSS instead of ITO guaranteed a good mechanical flexibility, with more than 80 % of the initial *PCE* maintained after 100 time bending with a bending radius of 14 mm in ambient atmosphere. Skorenko *et al.* [121] and Li *et al.* [122] independently

studied PEDOT produced via vapor phase polymerization (VPP) as an alternative for ITO replacement. The high electric conductivity and high resistance towards mechanical stress (bending and stretching) was shown for VPP-PEDOT. Li *et al.* in particular combined VPP-PEDOT with Ag grid to produce devices and showed significantly improved device stability for the sample based on the alternative electrode in comparison to the traditional Ag grid/PEDOT:PSS(PH1000) electrode configuration [122].

Silver nanowires (AgNW) have been extensively used as an ITO replacement and a range of recent publications discuss the clear advantage in mechanical flexibility of the samples with AgNW [123–129]. Nevertheless, in most cases the device stability in terms of air exposure does not show any improvement. Only when Lee *et al.* studied the hybrid combination of AgNW and graphene, where the transparent electrode was developed by dry-transferring a CVD-grown monolayer graphene onto an AgNW, the authors succeeded in showing a slight improvement in stability of devices with the hybrid configuration compared to single AgNW [130]. Ag nanomesh was fabricated on a flexible substrate by another group using nano-imprint lithography (NIL) [131]. The Ag nanomesh transparent conductive electrode exhibited high transmittance of >88% and low sheet resistance of 15 Ω sq^{-1}, as well as a good mechanical flexibility. The stability of the device Ag nanomesh/ZnOx/PTB7:$PCBM_{[70]}$/PEDOT:PSS/Ag stored in air under ambient conditions, was comparable to ITO based device.

6 Upscaling and packaging

So far, the majority of reported organic and polymer solar cells are typically fabricated on small glass sheets using spin coating methods and active cell sizes below 1 cm^2 [132]. Even though such cells can show record efficiencies beyond 10% [133–135], they are often measured under inert atmosphere and lack appropriate encapsulation or have glass lids attached using epoxy glue. Although, devices produced with such methods and architectures show the potential of the technology in terms of *PCE,* they are far from the envisioned commercial OPV products. For demonstrating the true potential of OPVs as a product it is vital to utilize and develop processing techniques that will enable large-scale cost efficient fabrication and architectures that will allow achieving long-term stability under real world conditions. The latter in particular has to be compatible with large-scale processing.

The ideal large-scale fabrication methods for polymer based organic solar cells are solution-based roll-to-roll (R2R) printing and coating methods such as flexo printing, inkjet printing, spray

coating, slot-die coating, gravure printing, screen printing, and eventually laser scribing [136,137]. These methods enable the fabrication of modules with sizes up to 100 m in length [138,139] and even modules with up to 14 layers in a tandem configuration [140]. Other studies deliver freely shaped solar cells [141] or devices with very high geometrical fill factor [142–145]. Small-molecule based organic solar cells can be manufactured on an industrial scale using R2R vacuum deposition tools and laser processing [146]. Most reports on upscaled organic solar cells however concentrate on the manufacture of devices, but neglect the importance of similar sized encapsulation procedures, which are important for making the solar cells stable against environmental impact. The post processing and integration into to the intended application is for a large majority completely neglected which is a testimony to rather unevolved technological level of OPV.

Rigid glass panels are the best known barriers where solar cells can be sandwiched in between two panels [147]. Solar cells need to be placed some centimeter away from the edges to avoid edge ingress and adhesives with low water vapor transmission rate (WVTR) and low intrinsic water levels need to be selected to improve lifetime. These large-area glass-glass encapsulations are typically used in building integrated photovoltaic (BIPV) products, such as glass facades [148]. The fabrication of 3rd generation photovoltaics directly on glass and additional glass encapsulation is a procedure commonly used for large area dye sensitized solar cells or in the future possibly for perovskite based technologies. The typical sealing method is based on heat fusing or laser assisted glass frit sealing [149–151]. The freedom in three-dimensional shape is limited and the natural flexibility of foil based solar cells is sacrificed. Although ultrathin flexible glass as a substrate and barrier is starting to gain attraction especially in the field of organic light emitting diodes (LEDs), the utilization for OPVs is currently limited [152].

The best flexible candidates for environmental protection are the foil-based barrier films ranging from food barriers to multilayer ultra-barrier films with WVTR reaching up to 10^{-6} g/m²/day. The barrier films are either commercially available from a variety of manufacturers (price is highly dependent on barrier performance) or manufactured in research laboratories using solution coating, vacuum deposition, sputtering, or atomic layer deposition (ALD) of metal oxides and polymer interlayers [153–156].

The rolls of flexible barrier films can easily be integrated in roll-to-roll and roll-to-batch production lines of OPVs and the solar cells can either be processed directly onto the barrier substrate [157] (in some cases with additional corona pretreatment) with subsequent encapsulation using an additional barrier film for the opposite side, or if the substrate does not possess barrier properties, then the complete device with substrate is sandwiched between two barrier foils. Various adhesive methods exist for making the barrier foil stick to the substrate [158] and many hundreds of meters

can be continuously laminated [138,139] or for architectural purposes processed in batches [142] in R2R process. The earliest R2R produced organic solar cells used *pressure sensitive adhesives* (PSA). PSAs are applied to the barrier foil as a separate step, and this barrier laminate (containing pressure sensitive glue on one side – similar to ordinary Scotch tape) is then laminated onto the substrate carrying the device [159,160]. Thus, PSA lamination requires several preprocessing steps to prepare the laminate and it produces waste in form of release-liner (coated paper or polymer film) in the same length as the barrier film. In contrast, *hotmelt* and *UV-curable* adhesives are directly applied onto the foil and used to attach the barrier film on the printed solar cells [158] (see Figure 17). In the case of hotmelt lamination, when the laminate is brought together with the substrate in a hot nip, the adhesive becomes momentarily liquid which allows contact between the substrate and barrier before the adhesive hardens upon cooling. For *UV curing* adhesive lamination UV curable adhesive is applied between the substrate and the barrier followed by exposure to UV-light in order to cure the adhesive. In both lamination processes the glues are fluid while entering the nip rollers and cooled or light activated after passing the nip. The fluid phase avoids the inclusion of tiny air bubbles that often occur with PSAs. Overall, according to Hösel *et al.* [158], the UV-curable adhesive leads to the highest stability of the three (UV > hotmelt > PSA sequence for better stability). The authors additionally conclude that the UV-adhesive makes a very efficient edge sealing. It should be noted here that UV-curable adhesive systems are typically based on epoxies or isocyanates, which can cause serious allergies and permanent skin damage in humans (see Figure 18).

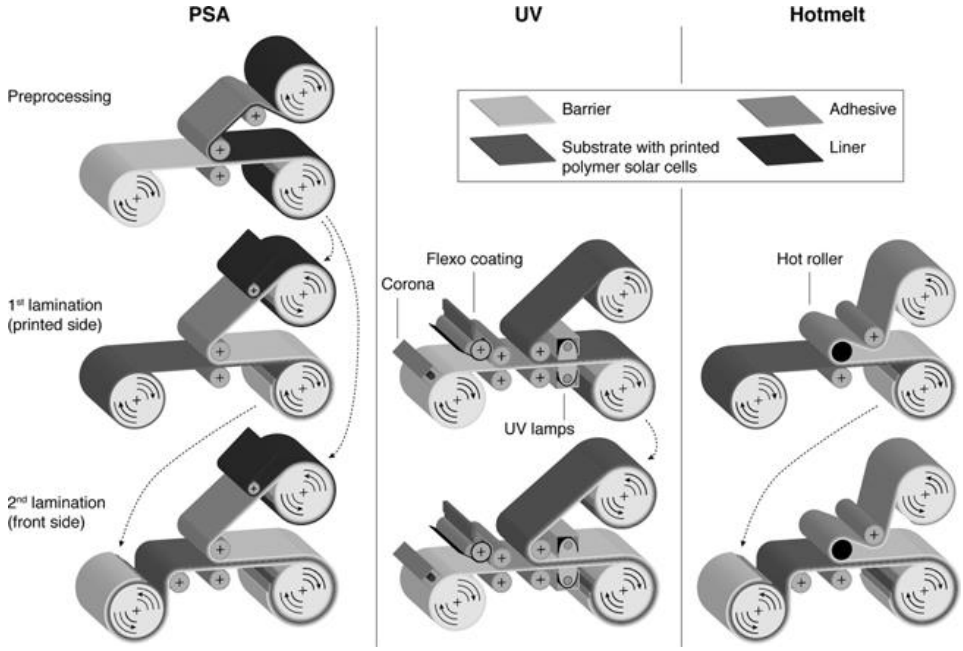

Figure 17 Process workflow for the R2R encapsulation of flexible OPV modules. Reproduced with permission from [158].

Figure 18. Permanent skin damage as a result of exposure to UV-curing epoxy resins. Great care must be excercised in the laboratory and when scaling up.

In another study, stability tests over more than 900 hours under illumination showed that single-sided lamination with UV-curable adhesive achieves better stability than double-side PSA lamination [161]. Long-term outdoor tests in Africa of double-side encapsulated large-area modules with hotmelt office lamination pouches proved the functionality of hotmelt as a glue, but failed due to the poor quality of the plastic film. Strong UV-radiation made the lamination pouch brittle and led to bleaching and delamination at the edges of the modules. This proves that barrier films need to be resistant against environmental impacts over the expected lifetime of the solar cells. More details can be found elsewhere on the descriptions of the different lamination process [162] and flexible barrier film preparation and properties [163].

Weerasinghe *et al.* recently showed that PSA barriers may contain significantly amounts of moisture after prolonged storage of the foil before device manufacturing and packaging of the device with such a barrier will significantly affected the device stability [164]. The authors showed that the stability of the encapsulated devices could be significantly increased by simply pre-outgassing the PSA barrier in a vacuum oven before encapsulation.

Edge sealing of continuously coated and cut solar cell modules was found to be highly important for the lifetime and stability of large-scale OPVs [105,165,166] and perovskite solar cells [167]. In particular, when Weerasinghe *et al.* described ‘hand lamination’ of small R2R processed solar cell modules either by PSA lamination or by hotmelt (Ethylene-vinyl acetate (EVA) adhesive) combined with barrier gasket applied along the perimeter of the OPV device, they showed an improved stability in both cases stressing the importance of the edge sealing [105,166]. It should be mentioned here that no reference studies were presented using only the hotmelt, so it is difficult to evaluate how much the increased stability can be ascribed to the introduction of the extra edge sealing gasket and how much can be ascribed to the EVA hotmelt adhesive. Nevertheless, water and oxygen ingress from the side

is a critical factor that has been addressed earlier and proved the necessity of large protective rims around OPVs [168]. Additionally, the electrical terminals of the modules can be the first direct entry point between the encapsulation layers for diffusions of the ambient agents. It has been shown in long term outdoor studies up to 10000 hours that water ingress through the contact points can lead to destructive degradation of parts of the solar cell next to the contacts [169], thus appropriate protections of the electrode is also an important necessity.

Other failures that have been shown in upscaled solar cells with flexible encapsulation are typically associated with delamination of the encapsulant, bubble formation, and bleaching from the edges, if not properly sealed [170,171]. Major destructive behavior was also observed in very large organic solar cell modules (100 m x 0.3 m) with high open circuit voltages of 10 kV, initiated possibly by pinholes, delamination, shunts, and water ingress [172]. The defective area formed hotspots that tend to form arcs and slowly melted the lamination foil until inflammation. The problems could be solved by cut-replace repair procedures that enabled modules with 150 W_{peak} after more than 4300 hours outdoors. The initial performance was well beyond 200 W_{peak} for one module under 1 sun illumination and after the initial burn in the module demonstrated around 400 days of lifetime calculated for the stabilized performance [16].

Meanwhile, a recent study by Nehm *et al.* on barrier properties of flexible PET substrates with an added Zinc-Tin-Oxide (ZTO) barrier showed and important link between device temperature and the performance of the barrier. In particular the authors showed that the water vapor transmission rate (WVTR) of the barrier not only has a linear relationship with humidity, but also linear logarithmic relationship with the reciprocal temperature (1/T) [173]. The study, which was based on calcium tests, also showed a clear dependency of whether the interface of Ca tester was with barrier film from the ZTO side or the PET side. Such dependence was ascribed to interface diffusion processes. This shows that barrier properties are not easily determined simply by a given WVTR, but that consideration of factors such as climate and device interfaces have to be taken into account.

7 Stability and lifetime characterization

An important element when aiming at improving OPV stability is the proper testing and characterization of the failure mechanisms, as well as correct stability rating of the photovoltaic performance. It is vital to be able to record and understand the mechanisms that cause the ageing of OPVs in order to protect the devices against these mechanisms. It is also important to be able to rate the stability of the samples in order to both enable easy comparison of the different device stabilities

produced by different laboratories and establish the progress of lifetime improvements. This chapter will first discuss the recent reports on various advanced characterization techniques that were utilized for characterization of failure mechanisms. This will then be followed by a discussion of the ISOS test guidelines that have commonly been used in the OPV field in the recent years. Recently proposed methods for identifying a generic marker of lifetime and comparing the lifetimes of various devices via a so called o-diagram are also discussed.

7.1 Advanced characterization of stability

Throughout the history, many different techniques have been employed for studying the stability, which range from simple IV-testing to advanced photo-electrical characterization, transient measurements and scanning microscopy. Such tools allow locating and recording specific ageing mechanisms and therefore, help eliminating these. This section outlines a number of advanced characterization techniques that have been employed recently for studying the device ageing.

Impedance spectroscopy has proven to be rather useful technique for studying the electric properties of individual layers and complete OPV devices. As an example Lin *et al.* has recently demonstrated the use of impedance spectroscopy for analyzing the stability behavior of individual layers in the traditional OPV device during the ageing process [174]. In particular using IV and IS measurements it was demonstrated that there is significant capacitance increase at the PEDOT:PSS/ITO interface, which indicated the increased amount of charge traps. This and the increased resistance at the PEDOT:PSS/active layer interface were claimed to be the main reasons for the initial rapid degradation (burn in) of the device. Guerrero *et al.* combined absorbance measurements, capacitance-voltage (c-v) and impedance spectroscopy in order to investigate the ageing mechanism of P3HT:PCBM based devices stored for one year in dark in glovebox [175]. Based on such optical and electrical characterizations the authors concluded that the main ageing mechanism was the development of localized charge transfer complexes ($P3HT^{\bullet+}$–$PCBM^{\bullet-}$), which not only reduced the photocurrent due to the reduction of the light absorption properties, but also reduced the voltage, since the formation of such complexes led to creation of electronic defect states, which affected the hole Fermi level resulting in decrease of V_{OC}. Karuthedath *et al.* used instead microsecond and femtosecond laser pulses to study the charge transients of P3HT:PCBM and Si-PCPDTBT:PCBM films and devices and determined that during the photoageing of the active mixtures the charge generation was intact, but the charge recombination was strongly reduced, which as a consequence reduced the charge mobility [176]. Table 2 below summarizes the list of other

recently reported advanced characterizations of ageing mechanisms including the ones discussed above. For other reported techniques the reader should refer to earlier published reviews [7,8]

Table 2 The list of various advanced characterization techniques reported in recent years and the short descriptions of the sample types and the ageing mechanisms discovered with the use of these techniques

Characterisation tools	Tested sample	Observations	Ref.
• Impedance spectroscopy	ITO/PEDOT:PSS (interface)	Increased amount of charge traps	[174]
	PEDOT:PSS / P3HT:PCBM (interface)	Increased resistance	
• Impedance spectroscopy	ITO / ZnOx / PTB7:$PCBM_{[70]}$ / MoOx / Ag (bulk and interfaces)	Charge accumulation at the electrodes	[177]
• Impedance spectroscopy • Absorbance measurement • Capacitance-voltage (C-V)	ITO / ZnOx / P3HT:PCBM / MoOx / Ag (bulk and interfaces)	Development of localized charge transfer complexes ($P3HT^{\bullet+}$–$PCBM^{\bullet-}$) as main ageing mechanism	[175]
• Transient measurements with femtosecond laser	P3HT:PCBM Si-PCPDTBT:PCBM (bulk)	Charge generation is intact during photo-oxidation, but charge recombination is strongly reduced indicating reduced charge mobility	[176]
• Atomic force microscopy AFM • X-ray photoelectron spectroscopy (XPS)	Si-PCPDTBT film surface	Rapid surface oxidation accompanied with loss of carbon and sulphur and swelling of the film, followed by gradual oxidation of the bulk and shrinking of the film. Oxidation of Si bridging atom is the first step in the photo-oxidation process of the film.	[178]
• UV–visible spectroscopy Infrared (IR) spectroscopy • Time-of-flight secondary ion mass spectrometry (TOF:SIMS)	Si-PCPDTBT film bulk		
• Damp-heat test • X-ray photoelectron spectroscopy • Scanning electron microscopy • Energy-dispersive X-ray analysis	ITO / ZnOx / Active Layer / PEDOT:PP / Ag	Migration of Ag atoms causing creation of shunts was observed. ZnOx etching by PEDOT:PSS was also suggested.	[179]
• Capacitance–temperature measurement • Confocal scanning microscopy	ITO / PEDOT:PSS / Active Layer / ZnOx / Ag	Threshold temperature T_{MAX}, at which the morphology becomes thermally unstable, is determined and allows determining thermal stability of materials and devices.	[180]
• Intensity-resolved EQE	Ag / PEDOT:PSS / P3HT:PCBM / LiF:Al	EQE shape dependence on light intensity reveals generation of traps in PCBM	[181]

7.2 Lifetime measurements and reporting

7.2.1 Before and after ISOS standards

One of the main milestones in the lifetime testing of organic photovoltaics was the establishment of ISOS guidelines, which were published in 2011 based on the consensus of the discussion and conclusions reached during the first 3 years of the International Summit on OPV Stability (ISOS) [182]. The guidelines offer directions on how to perform stability test of OPVs and similar technologies under different conditions, such as dark tests (shelf life), outdoor tests, indoor weathering and thermal cycling tests. Table 3 shows the short summary of the tests. One of the earlier interlaboratory studies demonstrated how different environmental conditions, such as relative humidity, temperature, light intensity or spectrum drastically affect the outcome of the stability test of an OPV device [183]. Therefore the purpose of the ISOS guidelines was to help the researchers in different laboratories to harmonize the testing procedures by choosing common testing conditions. To achieve this, the guidelines in particular recommend a number of important limitations, some of which were:

- Only light sources that resemble AM1.5G well must be used in indoor weathering tests. The light sources with poor performance in the UV range, such as classical sulphur plasma lamps or light emitting diodes with limited wavelength range do not qualify for ISOS tests.
- Specific sample temperatures or relative humidity of the environment must be used during certain indoor tests, as is specified in Table 3

Since, however the level of equipment of at different laboratories varies significantly, the guidelines addressed this by offering three levels of testing varying in complexity of the procedure and equipment requirements that can suit both advanced accredited test laboratories and research laboratories with limited equipment. Obviously, the higher level of tests is chosen the better accuracy in the tests can be achieved.

Table 3 Overview of different types of ISOS test protocols. Reproduced with permission from [182].

Three levels

Basic (Level 1)	"Hand held" measurements using the simplest equipment and few conditions
Intermediate (Level 2)	Fixed conditions and protocols suited for most labs
Advanced (Level 3)	Standardized tests applied in certified labs. Extended range of parameters to monitor, etc.

Test type	**Dark**			**Outdoor**		
Test ID	ISOS-D-1 Shelf	ISOS-D-2 High temp. storage	ISOS-D-3 Damp heat	ISOS-O-1 Outdoor	ISOS-O-2 Outdoor	ISOS-O-3 Outdoor
Light source	None	None	None	Sunlight	Sunlight	Sunlight
Temp.[a]	Ambient	65/85 °C	65/85 °C	Ambient	Ambient	Ambient
Relative humidity (R.H.)[a]	Ambient	Ambient (low)	85%	Ambient	Ambient	Ambient
Environment[a]	Ambient	Oven	Env. chamber	Outdoor	Outdoor	Outdoor
Characterization light source	Solar simulator or sunlight	Solar simulator	Solar simulator	Solar simulator	Sunlight	Sunlight and solar simulator
Load[b]	Open circuit	Open circuit	Open circuit	MPP or open circuit	MPP or open circuit	MPP

Test type	**Laboratory weathering testing**			**Thermal cycling**		
Test ID	ISOS-L-1 Laboratory weathering	ISOS-L-2 Laboratory weathering	ISOS-L-3 Laboratory weathering	ISOS-T-1 Thermal cycling	ISOS-T-2 Thermal cycling	ISOS- T-3 Thermal cycling
Light source	Simulator	Simulator	Simulator	None	None	None
Temp.[a]	Ambient	65/85 °C	65/85 °C	Between room temp. and 65/85 °C	Between room temp. and 65/85 °C	−40 to +85 °C
Relative humidity (R.H.)[a]	Ambient	Ambient	Near 50%	Ambient	Ambient	Near 55%
Environment/setup	Light only	Light & Temp.	Light, Temp. and R.H.	Hot plate/oven	Oven/env. chamb.	Env. chamb.
Characterization light source	Solar simulator	Solar simulator	Solar simulator	Solar simulator or sunlight	Solar simulator	Solar simulator
Load[b]	MPP or open circuit	MPP or open circuit	MPP	Open circuit	Open circuit	Open circuit

One of the recent studies demonstrated how following the ISOS guidelines can improve the reproducibility of the test results. In particular, identical samples were distributed among 7 laboratories in different countries and tests were conducted according to ISOS-D-2 (high temperature storage) and ISOS-D-3 (Damp heat) tests [184]. Figure 19 shows the good overlap among the curves of the samples tested at different laboratories. As a comparison, in the similar interlaboratory studies conducted before ISOS, where the laboratories did not follow common protocol the ageing rates of the dark tests varied by order of magnitude due to different temperature and humidity conditions used during the tests [183]. The recent analyses of literature related to OPV stability demonstrated how the publication of ISOS guidelines affected the reported lifetime data. In particular, all the reported stability data and test conditions were categorized according to if the conditions were compatible with ISOS guidelines or not. The compatibility was determined by if the test conditions sufficed the important ISOS criteria, such as device temperature, light source type etc. The reports were grouped into these published before year 2012 and from year 2012 (since ISOS guidelines were published right before 2012). Figure 20 shows the ratio of the number of compatible and non-compatible stability data reported before and from year 2012. From the plot it is clear that while the ISOS compatible data was around 40% before 2012, it reached 60% for articles published from year 2012. 25% of the articles published from year 2012 explicitly cite ISOS protocols. The majority of non-compatible data are the tests conducted in inert atmosphere or with light sources with poor UV component, although some publications erroneously regard these conditions as part of ISOS test guidelines. It is therefore important to clarify here that any ISOS testing procedure is intended for

tests in air and any tests in inert atmosphere cannot be qualified as ISOS protocols. Similarly, ISOS guidelines emphasize the importance of the use of light sources with appropriate UV component, since it is the UV part of the light that causes the main damage to the cell.

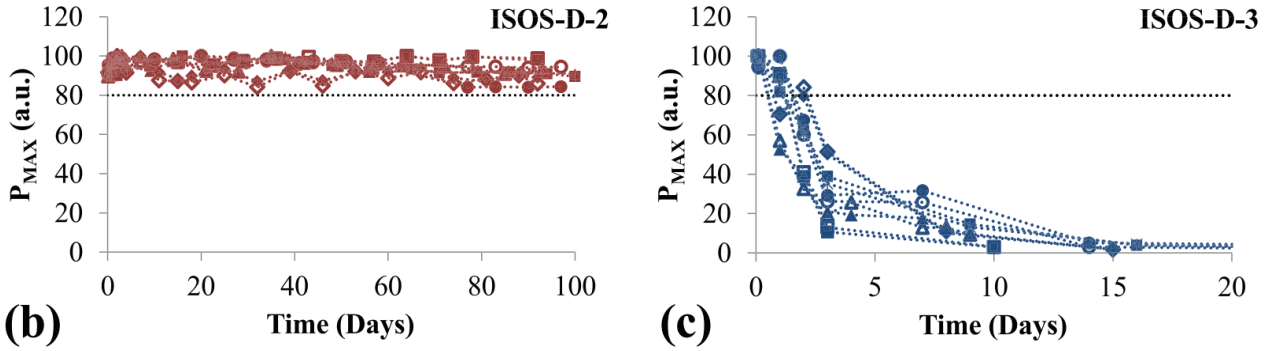

Figure 19 Testing of R2R manufactured and packaged flexible OPV modules under ISOS-D-2 (b) and ISOS-D-3 (c) test conditions in different laboratories. The plots represent the maximum power against the time. Reprinted with permission from [184].

It should be stressed that tests in inert atmosphere can merely be used for comparing two different samples in the same test conditions, but do not give a true insight into the device stability potential in real environment and cannot be utilized for comparative studies with other reports. Therefore the researchers are highly encouraged to refer instead to ISOS guidelines for evaluating the stability of their devices, if the purpose is eventually to truly assess the stability in real environment. It is also important to add that the low UV light or low intensity light soaking tests can be rather useful for imitating operation in indoor environments and unfortunately at this stage ISOS testing categories do not cover such tests. An extension of the ISOS guidelines in this direction would therefore be a useful effort and should be addressed by the ISOS community.

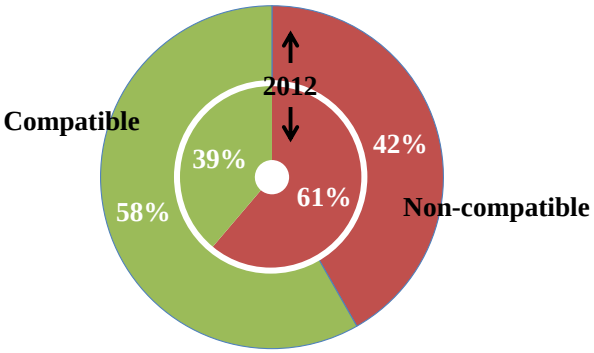

Figure 20 shows the percent of ISOS compatible (green) and non-compatible (red) stability data reported in literature published before (inner circle) and from (outer circle) year 2012.

Table 4 lists a number of recent publications that used ISOS guidelines to conduct lifetime measurements of OPV samples. The tests range from simple shelf life to sophisticated thermal cycling tests.

Table 4 presents the list of ISOS protocols used in the recent publications. The table provides also the types of the test samples and the observations made during the studies.

Test condition	Tested sample	Observations	Ref.
• ISOS-O-1	Ag-grid/ PEDOT:PSS / ZnOx / P3HT:PCBM / PEDOT:PSS / Ag-grid packaged in PET/SiOX barrier material	OPV was compared to Si performance in outdoor conditions for 4 months. At reduced light intensities OPV performance was reduced due to the lack of light doping. Positive temperature coefficient was identified for OPVs	[171]
• ISOS-D-1 • ISOS-O-1 • ISOS-L-1	ITO / PEDOT:PSS or MoOx / P3HT:ICBA / Ca / Al	MoOx based samples outperform PEDOT:PSS samples in dark and outdoor conditions, but similar *PCE* ageing is recorded for indoor light soaking tests (see section 4.1).	[89]
• ISOS-O-2 • ISOS-L-2	8 different device structures	Unprotected terminals of the devices were the main bottlenecks for stability	[185]
• ISOS-D-2 • ISOS-O-3	Ag-grid/ PEDOT:PSS / ZnOx / P3HT:PCBM / PEDOT:PSS / Ag-grid packaged in PET/SiOX barrier material	Demonstration of 2 years stability	[186]
• ISOS-T-3	ITO / ZnOx / P3HT:PCBM / PEDOT:PSS / Ag	Thermal cycling of 200 times does not affect device performance. Adhesion between active layer and PEDOT:PSS is strengthened due to the elevated temperature of the test	[187]

7.2.2 Lifetime marker

Operational lifetime in the PV field is commonly referred to the time when the sample degrades by 20 % from initial performance, marked as T_{80}. However, due to varying shapes of ageing curves for OPV devices, such a simple definition may not be sufficient for truly representing the device stability. Therefore, apart from the guidelines for conducting lifetime tests the ISOS protocols also suggested the method for reporting the lifetime [182]. Figure 21 depicts a typical ageing curve of an OPV and presents the parameters that describe the lifetime. In particular, ISOS suggests using two lifetime values to describe the ageing:

- T_{80} which is the time when the sample degrades by 20 % from the initial value E_0 (E is the parameter describing the sample performance, such as for example *PCE*)
- T_{S80} which is the time when the sample degrades by 20 % from arbitrarily defined E_S second starting value defined by the user and is calculated from the corresponding second starting time value T_S

E_S, T_S typically describe the point where the curve enters into a more stabilized phase, as can be seen in Figure 21 and T_{S80} will correspondingly describe the lifetime for the more stabilized performance of the device, while T_{80} describes the initial typically more rapid ageing, often called "burn in". It must be noted also that it is important to report also the E_0 and E_S values together with the lifetime values, as often the device performance stabilizes only after fully degrading and therefore, E_0 and E_S will allow distinguishing among well performing and degraded samples. Table 5 shows the list of all the ageing parameters defined by ISOS and their description.

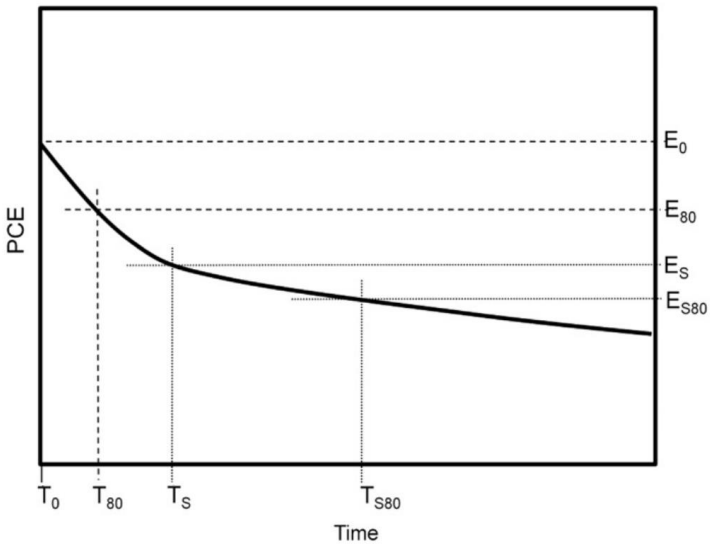

Figure 21 Example of a degradation curve with the stability markers. Reported with permissions from Elsevier [182]

Table 5 The list of the parameters describing the lifetime according to the ISOS guidelines

Parameter	Description
E_0, T_0	E_0 is the initial performance measured at time T_0 = 0,
E_S, T_S	E_S is the performance measured at time T_S, arbitrarily defined by the user
E_{80}, T_{80}	T_{80} is the lifetime calculated from T_0 that defines the time when the sample reaches E_{80} = 0.8 * E_0 performance
E_{S80}, T_{S80}	T_{S80} is the lifetime calculated from T_S that defines the time when the sample reaches E_{S80} = 0.8 * E_S performance

Although the representation of the lifetime via two parts of the curve gives a better insight into the device ageing, the E_S, T_S values randomly defined by the user may lead to ambiguity and may jeopardize the comparability of the data reported by different groups. Roesch *et al.* addressed this by proposing a method for mathematically determining the point T_S [188]. In particular, the approach is

based on the assumption that the degradation curve can be approximated using a biexponential function shown in (1):

$$\eta(t) \approx A \cdot e^{-\frac{t}{\tau_1}} + B \cdot e^{-\frac{t}{\tau_2}} \quad (1)$$

where the first term describes the fast decay and the second term the stabilized section of the curve. τ_1 and τ_2 are the respective time constants of the exponential decays and can be determined by fitting the model to the real curves. Authors suggest that the burn in stage comes to its end when the first term in the equation reaches 1 % of its initial performance. In other words, T_S can be determined by the equation (2):

$$A \cdot e^{-\frac{T_S}{\tau_1}} = 0.01 \cdot A \rightarrow T_S = -\tau_1 \cdot \ln 0.01 \quad (2)$$

Finally, the authors suggest using as a representative of lifetime a special figure of merit, the "lifetime energy yield" (*LEY*) to describe the energy produced by the device throughout its lifetime: *LEY* of the solar cells can be calculated by integrating the fitted double exponential function over the operational lifetime of the device until T_{S80} as defined in eq. (3) and shown in Figure 22:

$$LEY = \int_{t=0}^{T_{S80}} \eta(t)dt \cdot 1\ kW/m^{-2} \quad (3)$$

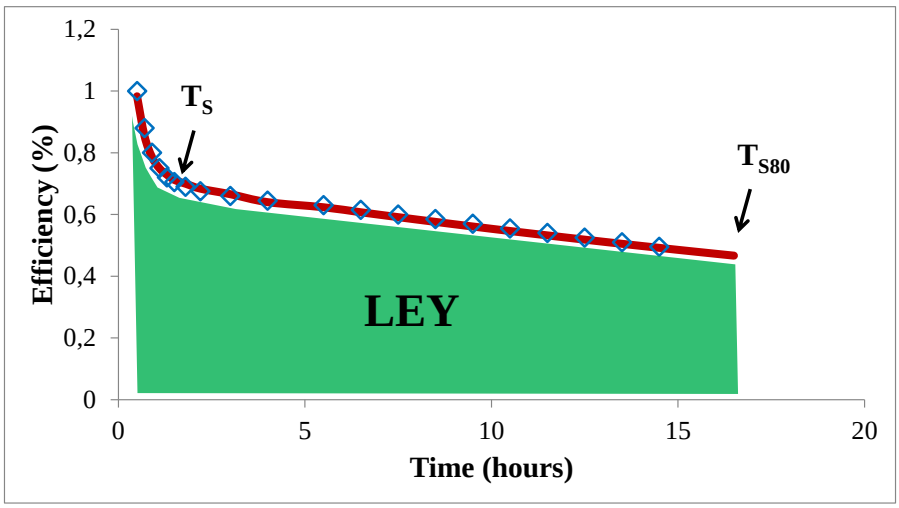

Figure 22 Example degradation curve with parameters calculated from a double exponential fit, marked: burn-in time T_S, operational lifetime T_{S80} and lifetime energy yield (*LEY*).

The proposed method of determining T_S however relies on the fitting of the curves with a double exponential, which imposes a limitation on the types of ageing curves the method can be applied to.

Slightly modified approach is therefore proposed here for determining T_S value. We first of all suggest defining *LEY´* as the lifetime energy yield determined by setting the integral boundaries from

T_S (instead of T_0) to T_{S80} (equation (3´)) and generalizing $\eta(t)$ as any function that fits the best for the particular curve, including linear function:

$$LEY' = \int_{T_S}^{T_{S80}} \eta(t)dt \cdot 1\ kW/m^{-2} \qquad (3')$$

As a next step T_S is chosen such, that it gives the largest possible LEY'. Geometrically speaking this will be proportional to simply maximizing the product E_S * T_{S80} calculated from the fitted function $\eta(t)$. Figure 23 (b) shows an example of the product E_S * T_{S80} as a function of T_S, calculated from the curves reported in Figure 23 (a) by using linear fitting function. For the curve "3" in Figure 23 (a) the section with the initial increase of performance, which is typically associated with device preconditioning, is simply neglected and the starting point T_0 is moved to the time where the curves reaches its maximum. From the Figure 23 (b) it is obvious that apart from curve "1" all the others curves show maximum energy at E_0 value, which means that these samples either never entered into a more stabilized phase or degraded before reasonable stabilization could be achieved. In this case the maximum lifetime energy yield is determined by setting $T_S = T_0$ and the pair E_0 & T_{80} and LEY (calculated from T_0 to T_{80}) will represent the device lifetime. Meanwhile, for the curve "1" in Figure 23 (b) there is a certain point after T_0, where the maximum lifetime energy yield is achieved and this point will define the T_S. The lifetime will then be represented by the pair E_S & T_{S80} and LEY_S (calculated from T_S to T_{S80}). The method allows generically determining T_S without limiting the function $\eta(t)$ to a single type and therefore, addressing various shapes of ageing curves.

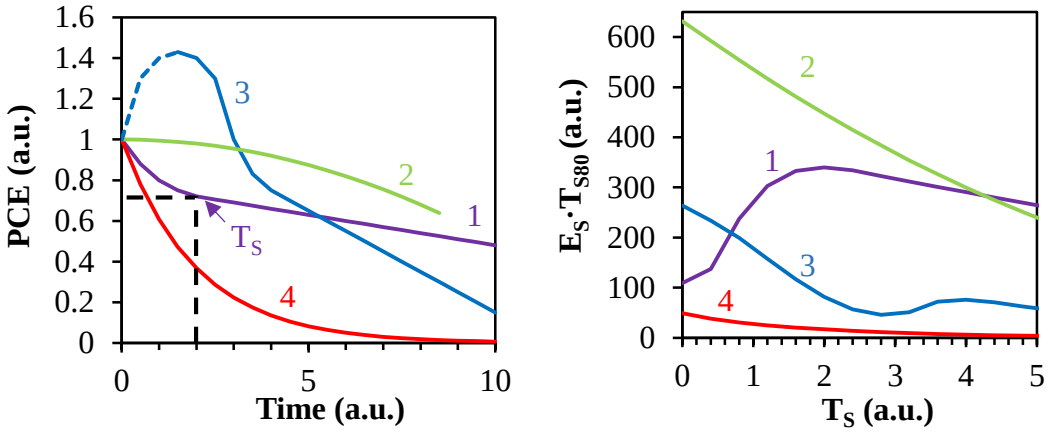

(a) (b)

Figure 23 (a) Ageing curves of different shapes take from real measurements and (b) the product E_S * T_{S80} as a function of T_S, calculated for the corresponding curves in (a).

Based on the discussions above we offer the following summary of steps to determine and report the lifetime of an OPV:

1. Conduct the ageing tests of the sample according to ISOS guideline and construct the ageing curve
2. Calculate the product $E_S * T_{S80}$ as a function of T_S using the most suitable function for the ageing curve and determine the point where the product $E_S * T_{S80}$ is maximum and define that point as T_S
3. Calculate *LEY* using the equation (3´) with boundaries of the integral set from T_S to T_{S80}
4. Report E_S, T_{S80} and *LEY*

It is our belief that the proposed methodology will allow generically determining the lifetime for any shapes of curves and will enable fair comparison of lifetime among research groups.

It is important to note here that extrapolation of the measured lifetime data that never reached T_{80} value was not discussed here, as this is a complex process that can be a source of large errors and therefore, requires a separate investigation. It is obvious however, that if the sample stability extends beyond a few years, extrapolation can be very useful for estimating the lifetime and this must be done with extra care and only for data with reasonable density of measurements. Even in this case however it is important to bear in mind that often secondary effects may accelerate the ageing of a sample at a later stage and therefore any extrapolated data can only be used as an indication rather than a proof of a device lifetime.

7.2.3 Lifetime comparison: O-diagram and baselines

One of the efficient ways for comparing the lifetime of different devices is plotting their initial performance E_0 versus the lifetime T_{80}. However, since the reported OPV lifetime often varies from minutes up to years, the time scale should then be used in logarithmic format for easier presentation. In our earlier publication we suggested logarithmic scale with base 4 for the time parameter *T*, which allowed splitting the time axes into time blocks, which could be associated with common time units such as hours, days, weeks etc. The plot was named O-diagram (o stands for OPV) and was utilized in a number of our studies for comparing the lifetime of different devices [184,189,190] and was also discussed earlier in this review in section 4.1. Figure 24 shows an example of o-diagrams, which were used to compare the stability of a large number of samples tested under different ISOS test conditions. In the figure six diagrams are presented each corresponding to one ISOS test distinguished by colors. Each diagram has Y-axes representing *PCE* and X-axes representing the lifetime. X-axes are presented in logarithmic scale with base 4 expressed in days, shown at the bottom, which are split into time blocks associated with the common time units shown on the top. The blue and red labels

represent the lifetime of the samples with and without encapsulation. The figure demonstrates how the samples tested under different conditions cluster in certain time blocks and therefore their lifetime can be categorized according to the common time units, such as for example samples tested under ISOS-D-1 (shelf life) and ISOS-D-2 (high temperature storage) conditions last mostly couple of seasons, while under harsh tests of ISOS-L-3 (indoor weathering under elevated temperatures and humidity) only days and weeks. In this study o-diagram was used to gauge and compare the lifetime of the same samples tested under different ISOS test conditions. Similarly, in another two studies the same approach was used to categorize the lifetime of all the devices that were reported in literature so far, which allowed both identifying certain trends in the OPV lifetime, determining the best reported lifetime and establishing baseline for OPV lifetime [16,191]. The latter studies are discussed in details in the next chapter.

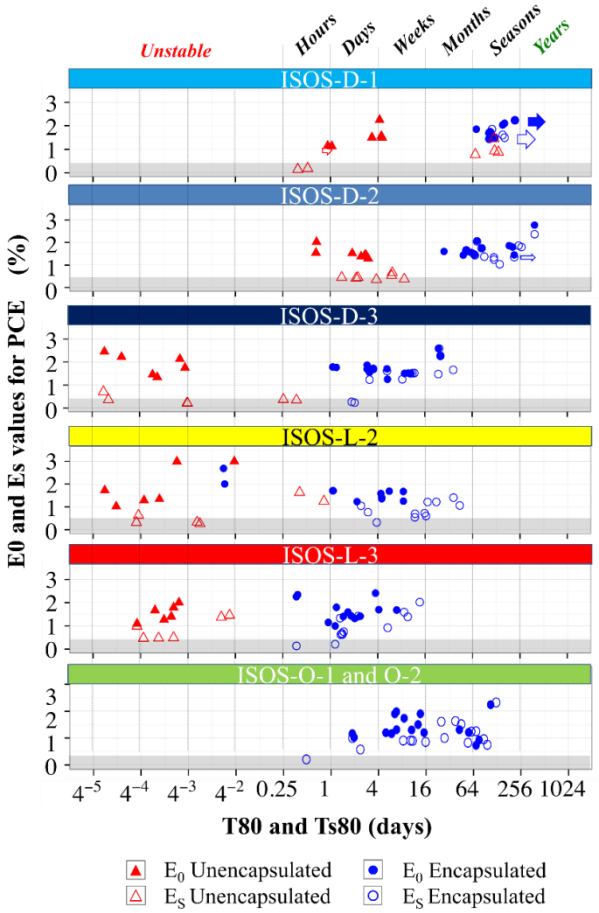

Figure 24 The o-diagram presents the E_0, T_{80} (solid markers) and E_S, T_{S80} (open markers) values for all the tested samples under different ISOS test conditions (the conditions of the tests are reported in the literature [182]). The blue circles and the red triangles represent correspondingly the devices with and without encapsulation. The grey zone marks the area where the devices are considered fully degraded (below 30% of initial performance). The arrow shows the data that represents T_{final} (the time of the last measurement) instead of T_{80}, which can be much higher. Reprinted with permission from Elsevier [190].

8 Current status and predictions of OPV lifetime

Recently two studies were reported, based on the meta-analyzes of OPV lifetime data reported in literature. The first one presented the analyzes of all the articles reporting lifetime data of OPVs published before mid-2013 [16] and the second one analyzing the remaining articles until mid-2015 [191]. The idea was to identify the pair of E_0 & T_{80} parameters for each ageing curve and combine these in the o-diagram for comparative analyzes. Sections 4.1 has already discussed an example of the use of this data for comparing samples with and without PEDOT:PSS in terms of lifetime.

A number of lessons were learned from these studies. In particular, Figure 25 shows the lifetime values extracted from literature data distributed versus the years of publications. The blue circles and green triangles represent both encapsulated and unencapsulated samples tested in dark and under light respectively. The black solid line shows the number of data points per year. The figure demonstrates how both the number of reports and the lifetime are rapidly increasing. This shows that the lifetime issue has become one of the most important and urgent challenges of OPV field and therefore, significant improvements can be seen in the past several years with reported lifetime values crossing the 2 years threshold.

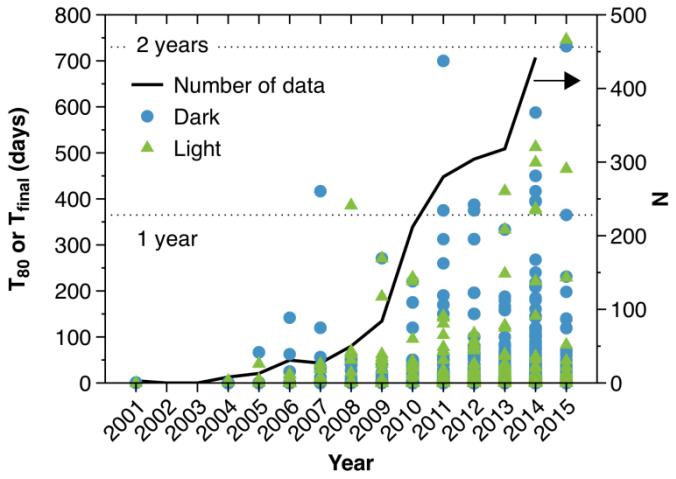

Figure 25 Lifetime of both encapsulated and unencapsulated device extracted from literature versus the year of publication. Blue circles and green triangles represent the data measured in dark and under light respectively. The black solid line shows the number of reports per year. Reprinted with permission from [191].

More importantly, the studies allowed determining the typical OPV performance under specific test conditions [191]. All the literature data were split into four categories: Group 1 and 2 – unencapsulated samples tested under light and in dark respectively, group 3 and 4 – encapsulated samples tested under light and dark respectively. Group 3 additionally was split into three categories – samples tested (a) under light sources with spectrum close to AM1.5G, (b) outdoors and (c) under

light sources with poor UV content or low intensity. The groups were additionally associated with but not limited to the corresponding ISOS guidelines marked in the legends of the plots. The distributions of the lifetime data in the time blocks (same scale as in o-diagram) were then constructed and are presented in Figure 26. The Y-axis represent the number of data points and X-axis the time. The blocks marked with red show the median and the green show the maximum number of samples with the corresponding lifetime values reported for each test condition. The table on the right lower corner lists all the median and maximum values for the different categories. For the unencapsulated samples tested in the dark (right upper corner) two distinct picks are identified, where the picks with lower and higher lifetime values correspond to the normal and inverted structures, respectively. These distributions are named as baselines for OPV lifetime and are suggested to be used in the following way:

For any newly developed (OPV) solar cell:

- If the achieved lifetime is beyond the median, then the sample has an improved stability.
- If the achieved lifetime is in the maximum region or beyond, then the sample has an outstanding or record lifetime, respectively.

The reason the category 3 was split according to the light source type was because the light source can have a significant impact on device lifetime, as was discussed in the ISOS guidelines.

From the figure it is additionally evident that while there is only little difference in stability for samples with and without encapsulation when tested in dark (especially for inverted structures), significant difference is observed for indoor light tests, where unencapsulated samples last mostly only couple of hours and reach several hundred hours when encapsulated. Nevertheless, the comparison is very generic and the ration may differ significantly from one type of devices or test conditions to another. Larger amount of data is therefore needed for more accurate comparison.

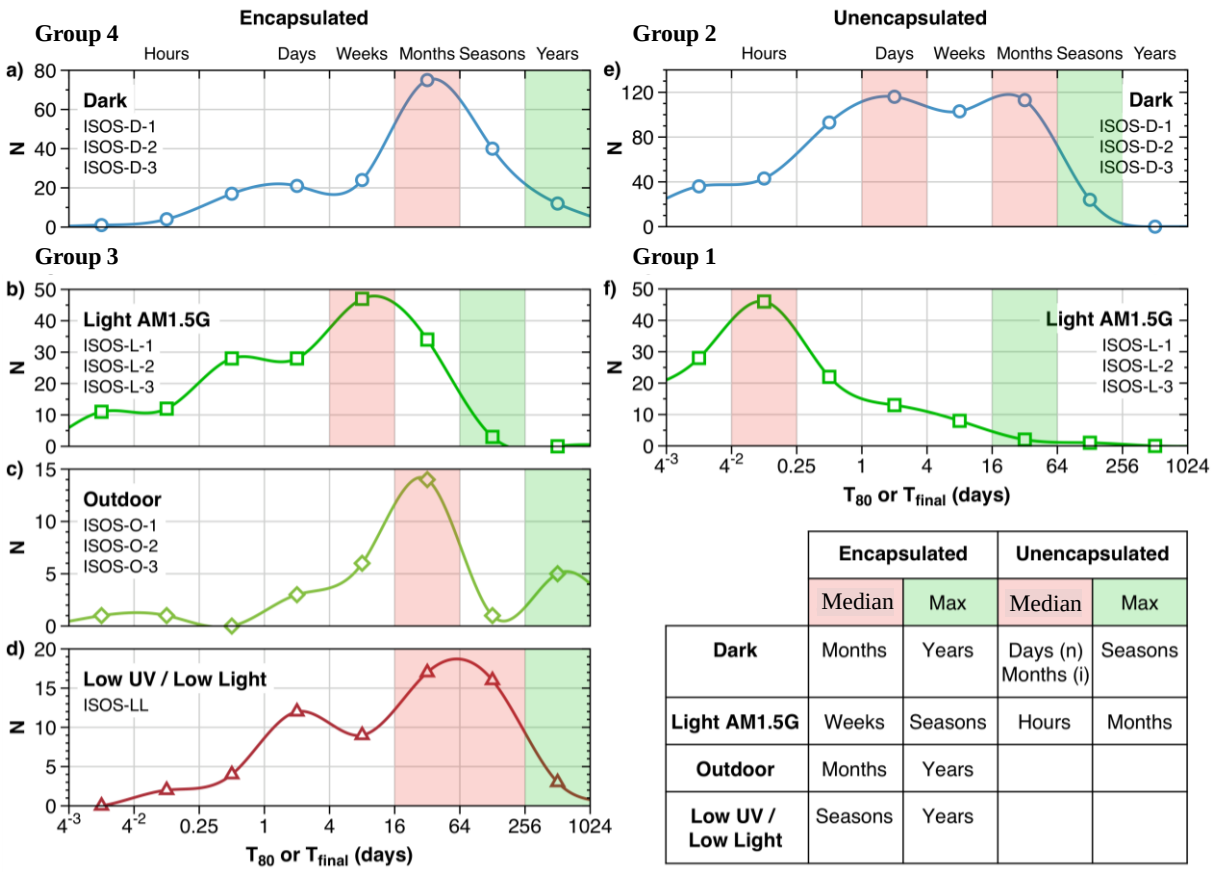

	Encapsulated		Unencapsulated	
	Median	Max	Median	Max
Dark	Months	Years	Days (n) Months (i)	Seasons
Light AM1.5G	Weeks	Seasons	Hours	Months
Outdoor	Months	Years		
Low UV / Low Light	Seasons	Years		

Figure 26 Baselines of the lifetime of OPVs tested under different ageing conditions for encapsulated (left plots) and unencapsulated (right plots) samples. The plots represent the number of data points distributed among the time blocks corresponding to the logarithmic scale with base 4 (similar to o-diagram). The scale is associated with the common time units shown on the top x-axis of each plot. The median and maximum lifetime values for each distribution are highlighted with red and green bands and are listed in the table on the right lower corner. For unencapsulated samples tested in the dark two distinct peaks, i.e., two median values corresponding to days and months, are associated with the normal and inverted structures. The test conditions are associated with, but not limited to the ISOS test conditions. Reprinted with permission from [191].

The literature data analyzes allowed also constructing the diagram of the best reported lifetimes of devices per year, which is shown in Figure 27. Four trends are shown for samples tested respectively in dark, under low UV light, in outdoor conditions and indoor under light source with spectrum close to AM1.5G. The diagram was reported in the earlier publication [191] and is now updated with the latest achievement of 4 years (1463 days) of shelf life for flexible R2R processed and packaged OPV modules manufactured at the Technical University of Denmark. The 4 years measurements are presented in Figure 28 and are a continuation of an earlier reported study, where over 2 years of lifetime was reported for roll-to-roll coated modules by Krebs *et al.* [186]. The details of the modules and the measurements can be found in the aforementioned publication.

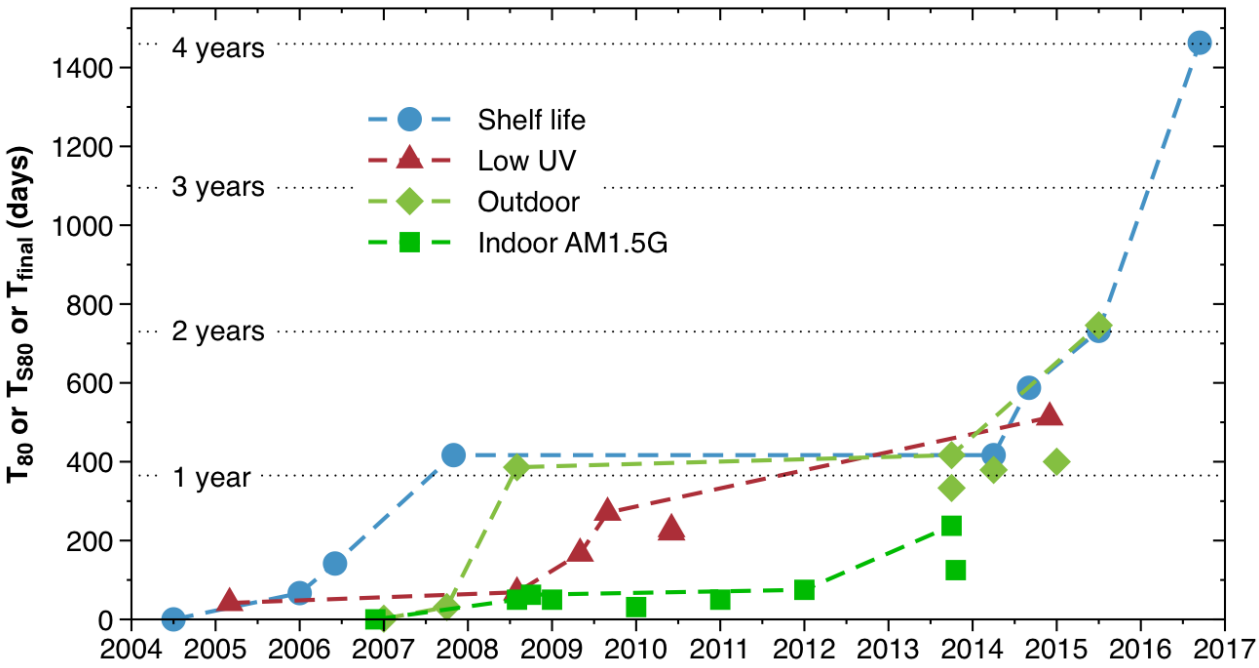

Indoor AM1.5G			Shelf life			Outdoor			Low UV		
PCE (%)	Lifetime (days)	Ref.	*PCE* (%)	Lifetime (days)	Ref.	*PCE* (%)	Lifetime (days)	Ref.	*PCE* (%)	Lifetime (days)	Ref.
1.08	0.083	[80]	0.8	0.042	[192]	0.0024	2	[193]	2.5	42	[194]
NA	50	[195]	0.035	67	[196]	4.2	31	[197]	4.1	69	[198]
NA	63	[199]	0.16	142	[200]	NA	386	[195]	2.32	167	[201]
1.09	50	[202]	2.8	417	[203]	1.43	417	[169]	5.9	271	[204]
3.54	31	[205]	1.27	417	[206]	1.43	333	[169]	2.7	229	[207]
NA	50	[208]	6.05	587.5	[72]	NA	379	[206]	6.07	221	[209]
2.1	75	[210]	1.06	732	[186]	1.42	400	[211]	2.7	513	[212]
3.42	125	[213]	1.06	1463	Continuation of [186]	1.11	746	[186]			
2.59	238	[214]									

Figure 27 Best lifetime values for different test conditions reported for each year. The table below shows the corresponding initial efficiencies and references. Some of the data points have been defined by the last measurement T_{final} of the experiment, since the 20% ageing threshold was not reached during the test. The dashed lines connect the data points to highlight the evolvement of record values. The horizontal dotted lines mark the 1 and 2 year values.

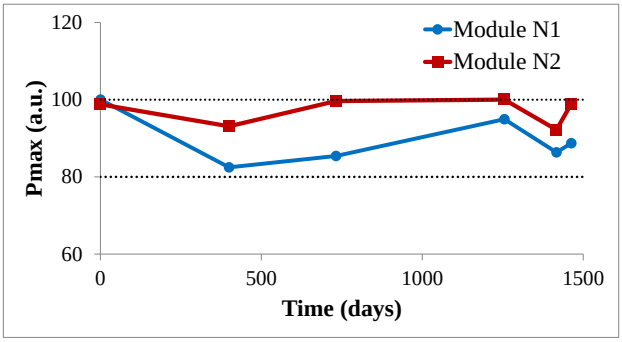

Figure 28 Shelf life of flexible R2R processed, ITO-free, encapsulated OPV modules manufactured at the Technical University of Denmark in 2012. The normalized values of maximum power P_{max} versus the time is presented. The two curves correspond to two identical modules stored in dark in air.

The diagram of the best lifetimes also highlights the fact that the lifetime of OPVs experienced rapid improvements in recent years and 2 years has already been achieved for outdoor tests and 4 years for shelf life.

Today at least one important question still remains: how to predict the lifetime of an OPV device based on accelerated tests? Methods for accurate prediction are necessary, since the lifetime of OPVs is gradually improving and the testing period becomes impractical for rapid scientific progress. While an answer to this question has not been given yet, steps are being taken towards addressing this issue. In particular, based on the collected literature data presented above a database was established, which is hosted online at the address http://plasticphotovoltaics.com/lifetime-predictor.html. The data is freely accessible for the public and a user friendly interface has been developed that allows analyzing the data by applying specific filters. The page also allows uploading any new data. The purpose of the online data is to gradually expand the lifetime database of OPVs and create sufficient data that will allow developing more accurate baselines particularly for ISOS tests and eventually establishing prediction tools for devices with prolonged lifetimes.

Meanwhile, based on the data presented above and the fact that in last two years the lifetime of OPVs was reported to improve from 1 year to 2-4 years, it is fair to assume that already today there are samples under test, that will last up to 3-4 years under light and much longer in dark and if the same progress continues, by 2020 samples will be produced that will last more than 7-8 years. Moreover, if we employ novel measures, such as *LEY* discussed in section 7.2.2 and instead of T_{80} threshold use perhaps another metric to define the usable lifetime span that is more true to when an OPV technology becomes unfit for use (for example. T_{50}), it would appear 7-15 years is within the reach in near future, if not already here. Therefore, with the given very low embedded energy in the production it is highly likely that within next few years the energy produced by stable OPVs will reach the cost level that will compete even with fossil fuels [215].

9 Conclusions

In conclusion, the review discussed the stability of organic solar cells by addressing the entire chain of challenges ranging from physical and chemical modifications in the atomic level to device upscaling and packaging and lifetime characterization. The importance of maintaining the compatibility of devices with final product design, while developing architectural solutions for device stabilization, was stressed. The ageing mechanisms in different layers of the devices were discussed and an overview of recently proposed solutions was presented. This included the overview of recent advances in chemical modifications of the active layer via side chain modifications, diversification

of the back bones and improvement of the acceptor materials. The latter involved cross linking of fullerenes or the use of fullerene free materials. The pros and cons of additives were discussed in terms of morphological stability of the films, as well as inclusion of third components in the active mixture. Mechanical stability of the layers and interfaces was additionally discussed, which gains increased attention in recent years. In particular, it was demonstrated that certain compatibilizers or a set of external stresses could improve the cohesion of certain layers in the device. Molecular weight or donor: acceptor rations were additional parameters affecting the mechanical stability of the layers. Device upscaling and packaging were addressed as well, and the importance of appropriate edge sealing was highlighted and supported with some examples. Characterization of device stability and lifetime were discussed, which included the overview of the recently reported advanced characterization techniques that were used for studying the ageing mechanism. The summary of ISOS guidelines for testing device lifetime was presented and accomplished by presentation of a generic marker for lifetime determination for any shapes of ageing curves and the lifetime energy yield as an additional marker for lifetime rating. The lifetime comparison of the different reports via an o-diagram was discussed as well. The review was concluded by presenting the status of OPV lifetime today and predicting its progress in near future. In particular, today up to 4 years of stability has been reported and if the same progress continues, by 2020 samples with lifetime up to 7-8 years will likely be achieved. Moreover, if different and perhaps more suitable metrics are defined that will better reflect the usefulness of OPV in operation for certain applications, such as for example the energy produced by the samples until T_{50} lifetime, up to 15 years stability can be envisaged for OPVs in the near future.

References

[1] Djurišić A B, Liu F, Ng A M C, Dong Q, Wong M K, Ng A and Surya C 2016 Stability issues of the next generation solar cells *Phys. status solidi - Rapid Res. Lett.* **10** 281–99

[2] Manceau M, Rivaton A, Gardette J L, Guillerez S and Lemaître N 2009 The mechanism of photo- and thermooxidation of poly(3-hexylthiophene) (P3HT) reconsidered *Polym. Degrad. Stab.* **94** 898–907

[3] Turkovic V, Engmann S, Gobsch G and Hoppe H 2012 Methods in determination of morphological degradation of polymer:fullerene solar cells *Synth. Met.* **161** 2534–9

[4] Waters H, Bristow N, Moudam O, Chang S W, Su C J, Wu W R, Jeng U S, Horie M and Kettle J 2014 Effect of processing additive 1,8-octanedithiol on the lifetime of PCPDTBT based Organic Photovoltaics *Org. Electron. physics, Mater. Appl.* **15** 2433–8

[5] Kim Y J, Chung D S and Park C E 2015 Highly thermally stable non-fullerene organic solar cells: p-DTS(FBTTh2)2:P(NDI2OD-T2) bulk heterojunction *Nano Energy* **15** 343–52

[6] Han D, Lee H, Jeong S, Lee J, Lee J-Y and Yoo S 2015 Stability enhancement of normal-geometry organic solar cells in a highly damp condition: A study on the effect of top electrodes *Org. Electron.* **25** 31–6

[7] Jørgensen M, Norrman K and Krebs F C 2008 Stability/degradation of polymer solar cells *Sol. Energy Mater. Sol. Cells* **92** 686–714

[8] Grossiord N, Kroon J M, Andriessen R and Blom P W M 2012 Degradation mechanisms in organic photovoltaic devices *Org. Electron.* **13** 432–56

[9] Jørgensen M, Norrman K, Gevorgyan S A, Tromholt T, Andreasen B and Krebs F C 2012 Stability of polymer solar cells *Adv. Mater.* **24** 580–612

[10] Lee J U, Jung J W, Jo J W and Jo W H 2012 Degradation and stability of polymer-based solar cells *J. Mater. Chem.* 24265–83

[11] Cao H, He W, Mao Y, Lin X, Ishikawa K, Dickerson J H and Hess W P 2014 Recent progress in degradation and stabilization of organic solar cells *J. Power Sources* **264** 168–83

[12] Giannouli M, Drakonakis V M, Savva A, Eleftheriou P, Florides G and Choulis S A 2015 Methods for Improving the Lifetime Performance of Organic Photovoltaics with Low-Costing Encapsulation *ChemPhysChem* **16** 1134–1154

[13] Cheng P and Zhan X 2016 Stability of organic solar cells: challenges and strategies *Chem. Soc. Rev.* **45** 2544–82

[14] Lloyd M T, Olson D C, Berry J J, Kopidakis N, Reese M O, Steirer K X and Ginley D S 2010 Enhanced lifetime in unencapsulated organic photovoltaics with air stable electrodes *2010 35th IEEE Photovoltaic Specialists Conference* (IEEE) pp 001060–3

[15] Voroshazi E, Cardinaletti I, Uytterhoeven G, Hadipour A, Rand B P and Aernouts T 2013 Role of electron and hole collecting buffer layers on the stability of inverted polymer: Fullerene photovoltaic devices *2013 IEEE 39th Photovoltaic Specialists Conference (PVSC)* (IEEE) pp 3212–5

[16] Gevorgyan S A, Madsen M V., Roth B, Corazza M, Hösel M, Søndergaard R R, Jørgensen M and Krebs F C 2016 Lifetime of Organic Photovoltaics: Status and Predictions *Adv. Energy Mater.* **6** 1–17

[17] Drakonakis V M, Savva A, Kokonou M and Choulis S A 2014 Investigating electrodes degradation in organic photovoltaics through reverse engineering under accelerated humidity lifetime conditions *Sol. Energy Mater. Sol. Cells* **130** 544–50

[18] Züfle S, Neukom M T, Altazin S, Zinggeler M, Chrapa M, Offermans T and Ruhstaller B 2015 An Effective Area Approach to Model Lateral Degradation in Organic Solar Cells *Adv. Energy Mater.* **5** 1500835

[19] Krebs F C, Hoesel M, Corazza M, Roth B, Madsen M V., Gevorgyan S a., Sondergaard R R, Karg D and Jorgensen M 2013 Freely Available OPV-The Fast Way to Progress *Energy Technol.* **1** 378–81

[20] Espinosa N, Hösel M, Jørgensen M and Krebs F C 2014 Large scale deployment of polymer solar cells on land, on sea and in the air *Energy Environ. Sci.* **7** 855

[21] Cardinaletti I, Kesters J, Bertho S, Conings B, Piersimoni F, D'Haen J, Lutsen L, Nesladek M, Van Mele B, Van Assche G, Vandewal K, Salleo A, Vanderzande D, Maes W and Manca J V. 2014 Toward bulk heterojunction polymer solar cells with thermally stable active layer morphology *J. Photonics Energy* **4**040997 (1-12)

[22] Rumer J W and McCulloch I 2015 Organic photovoltaics: Crosslinking for optimal morphology and stability *Mater. Today* **18** 425–35

[23] Lu L, Zheng T, Wu Q, Schneider A M, Zhao D and Yu L 2015 Recent Advances in Bulk Heterojunction Polymer Solar Cells *Chem. Rev.* **115** 12666–731

[24] Bundgaard E, Helgesen M, Carlé J E, Krebs F C and Jørgensen M 2013 Advanced functional polymers for increasing the stability of organic photovoltaics *Macromol. Chem. Phys.* **214** 1546–58

[25] Xu X, Wu Y, Fang J, Li Z, Wang Z, Li Y and Peng Q 2014 Side-chain engineering of benzodithiophene-fluorinated quinoxaline low-band-gap co-polymers for high-performance polymer solar cells *Chem. - A Eur. J.* **20** 13259–71

[26] Tournebize A, Gardette J-L, Taviot-Guého C, Bégué D, Arnaud M A, Dagron-Lartigau C, Medlej H, Hiorns R C, Beaupré S, Leclerc M and Rivaton A 2015 Is there a photostable conjugated polymer for efficient solar cells? *Polym. Degrad. Stab.* **112** 175–84

[27] Morse G E, Tournebize A, Rivaton A, Chassé T, Taviot-Gueho C, Blouin N, Lozman O R and Tierney S 2015 The effect of polymer solubilizing side-chains on solar cell stability *Phys. Chem. Chem. Phys.* **17** 11884–97

[28] Li Z, Wu F, Lv H, Yang D, Chen Z, Zhao X and Yang X 2015 Side-Chain Engineering for Enhancing the Thermal Stability of Polymer Solar Cells *Adv. Mater.* **27** 6999–7003

[29] Verstappen P, Kesters J, D'Olieslaeger L, Drijkoningen J, Cardinaletti I, Vangerven T, Bruijnaers B J, Willems R E M, D'Haen J, Manca J V., Lutsen L, Vanderzande D J M and Maes W 2015 Simultaneous Enhancement of Solar Cell Efficiency and Stability by Reducing the Side Chain Density on Fluorinated PCPDTQx Copolymers *Macromolecules* **48** 3873–82

[30] Vandenbergh J, Conings B, Bertho S, Kesters J, Spoltore D, Esiner S, Zhao J, Van Assche G, Wienk M M, Maes W, Lutsen L, Van Mele B, Janssen R A J, Manca J and Vanderzande D J M 2011 Thermal Stability of Poly[2-methoxy-5-(2'-phenylethoxy)-1,4-phenylenevinylene] (MPE-PPV): Fullerene Bulk Heterojunction Solar Cells *Macromolecules* **44** 8470–8

[31] Campo B J, Bevk D, Kesters J, Gilot J, Bolink H J, Zhao J, Bolsée J-C, Oosterbaan W D, Bertho S, D'Haen J, Manca J, Lutsen L, Van Assche G, Maes W, Janssen R A J and Vanderzande D 2013 Ester-functionalized poly(3-alkylthiophene) copolymers: Synthesis, physicochemical characterization and performance in bulk heterojunction organic solar cells *Org. Electron.* **14** 523–34

[32] Kesters J, Kudret S, Bertho S, Van Den Brande N, Defour M, Van Mele B, Penxten H, Lutsen L, Manca J, Vanderzande D and Maes W 2014 Enhanced intrinsic stability of the bulk heterojunction active layer blend of polymer solar cells by varying the polymer side chain pattern *Org. Electron. physics, Mater. Appl.* **15** 549–62

[33] Bertho S, Campo B, Piersimoni F, Spoltore D, D'Haen J, Lutsen L, Maes W, Vanderzande D and Manca J 2013 Improved thermal stability of bulk heterojunctions based on side-chain functionalized poly(3-alkylthiophene) copolymers and PCBM *Sol. Energy Mater. Sol. Cells* **110** 69–76

[34] Kesters J, Verstappen P, Raymakers J, Vanormelingen W, Drijkoningen J, D'Haen J, Manca J, Lutsen L, Vanderzande D and Maes W 2015 Enhanced Organic Solar Cell Stability by Polymer (PCPDTBT) Side Chain Functionalization *Chem. Mater.* **27** 1332–41

[35] Heckler I, Kesters J, Defour M, Madsen M, Penxten H, D'Haen J, Van Mele B, Maes W and Bundgaard E 2016 The Influence of Conjugated Polymer Side Chain Manipulation on the Efficiency and Stability of Polymer Solar Cells *Materials (Basel).* **9** 181

[36] Lee R-H, Chen W-Y and Shiau S-Y 2013 Synthesis and photovoltaic properties of a series of bulk heterojunction solar cells based on interchain-linked conjugated polymers *Polym. J.* **45** 744–57

[37] Manceau M, Bundgaard E, Carlé J E, Hagemann O, Helgesen M, Søndergaard R, Jørgensen M and Krebs F C 2011 Photochemical stability of π-conjugated polymers for polymer solar cells: a rule of thumb *J. Mater. Chem.* **21** 4132

[38] Gedefaw D, Tessarolo M, Prosa M, Bolognesi M, Henriksson P, Zhuang W, Seri M, Muccini M and Andersson M R 2016 Induced photodegradation of quinoxaline based copolymers for photovoltaic applications *Sol. Energy Mater. Sol. Cells* **144** 150–8

[39] Shin N, Yun H-J, Yoon Y, Son H J, Ju S-Y, Kwon S-K, Kim B and Kim Y-H 2015 Highly Stable Polymer Solar Cells Based on Poly(dithienobenzodithiophene- co -thienothiophene) *Macromolecules* **48** 3890–9

[40] Zhang S, Yang B, Liu D, Zhang H, Zhao W, Wang Q, He C and Hou J 2016 Correlations among Chemical Structure, Backbone Conformation, and Morphology in Two Highly Efficient Photovoltaic Polymer Materials *Macromolecules* **49** 120–6

[41] Carlé J E, Helgesen M, Zawacka N K, Madsen M V., Bundgaard E and Krebs F C 2014 A comparative study of fluorine substituents for enhanced stability of flexible and ITO-free high-performance polymer solar cells *J. Polym. Sci. Part B Polym. Phys.* **52** 893–9

[42] Nguyen T L, Choi H, Ko S-J, Uddin M a., Walker B, Yum S, Jeong J-E, Yun M H, Shin T J, Hwang S, Kim J Y and Woo H Y 2014 Semi-crystalline photovoltaic polymers with efficiency exceeding 9% in a ~300 nm thick conventional single-cell device *Energy Environ. Sci.* **7** 3040–51

[43] Livi F, Zawacka N K, Angmo D, Jørgensen M, Krebs F C and Bundgaard E 2015 Influence of Side Chain Position on the Electrical Properties of Organic Solar Cells Based on Dithienylbenzothiadiazole- alt -phenylene Conjugated Polymers *Macromolecules* **48** 3481–92

[44] Li F, Yager K G, Dawson N M, Yang J, Malloy K J and Qin Y 2013 Complementary Hydrogen Bonding and Block Copolymer Self-Assembly in Cooperation toward Stable Solar Cells with Tunable Morphologies *Macromolecules* **46** 9021–31

[45] Chen C-P, Huang C-Y and Chuang S-C 2014 Highly Thermal Stable and Efficient Organic Photovoltaic Cells with Crosslinked Networks Appending Open-Cage Fullerenes as Additives *Adv. Funct. Mater.* n/a-n/a

[46] Diacon A, Derue L, Lecourtier C, Dautel O, Wantz G and Hudhomme P 2014 Cross-linkable azido C 60 -fullerene derivatives for efficient thermal stabilization of polymer bulk-heterojunction solar cells *J. Mater. Chem. C* **2** 7163

[47] George Z, Xia Y, Sharma A, Lindqvist C, Andersson G G, Inganäs O, Moons E, Müller C and Andersson M R 2016 Two-in-one: cathode modification and improved solar cell blend stability through addition of modified fullerenes *J. Mater. Chem. A* 2663–9

[48] Wang S, Wang M, Chen Z and Yang X 2015 Selection strategy of porphyrins for achieving thermally stable polymer solar cells *J. Mater. Chem. A* **0** 1–9

[49] Li S, Liu W, Shi M, Mai J, Lau T-K, Wan J-H, Lu X, Li C-Z and Chen H 2016 A spirobifluorene and diketopyrrolopyrrole moieties based non-fullerene acceptor for efficient and thermally stable polymer solar cells with high open-circuit voltage *Energy Environ. Sci.* **9** 1–11

[50] Wang S, Qu Y, Li S, Ye F, Chen Z and Yang X 2015 Improved Thermal Stability of Polymer Solar Cells by Incorporating Porphyrins *Adv. Funct. Mater.* **25** 748–57

[51] Liao M-H, Tsai C-E, Lai Y-Y, Cao F-Y, Wu J-S, Wang C-L, Hsu C-S, Liau I and Cheng Y-J 2014 Morphological Stabilization by Supramolecular Perfluorophenyl-C 60 Interactions Leading to Efficient and Thermally Stable Organic Photovoltaics *Adv. Funct. Mater.* **24** 1418–29

[52] Lin Y and Zhan X 2014 Non-fullerene acceptors for organic photovoltaics: an emerging horizon *Mater. Horizons* **1** 470

[53] Chen L, Tian S and Chen Y 2014 Enhanced performance for organic bulk heterojunction solar cells by cooperative assembly of ter(ethylene oxide) pendants *Polym. Chem.* **5** 4480

[54] Wu Q, Bhattacharya M, Moore L M J and Morgan S E 2014 Air processed P3HT:PCBM photovoltaic cells: Morphology correlation to annealing, degradation, and recovery *J. Polym. Sci. Part B Polym. Phys.* **52** 1511–20

[55] Kim W, Kim J K, Kim E, Ahn T K, Wang D H and Park J H 2015 Conflicted Effects of a Solvent Additive on PTB7:PC 71 BM Bulk Heterojunction Solar Cells *J. Phys. Chem. C* **119** 5954–61

[56] Kettle J, Waters H, Ding Z, Horie M and Smith G C 2015 Chemical changes in PCPDTBT:PCBM solar cells using XPS and TOF-SIMS and use of inverted device structure for improving lifetime performance *Sol. Energy Mater. Sol. Cells* **141** 139–47

[57] Huang W, Gann E, Xu Z-Q, Thomsen L, Cheng Y-B and McNeill C R 2015 A facile approach to alleviate photochemical degradation in high efficiency polymer solar cells *J. Mater. Chem. A* **3** 16313–9

[58] Kettle J, Waters H, Horie M and Smith G C 2016 Alternative selection of processing additives to enhance the lifetime of OPVs *J. Phys. D. Appl. Phys.* **49** 85601

[59] Khiev S, Derue L, Ayenew G, Medlej H, Brown R, Rubatat L, Hiorns R C, Wantz G and Dagron-Lartigau C 2013 Enhanced thermal stability of organic solar cells by using photolinkable end-capped polythiophenes *Polym. Chem.* **4** 4145

[60] Bracher C, Yi H, Scarratt N W, Masters R, Pearson A J, Rodenburg C, Iraqi A and Lidzey D G 2015 The effect of residual palladium catalyst on the performance and stability of PCDTBT:PC70BM organic solar cells *Org. Electron.* **27** 266–73

[61] Cheng P and Zhan X 2015 Versatile third components for efficient and stable organic solar cells *Mater. Horiz.* **2** 462–85

[62] Derue L, Dautel O, Tournebize A, Drees M, Pan H, Berthumeyrie S, Pavageau B, Cloutet E, Chambon S, Hirsch L, Rivaton A, Hudhomme P, Facchetti A and Wantz G 2014 Thermal stabilisation of polymer-fullerene bulk heterojunction morphology for efficient photovoltaic solar cells. *Adv. Mater.* **26** 5831–8

[63] Kakavelakis G, Stratakis E and Kymakis E 2013 Aluminum nanoparticles for efficient and stable organic photovoltaics *RSC Adv.* **3** 16288

[64] Tore N, Parlak E A, Tumay T A, Kavak P, Sarıoğlan Ş, Bozar S, Günes S, Ulbricht C and Egbe D A M 2014 Improvement in photovoltaic performance of anthracene-containing PPE–PPV polymer-based bulk heterojunction solar cells with silver nanoparticles *J. Nanoparticle Res.* **16** 2298

[65] Mateker W R, Heumueller T, Cheacharoen R, Sachs-Quintana I T, McGehee M D, Warnan J, Beaujuge P M, Liu X and Bazan G C 2015 Molecular Packing and Arrangement Govern the Photo-Oxidative Stability of Organic Photovoltaic Materials *Chem. Mater.* **27** 6345–53

[66] Heumueller T, Mateker W R, Sachs-Quintana I T, Vandewal K, Bartelt J A, Burke T M, Ameri T, Brabec C J and McGehee M D 2014 Reducing burn-in voltage loss in polymer solar cells by increasing the polymer crystallinity *Energy Environ. Sci.* **7** 2974

[67] Heumueller T, Burke T M, Mateker W R, Sachs-Quintana I T, Vandewal K, Brabec C J and McGehee M D 2015 Disorder-Induced Open-Circuit Voltage Losses in Organic Solar Cells During Photoinduced Burn-In *Adv. Energy Mater.* **5** 1500111

[68] Hermenau M, Riede M, Leo K, Gevorgyan S A, Krebs F C and Norrman K 2011 Water and oxygen induced degradation of small molecule organic solar cells *Sol. Energy Mater. Sol. Cells* **95** 1268–77

[69] Oh J Y, Shin M, Lee H W, Lee Y-J, Baik H K and Jeong U 2014 Enhanced air stability of polymer solar cells with a nanofibril-based photoactive layer. *ACS Appl. Mater. Interfaces* **6** 7759–65

[70] Turkovic V, Engmann S, Tsierkezos N, Hoppe H, Ritter U and Gobsch G 2014 Long-term stabilization of organic solar cells using hindered phenols as additives. *ACS Appl. Mater. Interfaces* **6** 18525–37

[71] Voroshazi E, Cardinaletti I, Conard T and Rand B P 2014 Light-induced degradation of polymer: Fullerene photovoltaic devices: An intrinsic or material-dependent failure mechanism? *Adv. Energy Mater.* 1–7

[72] Kong J, Song S, Yoo M, Lee G Y, Kwon O, Park J K, Back H, Kim G, Lee S H, Suh H and Lee K 2014 Long-term stable polymer solar cells with significantly reduced burn-in loss *Nat. Commun.* **5** 5688

[73] Kim H J, Kim J-H, Ryu J-H, Kim Y, Kang H, Lee W B, Kim T-S and Kim B J 2014 Architectural engineering of rod-coil compatibilizers for producing mechanically and thermally stable polymer solar cells. *ACS Nano* **8** 10461–70

[74] Corazza M, Rolston N, Dauskardt R H, Beliatis M, Krebs F C and Gevorgyan S A 2016 Role of Stress Factors on the Adhesion of Interfaces in R2R Fabricated Organic Photovoltaics *Adv. Energy Mater.* 1501927

[75] Kim T, Kim J-H, Kang T E, Lee C, Kang H, Shin M, Wang C, Ma B, Jeong U, Kim T-S and Kim B J 2015 Flexible, highly efficient all-polymer solar cells. *Nat. Commun.* **6** 8547

[76] Savagatrup S, Rodriquez D, Printz A D, Sieval A B, Hummelen J C and Lipomi D J 2015 [70]PCBM and Incompletely Separated Grades of Methanofullerenes Produce Bulk Heterojunctions with Increased Robustness for Ultra-Flexible and Stretchable Electronics *Chem. Mater.* **27** 3902–11

[77] Savagatrup S, Printz A D, O'Connor T F, Zaretski A V. and Lipomi D J 2014 Molecularly Stretchable Electronics *Chem. Mater.* **26** 3028–41

[78] Bruner C, Novoa F, Dupont S and Dauskardt R 2014 Decohesion kinetics in polymer organic solar cells. *ACS Appl. Mater. Interfaces* **6** 21474–83

[79] Dupont S R, Voroshazi E, Heremans P and Dauskardt R H 2013 Adhesion properties of inverted polymer solarcells: Processing and film structure parameters *Org. Electron.* **14** 1262–70

[80] Kawano K, Pacios R, Poplavskyy D, Nelson J, Bradley D D C and Durrant J R 2006 Degradation of organic solar cells due to air exposure *Sol. Energy Mater. Sol. Cells* **90** 3520–30

[81] Voroshazi E, Verreet B, Buri A, Müller R, Di Nuzzo D and Heremans P 2011 Influence of cathode oxidation via the hole extraction layer in polymer:fullerene solar cells *Org. Electron. physics, Mater. Appl.* **12** 736–44

[82] Norrman K, Madsen M V., Gevorgyan S A and Krebs F C 2010 Degradation patterns in water and oxygen of an inverted polymer solar cell *J. Am. Chem. Soc.* **132** 16883–92

[83] Bulle-Lieuwma C W T, van Gennip W J H, van Duren J K J, Jonkheijm P, Janssen R A J and Niemantsverdriet J W 2003 Characterization of polymer solar cells by TOF-SIMS depth profiling *Appl. Surf. Sci.* **203**–**204** 547–50

[84] de Jong M P, Ijzendoorn L J Van and de Voigt M J A 2000 Stability of the interface between indium-tin-oxide in polymer light-emitting diodes *App. Phys. Lett.* **77** 2255–7

[85] Sapkota S B, Fischer M, Zimmermann B and Würfel U 2014 Analysis of the degradation mechanism of ITO-free organic solar cells under UV radiation *Sol. Energy Mater. Sol. Cells* **121** 43–8

[86] Lloyd M T, Olson D C, Lu P, Fang E, Moore D L, White M S, Reese M O, Ginley D S and Hsu J W P 2009 Impact of contact evolution on the shelf life of organic solar cells *J. Mater. Chem.* **19** 7638

[87] Bovill E, Scarratt N, Griffin J, Yi H, Iraqi a., Buckley a. R, Kingsley J W and Lidzey D G 2015 The role of the hole-extraction layer in determining the operational stability of a polycarbazole:fullerene bulk-heterojunction photovoltaic device *Appl. Phys. Lett.* **106** 73301

[88] Voroshazi E, Cardinaletti I, Uytterhoeven G, Li S, Empl M, Aernouts T and Rand B P 2014 Role of electron-and hole-collecting buffer layers on the stability of inverted polymer: Fullerene photovoltaic devices *IEEE J. Photovoltaics* **4** 265–70

[89] Kumar P, Bilen C, Vaughan B, Zhou X, Dastoor P C and Belcher W J 2016 Comparing the degradation of organic photovoltaic devices under ISOS testing protocols *Sol. Energy Mater. Sol. Cells* **149** 179–86

[90] Glen T S, Scarratt N W, Yi H, Iraqi A, Wang T, Kingsley J, Buckley A R, Lidzey D G and Donald A M 2016 Dependence on material choice of degradation of organic solar cells following exposure to humid air *J. Polym. Sci. Part B Polym. Phys.* **54** 216–24

[91] Greenbank W, Hirsch L, Wantz G and Chambon S 2015 Interfacial thermal degradation in inverted organic solar cells *Appl. Phys. Lett.* **107** 263301

[92] Savva A, Georgiou E, Papazoglou G, Chrusou A Z, Kapnisis K and Choulis S A 2015 Photovoltaic analysis of the effects of PEDOT:PSS-additives hole selective contacts on the efficiency and lifetime performance of inverted organic solar cells *Sol. Energy Mater. Sol. Cells* **132** 507–14

[93] Lee S J, Kim B S, Kim J-Y, Yusoff A R B M and Jang J 2015 Stable organic photovoltaic with PEDOT:PSS and MoOX mixture anode interfacial layer without encapsulation *Org. Electron.* **19** 140–6

[94] Lee J J, Lee S H, Kim F S, Choi H H and Kim J H 2015 Simultaneous enhancement of the efficiency and stability of organic solar cells using PEDOT:PSS grafted with a PEGME buffer layer *Org. Electron.* **26** 191–9

[95] Hou X, Li Q, Cheng T, Yu L, Wang F, Lin J, Dai S, Li Y and Tan Z 2015 Improvement of the power conversion efficiency and long term stability of polymer solar cells by incorporation of amphiphilic Nafion doped PEDOT-PSS as a hole extraction layer *J. Mater. Chem. A* **3** 18727–34

[96] Yuan Z, Wu Z, Bai S, Cui W, Liu J, Song T and Sun B 2015 Layered bismuth selenide utilized as hole transporting layer for highly stable organic photovoltaics *Org. Electron.* **26** 327–33

[97] Kim N, Xin G, Cho S M, Pang C and Chae H 2015 Microwave-reduced graphene oxide for efficient and stable hole extraction layers of polymer solar cells *Curr. Appl. Phys.* **15** 953–7

[98] Shi Y, Tan L, Chen L and Chen Y 2014 Self-assembled buffer layer from conjugated diblock copolymers with ethyleneoxide side chains for high efficiency polymer solar cells *J. Mater. Chem. C* **0** 1–11

[99] MacLeod B A, Tremolet de Villers B J, Schulz P, Ndione P F, Kim H, Giordano A J, Zhu K, Marder S R, Graham S, Berry J J, Kahn A and Olson D C 2015 Stability of inverted organic solar cells with ZnO contact layers deposited from precursor solutions *Energy Environ. Sci.* **8** 592–601

[100] Stubhan T, Oh H, Pinna L, Krantz J, Litzov I and Brabec C J 2011 Inverted organic solar cells using a solution processed aluminum-doped zinc oxide buffer layer *Org. Electron.* **12** 1539–43

[101] Chen M-H, Kuo Y-C, Lin H-H, Chao Y-P and Wong M-S 2015 Highly stable inverted organic photovoltaics using aluminum-doped zinc oxide as electron transport layers *J. Power Sources* **275** 274–8

[102] Kam Z, Wang X, Zhang J and Wu J 2015 Elimination of Burn-in Open-Circuit Voltage Degradation by ZnO Surface Modification in Organic Solar Cells *ACS Appl. Mater. Interfaces* **7** 1608–15

[103] Bai S, Jin Y, Liang X, Ye Z, Wu Z, Sun B, Ma Z, Tang Z, Wang J, Würfel U, Gao F and Zhang F 2015 Ethanedithiol Treatment of Solution-Processed ZnO Thin Films: Controlling the Intragap States of Electron Transporting Interlayers for Efficient and Stable Inverted Organic Photovoltaics *Adv. Energy Mater.* **5** 1401606

[104] George Z, Voroshazi E, Lindqvist C, Kroon R, Zhuang W, Wang E, Henriksson P, Hadipour A and Andersson M R 2015 Improved performance and life time of inverted organic photovoltaics by using polymer interfacial materials *Sol. Energy Mater. Sol. Cells* **133** 99–104

[105] Weerasinghe H C, Rolston N, Vak D, Scully A D and Dauskardt R H 2016 A stability study of roll-to-roll processed organic photovoltaic modules containing a polymeric electron-selective layer *Sol. Energy Mater. Sol. Cells* **152** 133–40

[106] Raïssi M, Leroy-Lhez S and Ratier B 2016 Enhanced photocurrent and stability of organic solar cells using solution-based TS-CuPc interfacial layer *Org. Electron.* **37** 183–9

[107] Wang D, Zeng W, Chen S, Su X, Wang J and Zhang H 2015 Effect of a cathode buffer layer on the stability of organic solar cells *Semicond. Sci. Technol.* **30** 85017

[108] Chen L, Liu X, Wei Y, Wu F and Chen Y 2016 Alcohol-soluble interfacial fluorenes for inverted polymer solar cells: sequence induced spatial conformation dipole moment *Phys. Chem. Chem. Phys.* **18** 2219–29

[109] Glen T S, Scarratt N W, Yi H, Iraqi A, Wang T, Kingsley J, Buckley A R, Lidzey D G and Donald A M 2015 Grain size dependence of degradation of aluminium/calcium cathodes in organic solar cells following exposure to humid air *Sol. Energy Mater. Sol. Cells* **140** 25–32

[110] Yeom H R, Heo J, Kim G-H, Ko S-J, Song S, Jo Y, Kim D S, Walker B and Kim J Y 2015 Optimal top electrodes for inverted polymer solar cells. *Phys. Chem. Chem. Phys.* **17** 2152–9

[111] Voroshazi E, Uytterhoeven G, Cnops K, Conard T, Favia P, Bender H, Muller R and Cheyns D 2015 Root-Cause Failure Analysis of Photocurrent Loss in Polythiophene:Fullerene-Based Inverted Solar Cells *ACS Appl. Mater. Interfaces* **7** 618–23

[112] Romero-Gomez P, Betancur R, Martinez-Otero A, Elias X, Mariano M, Romero B, Arredondo B, Vergaz R and Martorell J 2015 Enhanced stability in semi-transparent PTB7/PC71BM photovoltaic cells *Sol. Energy Mater. Sol. Cells* **137** 44–9

[113] Ghosh D S, Liu Q, Mantilla-Perez P, Chen T L, Mkhitaryan V, Huang M, Garner S, Martorell J and Pruneri V 2015 Highly Flexible Transparent Electrodes Containing Ultrathin Silver for Efficient Polymer Solar Cells *Adv. Funct. Mater.* **25** 7309–16

[114] Espinosa N, García-Valverde R, Urbina A, Lenzmann F, Manceau M, Angmo D and Krebs F C 2012 Life cycle assessment of ITO-free flexible polymer solar cells prepared by roll-to-roll coating and printing *Sol. Energy Mater. Sol. Cells* **97** 3–13

[115] Peng C, Jia Z, Bianculli D, Li T and Lou J 2011 In situ electro-mechanical experiments and mechanics modeling of tensile cracking in indium tin oxide thin films on polyimide substrates *J. Appl. Phys.* **109** 103530

[116] Galagan Y, Mescheloff A, Veenstra S C, Andriessen R and Katz E A 2015 Reversible degradation in

ITO-containing organic photovoltaics under concentrated sunlight. *Phys. Chem. Chem. Phys.* **17** 3891–7

[117] Chen D, Zhang C, Wang Z, Zhang J, Tang S, Wei W, Sun L and Hao Y 2014 High efficient ITO free inverted organic solar cells based on ultrathin Ca modified AZO cathode and their light soaking issue *Org. Electron.* **15** 3006–15

[118] Wang W, Song M, Bae T-S, Park Y H, Kang Y-C, Lee S-G, Kim S-Y, Kim D H, Lee S, Min G, Lee G-H, Kang J-W and Yun J 2014 Transparent Ultrathin Oxygen-Doped Silver Electrodes for Flexible Organic Solar Cells *Adv. Funct. Mater.* **24** 1551–61

[119] Xue Z, Liu X, Zhang N, Chen H, Zheng X, Wang H and Guo X 2014 High-performance NiO/Ag/NiO transparent electrodes for flexible organic photovoltaic cells. *ACS Appl. Mater. Interfaces* **6** 16403–8

[120] Fan X, Wang J, Wang H, Liu X and Wang H 2015 Bendable ITO-free Organic Solar Cells with Highly Conductive and Flexible PEDOT:PSS Electrodes on Plastic Substrates. *ACS Appl. Mater. Interfaces* **7** 16287–95

[121] Skorenko K H, Faucett A C, Liu J, Ravvin N A, Bernier W E, Mativetsky J M and Jones W E 2015 Vapor phase polymerization and mechanical testing of highly electrically conductive poly(3,4-ethylenedioxythiophene) for flexible devices *Synth. Met.* **209** 297–303

[122] Li Y, Mao L, Tang F, Chen Q, Wang Y, Ye F, Chen L, Li Y, Wu D, Cui Z, Cai J and Chen L 2015 Ambient stable large-area flexible organic solar cells using silver grid hybrid with vapor phase polymerized poly(3,4-Ethylenedioxythiophene) cathode *Sol. Energy Mater. Sol. Cells* **143** 354–9

[123] Jin Y, Li L, Cheng Y, Kong L, Pei Q and Xiao F 2015 Cohesively Enhanced Conductivity and Adhesion of Flexible Silver Nanowire Networks by Biocompatible Polymer Sol-Gel Transition *Adv. Funct. Mater.* **25** 1581–7

[124] Lee H, Han G, Kim M, Ahn H and Lee H 2015 High mechanical and tribological stability of an elastic ultrathin overcoating layer for flexible silver nanowire films. *Adv. Mater.* **27** 2252–9

[125] Song Y, Jiang Y, Shi L, Cao S, Feng X, Miao M and Fang J 2015 Solution-processed assembly of ultrathin transparent conductive cellulose nanopaper embedding AgNWs. *Nanoscale* **7** 13694–701

[126] Song M, Park J H, Kim C S, Kim D-H, Kang Y-C, Jin S-H, Jin W-Y and Kang J-W 2014 Highly flexible and transparent conducting silver nanowire/ZnO composite film for organic solar cells *Nano Res.* **7** 1370–9

[127] Song M, Kim J-K, Yang S-Y and Kang J-W 2014 Solution-processed silver nanowires as a transparent conducting electrode for air-stable inverted organic solar cells *Thin Solid Films* **573** 14–7

[128] Kim Y, Ryu T I, Ok K-H, Kwak M-G, Park S, Park N-G, Han C J, Kim B S, Ko M J, Son H J and Kim J-W 2015 Inverted Layer-By-Layer Fabrication of an Ultraflexible and Transparent Ag Nanowire/Conductive Polymer Composite Electrode for Use in High-Performance Organic Solar Cells *Adv. Funct. Mater.* **25** 4580–9

[129] He X, He R, Liu A, Chen X, Zhao Z, Feng S, Chen N and Zhang M 2014 A highly conductive, flexible, transparent composite electrode based on the lamination of silver nanowires and polyvinyl alcohol *J. Mater. Chem. C* **2** 9737–45

[130] Lee D, Lee H, Ahn Y, Jeong Y, Lee D-Y and Lee Y 2013 Highly stable and flexible silver nanowire-graphene hybrid transparent conducting electrodes for emerging optoelectronic devices. *Nanoscale* **5** 7750–5

[131] Song M, Kim H-J, Kim C S, Jeong J-H, Cho C, Lee J-Y, Jin S-H, Choi D-G and Kim D-H 2015

ITO-free highly bendable and efficient organic solar cells with Ag nanomesh/ZnO hybrid electrodes *J. Mater. Chem. A* **3** 65–70

[132] Jørgensen M, Carlé J E, Søndergaard R R, Lauritzen M, Dagnæs-Hansen N A, Byskov S L, Andersen T R, Larsen-Olsen T T, Böttiger A P L, Andreasen B, Fu L, Zuo L, Liu Y, Bundgaard E, Zhan X, Chen H and Krebs F C 2013 The state of organic solar cells - A meta analysis *Sol. Energy Mater. Sol. Cells* **119** 84–93

[133] You J, Dou L, Yoshimura K, Kato T, Ohya K, Moriarty T, Emery K, Chen C-C, Gao J, Li G and Yang Y 2013 A polymer tandem solar cell with 10.6% power conversion efficiency. *Nat. Commun.* **4** 1446

[134] Zhou H, Zhang Y, Mai C-K, Collins S D, Bazan G C, Nguyen T-Q and Heeger A J 2015 Polymer Homo-Tandem Solar Cells with Best Efficiency of 11.3% *Adv. Mater.* **27** 1767–73

[135] Zhao J, Li Y, Yang G, Jiang K, Lin H, Ade H, Ma W and Yan H 2016 Efficient organic solar cells processed from hydrocarbon solvents *Nat. Energy* **1** 15027

[136] Søndergaard R, Hösel M, Angmo D, Larsen-Olsen T T and Krebs F C 2012 Roll-to-roll fabrication of polymer solar cells *Mater. Today* **15** 36–49

[137] Krebs F C 2009 Fabrication and processing of polymer solar cells: A review of printing and coating techniques *Sol. Energy Mater. Sol. Cells* **93** 394–412

[138] Sommer-Larsen P, Jørgensen M, Søndergaard R R, Hösel M and Krebs F C 2013 It is all in the Pattern-High-Efficiency Power Extraction from Polymer Solar Cells through High-Voltage Serial Connection *Energy Technol.* **1** 15–9

[139] Krebs F C, Espinosa N, Hösel M, Søndergaard R R and Jørgensen M 2014 25th anniversary article: Rise to power - OPV-based solar parks *Adv. Mater.* **26** 29–39

[140] Andersen T R, Dam H F, Hosel M, Helgesen M, Carle J E, Larsen-Olsen T T, Gevorgyan S A, Andreasen J W, Adams J, Li N, Machui F, Spyropoulos G D, Ameri T, Lemaitre N, Legros M, Scheel A, Gaiser D, Kreul K, Berny S, Lozman O R, Nordman S, Valimaki M, Vilkman M, Sondergaard R R, Jorgensen M, Brabec C J and Krebs F C 2014 Scalable, ambient atmosphere roll-to-roll manufacture of encapsulated large area, flexible organic tandem solar cell modules *Energy Environ. Sci.* **7** 2925–33

[141] Eggenhuisen T M, Galagan Y, Biezemans A F K V., Slaats T M W L, Voorthuijzen W P, Kommeren S, Shanmugam S, Teunissen J P, Hadipour A, Verhees W J H, Veenstra S C, Coenen M J J, Gilot J, Andriessen R and Groen W A 2015 High efficiency, fully inkjet printed organic solar cells with freedom of design *J. Mater. Chem. A* **3** 7255–62

[142] Berny S, Blouin N, Distler A, Egelhaaf H-J, Krompiec M, Lohr A, Lozman O R, Morse G E, Nanson L, Pron A, Sauermann T, Seidler N, Tierney S, Tiwana P, Wagner M and Wilson H 2016 Solar Trees: First Large-Scale Demonstration of Fully Solution Coated, Semitransparent, Flexible Organic Photovoltaic Modules *Adv. Sci.* **3** 1500342

[143] Galagan Y, Fledderus H, Gorter H, 't Mannetje H H, Shanmugam S, Mandamparambil R, Bosman J, Rubingh J-E J M, Teunissen J-P, Salem A, de Vries I G, Andriessen R and Groen W A 2015 Roll-to-Roll Slot-Die Coated Organic Photovoltaic (OPV) Modules with High Geometrical Fill Factors *Energy Technol.* **3** 834–42

[144] Spyropoulos G D, Ramirez Quiroz C O, Salvador M, Hou Y, Gasparini N, Schweizer P, Adams J, Kubis P, Li N, Spiecker E, Ameri T, Egelhaaf H-J and Brabec C J 2016 Organic and perovskite solar modules innovated by adhesive top electrode and depth-resolved laser patterning *Energy Environ. Sci.* **9** 2302–13

[145] Kubis P, Li N, Stubhan T, Machui F, Matt G J, Voigt M M and Brabec C J 2015 Patterning of organic photovoltaic modules by ultrafast laser *Prog. Photovoltaics Res. Appl.* **23** 238–46

[146] Uhrich C L, Falkenberg C, Rabe J, Heimke B, Klemet M, Wilde C, Wichtendahl R and Pfeiffer M 2014 Organic solar cells: from lab to roll-to-roll production ed Z H Kafafi, P A Lane and I D W Samuel p 918415

[147] Yan F, Noble J, Peltola J, Wicks S and Balasubramanian S 2012 Semitransparent OPV modules pass environmental chamber test requirements *Sol. Energy Mater. Sol. Cells* **114** 214–8

[148] Heliatek 2014 Heliatek announces largest BIOPV façade installation

[149] Hinsch A, Veurman W, Brandt H, Flarup Jensen K and Mastroianni S 2014 Status of Dye Solar Cell Technology as a Guideline for Further Research *ChemPhysChem* **15** 1076–87

[150] Ribeiro F, Maçaira J, Cruz R, Gabriel J, Andrade L and Mendes A 2012 Laser assisted glass frit sealing of dye-sensitized solar cells *Sol. Energy Mater. Sol. Cells* **96** 43–9

[151] Sastrawan R, Beier J, Belledin U, Hemming S, Hinsch A, Kern R, Vetter C, Petrat F M, Prodi-Schwab A, Lechner P and Hoffmann W 2006 A glass frit-sealed dye solar cell module with integrated series connections *Sol. Energy Mater. Sol. Cells* **90** 1680–91

[152] Formica N, Mantilla-Perez P, Ghosh D S, Janner D, Chen T L, Huang M, Garner S, Martorell J and Pruneri V 2015 An Indium Tin Oxide-Free Polymer Solar Cell on Flexible Glass *ACS Appl. Mater. Interfaces* **7** 4541–8

[153] Fahlteich J, Steiner C, Top M, Wynands D, Wanski T, Mogck S, Kucukpinar E, Amberg-Schwab S, Boeffel C and Schiller N 2015 10.1: Invited Paper : Roll-to-Roll Manufacturing of Functional Substrates and Encapsulation Films for Organic Electronics: Technologies and Challenges *SID Symp. Dig. Tech. Pap.* **46** 106–10

[154] Charton C, Schiller N, Fahland M, Holländer A, Wedel A and Noller K 2006 Development of high barrier films on flexible polymer substrates *Thin Solid Films* **502** 99–103

[155] Carcia P F, McLean R S, Groner M D, Dameron A A and George S M 2009 Gas diffusion ultrabarriers on polymer substrates using Al2O3 atomic layer deposition and SiN plasma-enhanced chemical vapor deposition *J. Appl. Phys.* **106** 23533

[156] Fahlteich J, Schönberger W, Fahland M and Schiller N 2011 Characterization of reactively sputtered permeation barrier materials on polymer substrates *Surf. Coatings Technol.* **205** S141–4

[157] Angmo D, Hösel M and Krebs F C 2012 All solution processing of ITO-free organic solar cell modules directly on barrier foil *Sol. Energy Mater. Sol. Cells* **107** 329–36

[158] Hösel M, Søndergaard R R, Jørgensen M and Krebs F C 2013 Comparison of UV-curing, hotmelt, and pressure sensitive adhesive as roll-to-roll encapsulation methods for polymer solar cells *Adv. Eng. Mater.* **15** 1068–75

[159] Krebs F C, Tromholt T and Jørgensen M 2010 Upscaling of polymer solar cell fabrication using full roll-to-roll processing. *Nanoscale* **2** 873–86

[160] Krebs F C, Fyenbo J and Jørgensen M 2010 Product integration of compact roll-to-roll processed polymer solar cell modules: methods and manufacture using flexographic printing, slot-die coating and rotary screen printing *J. Mater. Chem.* **20** 8994

[161] Emmott C J M, Moia D, Sandwell P, Ekins-Daukes N, Hösel M, Lukoschek L, Amarasinghe C, Krebs F C and Nelson J 2016 In-situ, long-term operational stability of organic photovoltaics for off-grid applications in Africa *Sol. Energy Mater. Sol. Cells* **149** 284–93

[162] Søndergaard R R, Hösel M and Krebs F C 2013 Roll-to-Roll fabrication of large area functional organic materials *J. Polym. Sci. Part B Polym. Phys.* **51** 16–34

[163] Ahmad J, Bazaka K, Anderson L J, White R D and Jacob M V. 2013 Materials and methods for encapsulation of OPV: A review *Renew. Sustain. Energy Rev.* **27** 104–17

[164] Weerasinghe H C, Watkins S E, Duffy N, Jones D J and Scully A D 2015 Influence of moisture out-gassing from encapsulant materials on the lifetime of organic solar cells *Sol. Energy Mater. Sol. Cells* **132** 485–91

[165] Tanenbaum D M, Dam H F, Rösch R, Jørgensen M, Hoppe H and Krebs F C 2012 Edge sealing for low cost stability enhancement of roll-to-roll processed flexible polymer solar cell modules *Sol. Energy Mater. Sol. Cells* **97** 157–63

[166] Weerasinghe H C, Vak D, Robotham B, Fell C J, Jones D and Scully A D 2016 New barrier encapsulation and lifetime assessment of printed organic photovoltaic modules *Sol. Energy Mater. Sol. Cells* **155** 108–16

[167] Weerasinghe H C, Dkhissi Y, Scully A D, Caruso R A and Cheng Y-B 2015 Encapsulation for improving the lifetime of flexible perovskite solar cells *Nano Energy* **18** 118–25

[168] Adams J, Salvador M, Lucera L, Langner S, Spyropoulos G D, Fecher F W, Voigt M M, Dowland S A, Osvet A, Egelhaaf H-J and Brabec C J 2015 Water Ingress in Encapsulated Inverted Organic Solar Cells: Correlating Infrared Imaging and Photovoltaic Performance *Adv. Energy Mater.* **5** 1501065

[169] Gevorgyan S A, Madsen M V., Dam H F, Jørgensen M, Fell C J, Anderson K F, Duck B C, Mescheloff A, Katz E A, Elschner A, Roesch R, Hoppe H, Hermenau M, Riede M and Krebs F C 2013 Interlaboratory outdoor stability studies of flexible roll-to-roll coated organic photovoltaic modules: Stability over 10,000 h *Sol. Energy Mater. Sol. Cells* **116** 187–96

[170] Loi A, Muellejans H, Sample T, Dunlop E and Bardizza G 2016 Accelerated ageing test of organic photovoltaic mini-modules: study of the electrical performances after exposure at different humidity, irradiance and temperature conditions *Eu PVSEC proceedings*

[171] Bristow N and Kettle J 2015 Outdoor performance of organic photovoltaics: Diurnal analysis, dependence on temperature, irradiance, and degradation *J. Renew. Sustain. Energy* **7** 13111

[172] Hösel M, Søndergaard R R, Jørgensen M and Krebs F C 2014 Failure modes and fast repair procedures in high voltage organic solar cell installations *Adv. Energy Mater.* **4** 1–7

[173] Nehm F, Dollinger F, Fahlteich J, Klumbies H, Leo K and Müller-Meskamp L 2016 Importance of Interface Diffusion and Climate in Defect Dominated Moisture Ultrabarrier Applications *ACS Appl. Mater. Interfaces* **8** 19807–12

[174] Ke L, Zhang N, Low E, Wang R, Kam Z M, Wang X, Liu B and Zhang J 2015 Organic photovoltaic initial stage degradation analysis using impedance spectroscopy *Synth. Met.* **202** 63–7

[175] Guerrero A, Heidari H, Ripolles T S, Kovalenko A, Pfannmöller M, Bals S, Kauffmann L-D, Bisquert J and Garcia-Belmonte G 2015 Shelf Life Degradation of Bulk Heterojunction Solar Cells: Intrinsic Evolution of Charge Transfer Complex *Adv. Energy Mater.* **5** 1401997

[176] Karuthedath S, Sauermann T, Egelhaaf H-J, Wannemacher R, Brabec C J and Lüer L 2015 The effect of oxygen induced degradation on charge carrier dynamics in P3HT:PCBM and Si-PCPDTBT:PCBM thin films and solar cells *J. Mater. Chem. A* **3** 3399–408

[177] Arredondo B, Martín-López M B, Romero B, Vergaz R, Romero-Gomez P and Martorell J 2016 Monitoring degradation mechanisms in PTB7:PC71BM photovoltaic cells by means of impedance spectroscopy *Sol. Energy Mater. Sol. Cells* **144** 422–8

[178] Tournebize A, Seck M, Vincze A, Distler A, Egelhaaf H-J, Brabec C J, Rivaton A, Peisert H and Chassé T 2016 Photodegradation of Si-PCPDTBT:PCBM active layer for organic solar cells applications: A surface and bulk investigation *Sol. Energy Mater. Sol. Cells* **155** 323–30

[179] Kim S H, Son H J, Park S H, Hahn J S and Kim D H 2016 A study for degradation of flexible organic photovoltaic modules via damp-heat test: By accessing individual layers of the module *Sol. Energy Mater. Sol. Cells* **144** 187–93

[180] Tessarolo M, Guerrero A, Gedefaw D, Bolognesi M, Prosa M, Xu X, Mansour M, Wang E, Seri M, Andersson M R, Muccini M and Garcia-Belmonte G 2015 Predicting thermal stability of organic solar cells through an easy and fast capacitance measurement *Sol. Energy Mater. Sol. Cells* **141** 240–7

[181] Katz E A, Mescheloff A, Visoly-Fisher I and Galagan Y 2016 Light intensity dependence of External Quantum Efficiency of fresh and degraded organic photovoltaics *Sol. Energy Mater. Sol. Cells* **144** 273–80

[182] Reese M O, Gevorgyan S A, Jørgensen M, Bundgaard E, Kurtz S R, Ginley D S, Olson D C, Lloyd M T, Morvillo P, Katz E a., Elschner A, Haillant O, Currier T R, Shrotriya V, Hermenau M, Riede M, Kirov K R, Trimmel G, Rath T, Inganäs O, Zhang F, Andersson M, Tvingstedt K, Lira-Cantu M, Laird D, McGuiness C, Gowrisanker S, Pannone M, Xiao M, Hauch J, Steim R, Delongchamp D M, Rösch R, Hoppe H, Espinosa N, Urbina A, Yaman-Uzunoglu G, Bonekamp J B, Van Breemen A J J M, Girotto C, Voroshazi E and Krebs F C 2011 Consensus stability testing protocols for organic photovoltaic materials and devices *Sol. Energy Mater. Sol. Cells* **95** 1253–67

[183] Gevorgyan S A, Medford A J, Bundgaard E, Sapkota S B, Schleiermacher H F, Zimmermann B, Würfel U, Chafiq A, Lira-Cantu M, Swonke T, Wagner M, Brabec C J, Haillant O, Voroshazi E, Aernouts T, Steim R, Hauch J a., Elschner A, Pannone M, Xiao M, Langzettel A, Laird D, Lloyd M T, Rath T, Maier E, Trimmel G, Hermenau M, Menke T, Leo K, Rösch R, Seeland M, Hoppe H, Nagle T J, Burke K B, Fell C J, Vak D, Singh T B, Watkins S E, Galagan Y, Manor A, Katz E a., Kim T, Kim K, Sommeling P M, Verhees W J H, Veenstra S C, Riede M, Greyson Christoforo M, Currier T, Shrotriya V, Schwartz G and Krebs F C 2011 An inter-laboratory stability study of roll-to-roll coated flexible polymer solar modules *Sol. Energy Mater. Sol. Cells* **95** 1398–416

[184] Gevorgyan S A, Corazza M, Madsen M V., Bardizza G, Pozza A, Müllejans H, Blakesley J C, Dibb G F a., Castro F a., Trigo J F, Guillén C M, Herrero J R, Morvillo P, Maglione M G, Minarini C, Roca F, Cros S, Seraine C, Law C H, Tuladhar P S, Durrant J R and Krebs F C 2014 Interlaboratory indoor ageing of roll-to-roll and spin coated organic photovoltaic devices: Testing the ISOS tests *Polym. Degrad. Stab.* **109** 162–70

[185] Owens C, Ferguson G, Hermenau M, Voroshazi E, Galagan Y, Zimmermann B, Rösch R, Angmo D, Teran-Escobar G, Uhrich C, Andriessen R, Hoppe H, Würfel U, Lira-Cantu M, Krebs F and Tanenbaum D 2015 Comparative Indoor and Outdoor Degradation of Organic Photovoltaic Cells via Inter-laboratory Collaboration *Polymers (Basel).* **8** 1

[186] Angmo D and Krebs F C 2015 Over 2 Years of Outdoor Operational and Storage Stability of ITO-Free, Fully Roll-to-Roll Fabricated Polymer Solar Cell Modules *Energy Technol.* **3** 774–83

[187] Balcaen V, Rolston N, Dupont S R, Voroshazi E and Dauskardt R H 2015 Thermal cycling effect on mechanical integrity of inverted polymer solar cells *Sol. Energy Mater. Sol. Cells* **143** 418–23

[188] Roesch R, Faber T, von Hauff E, Brown T M, Lira-Cantu M and Hoppe H 2015 Procedures and Practices for Evaluating Thin-Film Solar Cell Stability *Adv. Energy Mater.* **5**

[189] Corazza M, Krebs F C and Gevorgyan S A 2014 Predicting, categorizing and intercomparing the lifetime of OPVs for different ageing tests *Sol. Energy Mater. Sol. Cells* **130** 99–106

[190] Corazza M, Krebs F C and Gevorgyan S A 2015 Lifetime of organic photovoltaics: Linking outdoor and indoor tests *Sol. Energy Mater. Sol. Cells* **143** 467–72

[191] Gevorgyan S A, Espinosa N, Ciammaruchi L, Roth B, Livi F, Tsopanidis S, Züfle S, Queirós S, Gregori A, Benatto G A dos R, Corazza M, Madsen M V., Hösel M, Beliatis M J, Larsen-Olsen T T, Pastorelli F, Castro A, Mingorance A, Lenzi V, Fluhr D, Roesch R, Maria Duarte Ramos M, Savva A, Hoppe H, Marques L S A, Burgués I, Georgiou E, Serrano-Luján L and Krebs F C 2016 Baselines for Lifetime of Organic Solar Cells *Adv. Energy Mater.* 1600910

[192] Heutz S, Sullivan P, Sanderson B M, Schultes S M and Jones T S 2004 Influence of molecular architecture and intermixing on the photovoltaic, morphological and spectroscopic properties of CuPc-C60 heterojunctions *Sol. Energy Mater. Sol. Cells* **83** 229–45

[193] Katz E A, Gevorgyan S, Orynbayev M S and Krebs F C 2006 Out-door testing and long-term stability of plastic solar cells *Eur. Phys. J. Appl. Phys.* **36** 307–11

[194] Yang X, Loos J, Veenstra S C, Verhees W J H, Wienk M M, Kroon J M, Michels M a J and Janssen R a J 2005 Nanoscale morphology of high-performance polymer solar cells *Nano Lett.* **5** 579–83

[195] Hauch J A, Schilinsky P, Choulis S A, Childers R, Biele M and Brabec C J 2008 Flexible organic P3HT:PCBM bulk-heterojunction modules with more than 1 year outdoor lifetime *Sol. Energy Mater. Sol. Cells* **92** 727–31

[196] Dennler G, Lungenschmied C, Neugebauer H, Sariciftci N S and Labouret A 2005 Flexible, conjugated polymer-fullerene-based bulk-heterojunction solar cells: Basics, encapsulation, and integration *J. Mater. Res.* **20** 3224–33

[197] Laird D W, Vaidya S, Li S, Mathai M, Woodworth B, Sheina E, Williams S and Hammond T 2007 Advances in Plexcore active layer technology systems for organic photovoltaics: roof-top and accelerated lifetime analysis of high performance organic photovoltaic cells *SPIE 6656, Organic Photovoltaics VIII* p 66560X–66560X–8

[198] Franke R, Maennig B, Petrich A and Pfeiffer M 2008 Long-term stability of tandem solar cells containing small organic molecules *Sol. Energy Mater. Sol. Cells* **92** 732–5

[199] Hauch J A, Schilinsky P, Choulis S A, Rajoelson S and Brabec C J 2008 The impact of water vapor transmission rate on the lifetime of flexible polymer solar cells *Appl. Phys. Lett.* **93** 103306

[200] Lungenschmied C, Dennler G, Czeremuzskin G, Latrèche M, Neugebauer H and Sariciftci N S 2006 Flexible encapsulation for organic solar cells *SPIE 6197, Photonics for Solar Energy Systems* pp 619712-619712–8

[201] Zimmermann B, Würfel U and Niggemann M 2009 Longterm stability of efficient inverted P3HT:PCBM solar cells *Sol. Energy Mater. Sol. Cells* **93** 491–6

[202] Tipnis R, Bernkopf J, Jia S, Krieg J, Li S, Storch M and Laird D 2009 Large-area organic photovoltaic module-Fabrication and performance *Sol. Energy Mater. Sol. Cells* **93** 442–6

[203] Potscavage W J, Yoo S, Domercq B, Kim J, Holt J and Kippelen B 2007 Integrated organic photovoltaic modules *SPIE 6656, Organic Photovoltaics VIII* p 66560R–66560R–10

[204] Schwartz G, Maennig B, Uhrich C, Gnehr W, Sonntag S, Erfurth O, Wollrab E, Walzer K and Pfeiffer M 2009 Efficient and long-term stable organic vacuum deposited tandem solar cells *SPIE 7416, Organic Photovoltaics X* p 74160K–74160K–11

[205] Gao D, Helander M G, Wang Z Bin, Puzzo D P, Greiner M T and Lu Z H 2010 C60:LiF blocking layer for environmentally stable bulk heterojunction solar cells *Adv. Mater.* **22** 5404–8

[206] Angmo D, Sommeling P M, Gupta R, Hösel M, Gevorgyan S A, Kroon J M, Kulkarni G U and Krebs F C 2014 Outdoor operational stability of indium-free flexible polymer solar modules over 1 year studied in India, Holland, and Denmark *Adv. Eng. Mater.* **16** 976

[207] Hermenau M, Leo K and Riede M 2010 Comparison of different conditions for accelerated ageing of small molecule organic solar cells *SPIE 7722, Organic Photonics IV* p 77220K–77220K–10

[208] Cros S, De Bettignies R, Berson S, Bailly S, Maisse P, Lemaitre N and Guillerez S 2011 Definition of encapsulation barrier requirements: A method applied to organic solar cells *Sol. Energy Mater. Sol. Cells* **95** S65–9

[209] Uhrich C L, Schwartz G, Maennig B, Gnehr W M, Sonntag S, Erfurth O, Wollrab E, Walzer K, Foerster J, Weiss A, Tsaryova O, Leo K, Riede M K and Pfeiffer M 2010 Efficient and long-term stable organic vacuum deposited tandem solar cells *SPIE 7722, Organic Photonics IV* p 77220G–77220G–8

[210] Tanenbaum D M, Hermenau M, Voroshazi E, Lloyd M T, Galagan Y, Zimmermann B, Hösel M, Dam H F, Jørgensen M, Gevorgyan S A, Kudret S, Maes W, Lutsen L, Vanderzande D, Würfel U, Andriessen R, Rösch R, Hoppe H, Teran-Escobar G, Lira-Cantu M, Rivaton A, Uzunoğlu G Y, Germack D, Andreasen B, Madsen M V., Norrman K and Krebs F C 2012 The ISOS-3 inter-laboratory collaboration focused on the stability of a variety of organic photovoltaic devices *RSC Adv.* **2** 882

[211] Roth B, dos Reis Benatto G A, Corazza M, Søndergaard R R, Gevorgyan S A, Jørgensen M and Krebs F C 2015 The Critical Choice of PEDOT:PSS Additives for Long Term Stability of Roll-to-Roll Processed OPVs *Adv. Energy Mater.* **5** 1401912

[212] Sapkota S B, Spies A, Zimmermann B, Dürr I and Würfel U 2014 Promising long-term stability of encapsulated ITO-free bulk-heterojunction organic solar cells under different aging conditions *Sol. Energy Mater. Sol. Cells* **130** 144–50

[213] Roesch R, Eberhardt K R, Engmann S, Gobsch G and Hoppe H 2013 Polymer solar cells with enhanced lifetime by improved electrode stability and sealing *Sol. Energy Mater. Sol. Cells* **117** 59–66

[214] Karpinski A, Berson S, Terrisse H, Mancini-Le Granvalet M, Guillerez S, Brohan L and Richard-Plouet M 2013 Anatase colloidal solutions suitable for inkjet printing: Enhancing lifetime of hybrid organic solar cells *Sol. Energy Mater. Sol. Cells* **116** 27–33

[215] Mulligan C J, Bilen C, Zhou X, Belcher W J and Dastoor P C 2015 Levelised cost of electricity for organic photovoltaics *Sol. Energy Mater. Sol. Cells* **133** 26–31